PERFORMANCE EVALUATION AND MODELING OF TWIN SCREW PUMPS

A Dissertation

by

PENG LIU

Submitted to the Office of Graduate and Professional Studies of
Texas A&M University
in partial fulfillment of the requirements for the degree of

DOCTOR OF PHILOSOPHY

Chair of Committee,	Gerald L. Morrison
Committee Members,	Andrea Strzelec
	Je-Chin Han
	Robert Randall
Head of Department,	Andreas A. Polycarpou

May 2016

Major Subject: Mechanical Engineering

ABSTRACT

The Electric Submersible Pump (ESP) is used in the oil wells where the reservoir pressure is insufficient to push the fluid to the surface. Conventional ESP consists of a series of centrifugal pumps. However, the improvement of twin screw technology leads to the invention of a type of novel ESP, Electric Submersible Twin Screw Pump (ESTSP). To determine the performance of the ESTSP, multiphase tests have been performed with different working conditions and different working fluids.

In this research, the effect of the pressure rise, Gas Volumetric Fraction (GVF) and pump rotating speed on the behavior of the ESTSP has been studied. The pump was tested with a maximum pressure rise of 1000 psig. Hydraulic oil and water were selected as the working fluid to test the pump. The GVF varies from 0% to 85%. To evaluate the performance of the ESTSP, the pressure and temperature distribution, the flow rate capacity and the power consumption were recorded during the test. The performance of the ESTSP was compared with that of a Colfax pump to investigate the difference between the multistage pump and the one-stage pump.

The performance prediction of multiphase twin screw pumps has been a challenge. A new model is proposed to study the leakage flow in the twin screw pump. Adiabatic compressible flow is assumed in the circumferential clearance. The acceleration of the two-phase flow is taken into account in the new model. The change of Mach number of

the leakage flow in the clearance and the possibility of choked flow at the outlet of the clearance will be studied.

To verify the leakage model, experimental data of four different twin screw pumps is used to compare with the prediction by the model.

DEDICATION

To my dear wife — for her support of all that I do

ACKNOWLEDGEMENTS

My study at Texas A&M University will soon come to an end. At the completion of my dissertation, I wish to express my sincere gratitude to all those who have offered my invaluable assistance during the three years in the Turbomachinery Lab.

First, I would like to express my gratitude to Dr. Gerald Morrison, my supervisor, for his guidance and encouragement. He always supported me with intelligence and expertise whenever I met with difficulties.

Also, I would like to thank my committee members, Dr. Andrea Strzelec, Dr. Je-Chin Han and Dr. Robert E. Randall, for their guidance and support throughout this research. Thanks to Dr. Jun Xu at Shell Exploration & Production and Dr. Pradeep Dass at Can-K Group of companies for their continuous inputs and supports of this project. Thanks also to my friends Klayton Kirkland, Scott Chien, Sahand Prouzpaneh, Sujan Reddy, Yi Chen, and Wenfei Zhang for making my time at Texas A&M University a great experience.

Finally, thanks to my mother and father for their encouragement and to my wife for her patience and love.

NOMENCLATURE

ASD	Adjustable speed drive
CFD	Computational fluid dynamics
CC	Circumferential clearance
FC	Flank clearance
RC	Root clearance or radial clearance
ESP	Electric submersible pump
ESTSP	Electric submersible twin screw pump
GVF	Gas volume fraction
GUI	Graphical user interface
Re	Reynolds number
P&ID	Pipe and instruments diagram
M	Mach number
N	Total stage
K	Roughness factor
T	Temperature
Q	Flow rate
V	Volume
P_{drive}	Drive power
$P_{net,\ isothermal}$	Work done for isothermal compression
$P_{net,\ polytropic}$	Work done for polytropic compression

$Q_{s,i}$	Leakage across screw i
$A_{s,t}$	Effective leakage area in the circumferential clearance
X_P	Mass fraction
X	Friction factor
Z	Compressibility factor
U	Internal energy
ϕ_L^2	Two-phase friction multiplier
Δt	Time step
c	Speed of sound
c_p	Specific heat of constant pressure
c_v	Specific heat of constant volume
d_h	Hydraulic diameter
f	Friction factor
h	Enthalpy
l	Clearance length
Δp	Differential pressure
p	Pressure
v	Velocity
$\dot{m}$	Mass flow rate
n	Polytropic coefficient
s	Width of the clearance
v	Velocity

k_e	Loss coefficient
f_t	Ratio of circumferential leakage to total leakage
y	Gap depth
m_h	Half of hydraulic mean gap
n_p	Screw number
ω	Pump speed
α	GVF
η_v	Volumetric efficiency
η_{mech}	Mechanical efficiency
η_{eff}	Pump effectiveness
ρ	Density
μ_m	Viscosity
τ	Period of one revolution
Subscript	
l	Liquid
g	Gas
in	Inlet
out	Outlet
i	Chamber index
0	Chamber condition
m	Mean value
t	Time

N	Iteration number
w	Water
o	Oil
rev	Revolution
th	Theoretical
a	Actual
r	Recirculation

TABLE OF CONTENTS

Page

LIST OF FIGURES

Page

LIST OF TABLES

Page

1 INTRODUCTION

In the oil industry, artificial lift is an effective tool to sustain and increase the production of an oil well where the reservoir pressure is insufficient to drive the oil to the surface. According to a survey result from Schlumberger, only approximately 5% of the one million oil wells around the world flow naturally. [1] As a consequence, most of the oil production in the world intensely relies upon the artificial lift technology. Artificial lift has become a well-developed industry. However, innovations in artificial lift technology continue to be developed to meet the increasing challenges in the petroleum industry. In this chapter, the introduction of the main artificial lift methods will be presented. An innovation in artificial lift methods arose recently which will be presented and the related previous research will be summarized.

The most common artificial lift methods include rod pumps, gas lift, hydraulic pumps, electrical submersible pumps (ESP), etc. [2] The rod pump system transfers well fluids by a reciprocating piston (plunger). The plunger connects to the surface pumping unit by a rod. The rod pump is simple and familiar to most operators, so it is used widely. But it is limited in the wells with high GVF flow. The rod pump system needs a large surface footprint and high capital investment. Also depth limited and directional drilling can limit its usage.

The principle of gas lift is to inject compressed gas into the well to reduce the mixture density. Thus, the backpressure is reduced and the reservoir pressure is able to push the

fluids up to the surface. The gas lift is highly flexible, and it is highly tolerant with sand. However, the gas lift is limited in the oil wells with high back pressure.

The hydraulic pumping system conveys power to the downhole by pressurized fluid, which drives the subsurface pump to push fluid. The hydraulic pump is expensive and it is usually employed where other artificial methods are not available.

Electrical submersible pump system usually consists of subsurface pump (electrical submersible pump), electrical motor, protector for motor, and surface control equipment. The electric submersible pump is composed of multi-stages pumping units installed in series.

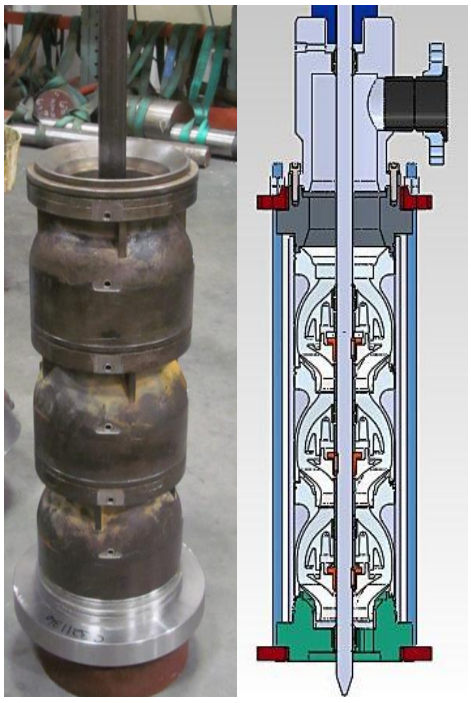

Figure 1.1 Conventional ESP [3]

The ESP system is one of the most common artificial lift methods due to its high efficiency and flexibility. The electric submersible pump is typically used to pump high flow rates in the deep oil wells. Compared with other artificial lift equipment, the electric submersible pump has significant advantages in the offshore application, because it needs the least space of surface construction. [2] A typical ESP pump is shown in Figure 1.1.

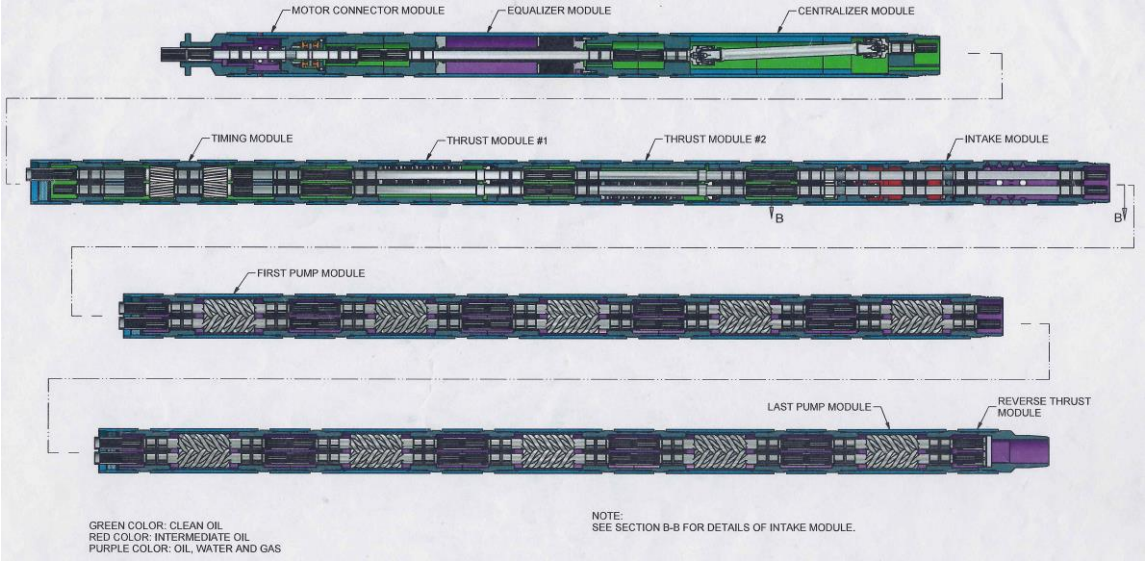

Figure 1.2 Drawing of the Can-K 425 ESTSP

The ESP technology has undertaken significant improvements since its invention in the 1910s. Conventional ESPs are composed of a series of centrifugal pumps as shown in Figure 1.1. However, a new type of ESP has emerged recently due to the development of twin screw pump technology. The Can-K Group of Companies Inc. designed and

manufactured an electrical submersible twin screw pump (ESTSP) to challenge the traditional ESPs. The pump consists of 10 stages of twin screw pump elements in series.

As shown in Figure 1.2, the diameter of the ESTSP is designed very small to fit into the oil well casing. In the downhole application, it is often required to handle high pressure conditions. With multiple stages, the new twin screw pump contains a great number of seals which enable it to keep its performance at high pressure operation. [4]

1.1 Introduction of Twin Screw Pumps

The twin screw pump is a type of positive displacement pump. It has two intermeshed screws, which form a series of closed chambers with the surrounding housing. When the pump runs, the liquid is carried by the moving chambers axially from the pump inlet to the outlet. As a displacement pump, the twin screw pump can handle very high GVF flow. In addition, the twin screw pump shows better erosion resistance due to the relatively low fluid velocity in the pump. The twin screw pump has been one of the most popular multiphase pumps in the petroleum industry.

Typically, there are two types of arrangements for twin screw pumps, single-end and double-end. The double-end arrangement is more popular and has been widely used due to its simplicity and compactness. As shown in Figure 1.3, the double-end pump is composed by two opposed pump elements with a common driving rotor. The working fluid flow through entrance and is absorbed into the pump elements at the both sides. The two pump elements produce equal and opposite axial thrust eliminating the need for

axial thrust bearings. The double-end pump is widely used as surface pump in the petroleum industry for the low and medium pressure multiphase pumping. [5]

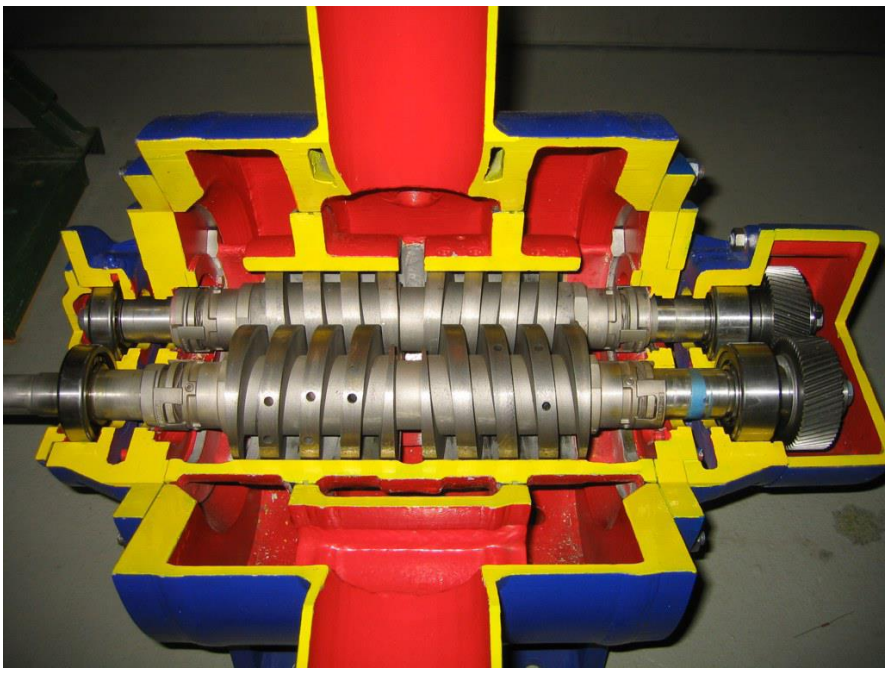

Figure 1.3 Cutaway of a multiphase twin-screw pump [6]

Compared with double-end arrangement, the single-end arrangement usually has longer screws. Hence, there are more closed chambers and seals in this type of pump. The working fluid enters the pump at one end and it is discharged at the other end. With more seals, the single-end pump has significant advantages to handle high pressure and GVF applications. Also, the unique design makes the single-end pump able to be

employed for subsurface applications. This design does require large capacity thrust bearing as shown in Figure 1.2.

The twin screw pump has been widely used for multiphase pumping in the petroleum industry. Extensive research has been done to investigate the working principle of twin screw pumps for multiphase flow.

1.2 Literature Review

1.2.1 Experiment and Modeling

Performance test and leakage flow analysis of the twin screw pump have been the research focus over the past decades. Since the twin screw pump is a positive displacement pump, theoretically it conveys a fixed volume of fluid in one revolution. However, if there is a pressure rise from the pump inlet to outlet, leakage flow will occur from the pump discharge side to the pump suction side through the internal clearances. Thus, the actually flow rate of a twin screw pump is always less than the theoretical flow rate. The leakage flow rate is usually affected by the dimensions of the clearances, the liquid viscosity, the differential pressures, GVF, etc.

The leakage flow can impose a serious impact on the performance of twin screw pumps. As a result, numerous experimental tests have been conducted to study its performance. These experiments were basically performed with water and air. Analytical models and CFD simulations have been proposed to understand the working principle of the leakage flow. In this section, the previous research on the twin screw pump will be summarized.

Vetter and Wincek [7] investigated the performance of two commercial twin screw pumps and they developed the first computer model to predict the pump performance for both single and two phase operation. In the computer model, the compression process was assumed to be isothermal due to the high specific heat of the liquid compared with the gas. It was also assumed that all clearances are filled with liquid only. In addition, the liquid backflow is the only factor that leads to the gas compression. The internal leakage flow velocity was calculated according to the differential pressure between the two adjacent cavities with the equation below,

$$\Delta p = f \frac{l}{d_h} \frac{\rho_l}{2} v^2 \tag{1.1}$$

where λ is the friction factor depending on the flow mode. For the laminar flow,

$$f = \frac{96}{Re} \tag{1.2}$$

For the turbulent smooth clearance,

$$f = \frac{0.3322}{Re^{0.25}} \tag{1.3}$$

For the turbulent rough clearance, the friction factor can be found by

$$\frac{1}{\sqrt{f}} = 2 \cdot log\left(\frac{2s}{K}\right) + 0.97 \tag{1.4}$$

The steady state operating conditions were obtained by iteration. Figure 1.4 shows the predicted pressure distributions by the computer model for single phase and two phase flow.

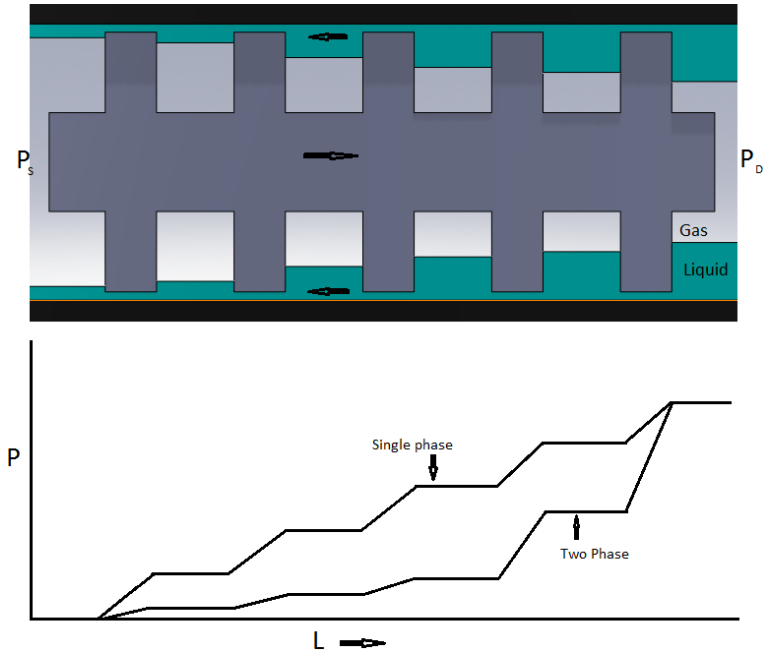

Figure 1.4 Pressure distributions in the screw pump [4]

Vetter evaluated the multiphase performance of two commercial screw pumps from Leistritz Corporation and Bornemann Corporation. The power consumption, isothermal efficiency, and volumetric flow rate capacity were investigated in this study.

Vetter verified the model prediction with the experimental data. The prediction results shows good agreement with experimental results when the inlet GVF is below 50%. However, the predictions deviate from the experimental data at 50% and 90% GVFs. In this case, the assumption of the totally liquid-filled clearances is no longer true and the gas injection in the clearance should be considered.

Egashira [8] investigated the performance characteristics of a twin screw pump and proposed a physical model to simulate the backflow. The experiment was conducted with single phase flow and two phase flow. The relation of backflow rate with the pressure distribution was investigated. In the physical model, the leakage flow rate and the pressure drop was related by the following equation,

$$\Delta p = \frac{\rho v^2}{2}\left[\frac{fy}{4m_h} + 1.5\right] \tag{1.5}$$

An empirical relationship of the pressure distribution along the screws was developed to calculate the leakage flow rate, which is expressed as,

$$\left(\frac{p_i - p_{in}}{p_{out} - p_{in}}\right) = \left(\frac{n}{n_p + 1}\right)^{p_d} \tag{1.6}$$

Where p_d equals to 1 for the single-phase flow and it increases with the compressibility of working fluid. The prediction of the model was compared with the experimental data. The model was confirmed to be effective within the test conditions.

Feng *et al* [9] performed a thermodynamic simulation for a multiphase twin screw pump. The back flow through the circumferential clearance was assumed to be incompressible viscous flow through a narrow channel. The backflow rate through the circumferential clearance was calculated by the equation as follows,

$$\dot{m} = \frac{\rho_l \pi d_l h^3 \Delta p}{12 \mu_l L} \tag{1.7}$$

The two-phase flow was assumed for the leakage through the flank clearance and the root clearance. An experimental test rig was established to obtain performance data for

different operating conditions. Feng compared the simulation results and the experimental data. The prediction showed good agreement with the test data within the test conditions.

Nakashima *et al* [10] proposed a thermodynamic model to predict the absorbed power, backflow rate and the discharge conditions. The compression process in the pump was considered to be adiabatic. In this model, Nakashima developed the equations to calculate the backflow based on the work of Wincek. The effect of local losses and the roughness in the new model was taken into account. Nakashima used both of the new model and Wincek's model to calculate the backflow of a multiphase twin screw pump tested by Egashira. It shows that Wincek's prediction is closer to the experimental data.

Martin and Scott [11] proposed a model which is able to predict the multiphase performance of the twin screw pump without knowing the dimensions of the clearances. It assumed that all the leakage flow is through an effective clearance, which can be estimated by the 100% water performance data. In this model, the leakage flow path was simplified to a two-dimensional flow between two plates. As a result, the pressure drop across the screws can be calculated as,

$$\Delta p = f \cdot \left(\frac{l}{2c}\right) \cdot \frac{\rho v^2}{2} \tag{1.8}$$

In this model, the pump surface was assumed to be smooth. Consequently, the friction factor can be calculated by following equation,

$$f = 0.316 \cdot Re^{-0.25} \tag{1.9}$$

At the end, the leakage flow rate across one screw was reduced to,

$$q_l = C_l \cdot \Delta p^{0.57} \tag{1.10}$$

Where C_l is only determined by the effectual clearance and other pump dimensions. If the single-phase performance data is available, C_l can be calculated by performing a linear regression.

The compression process in the chamber was assumed to be isothermal. A system of mass balance equations for each chamber was derived as following and they can be solved simultaneously,

$$V_s\left[\frac{p_s Z_1}{p_1 Z_s} - 1\right] + (q_1 - q_0)\Delta t = 0 \tag{1.11}$$

$$V_1\left[\frac{P_1 Z_2}{P_2 Z_1} - 1\right] + (q_2 - q_1)\Delta t = 0 \tag{1.12}$$

$$\vdots$$

$$V_{i-1}\left[\frac{p_{i-1} Z_i}{p_i Z_{i-1}} - 1\right] + (q_i - q_{i-1})\Delta t = 0 \tag{1.13}$$

$$\vdots$$

$$V_{n-1}\left[\frac{p_{n-1} Z_D}{p_D Z_{n-1}} - 1\right] + (q_n - q_{n-1})\Delta t = 0 \tag{1.14}$$

Prang and Cooper [12] proposed a prediction model for the twin screw pumps. In this model, Prang adopted Vetter's assumption that only liquid leaks across the clearances, but the effect of viscous heating on the friction factor in the clearance due to the shearing

of the leaking liquid was taken into account. The pressure distribution was simplified to be constant in one rotation and can be calculated by the following equation,

$$p_{i+1} - p = \rho_l \times \left(k_e + f\frac{l}{d_h}\right) \times \frac{\left(\frac{Q_{s,i}}{A_{s,t}} \times f_t\right)^2}{2} \quad 1.15$$

Where the leakage flow rate $Q_{s,i}$ is determined by the isothermal compression of the gas. For the multiphase flow, the gas volume in the chamber is calculated by

$$Q_{g,i+1} = Q_{g,i} \times \frac{p_i}{p_{i+1}} \quad 1.16$$

The slip $Q_{s,i}$ and the gas volume $Q_{g,i}$ is related by

$$Q_{s,i} = Q_d - Q_l - Q_{g,i} \quad 1.17$$

Solving equations 1.15 to 1.17 gives the leakage flow rate and the pressure distribution across the screws. To prove the validation of the model, various twin screw pumps were tested with different operating conditions. The prediction of the model showed good agreement with the experimental results. However, this model predicting zero leakage at extreme high GVF is doubtable since experimental results have proved that the volumetric efficiency will drop severely when the GVF is larger than a critical value.

Rausch and Vauth [13] established a leakage model which detailed the mass and energy balance equations in a chamber. Though Rausch developed the differential equations to describe the two-phase flow of the liquid and the gas in the clearance, the leakage flows in this model are considered to be liquid only. He also developed the differential equations for energy balance by assuming an adiabatic compression in the pump. The

model was verified by the experimental tests. It shows that the model works well with pure water. However, the predicted efficiency is higher than experimental results at low speeds and high GVFs.

So far, all the analytical research on the leakage flow is based on the common assumption that the leakage flow is single phase. That is to say, the clearances are filled with liquid only. As a result, the leakage flow rate and pressure change across one screw can be related by the following equation,

$$\Delta p = \lambda \frac{l}{d_h} \frac{\rho_l}{2} v^2 \tag{1.18}$$

However, a wide variety of experimental results have proved that this assumption is no longer true when the GVF above 80%. In order to study the performance of twin screw pumps working with high GVF flows, the effect of gas infiltration into the gap must be taken into consideration.

Vetter *et al* [14] modeled the hydrodynamic performance and hydroabrasive wear of the twin screw pumps. In this research, Vetter also put forward important improvement for the computer model by considering the influence of gas volume fraction in the clearance. The flow patterns and basic theory of the leakage flows were concluded. The mean density and the mean viscosity of two phase leakage flow were modeled by following equations,

$$\rho_c = \frac{\alpha \rho_g + (1+\alpha)\rho_l}{\alpha \frac{\rho_s}{\rho_c} + (1-\alpha)} \tag{1.19}$$

$$\mu_c = \frac{\alpha\rho_g\mu_g + (1-\alpha)\rho_l\mu_l}{\alpha\rho_g + (1-\alpha)\rho_l} \quad 1.20$$

In the new model, the mean density and the mean viscosity were used to calculate the leakage flow rate for the high GVF conditions. It should be noted that the compressibility of the two phase flow was not taken into consideration in the calculation. The density and the viscosity of the fluid in the clearance are assumed to be constant. In this study, Vetter also investigated the hydrodynamic performance and hydroabrasive wear of twin screw pumps.

Nakashima *et al* [15] proposed a thermos-hydraulic model. Nakashima evaluated the effect of hydrocarbon mixtures as working fluids and made a comparison with water-air. Infiltration of gas when suction GVF is above 80%. In the new model, the leakage was considered to be two phase when the GVF in the chamber is higher than 80%. The gas content in the clearances was estimated by the following equation,

$$GVF_P = \frac{GVF_k - 0.8}{0.2}, GVF_k \geq 0.8 \quad 1.21$$

The density and the viscosity were calculated with Beattie and Whalley correlations,

$$\rho_{gl} = \left(\frac{X_P}{\rho_g} + \frac{1-X_P}{\rho_l}\right)^{-1} \quad 1.22$$

$$\mu_{gl} = (1 - GVF_P)(1 + 2.5GVF_P)\mu_l + GVF_P\mu_g \quad 1.23$$

Where X_P is the mass fraction. As the leakage flow through the clearance, the change of the fluid properties was evaluated in this model. In this model, the leakage flow between two chambers is still calculated by the following equation of channel flow,

$$\Delta p = \lambda \frac{l}{d_h} \frac{\rho_l}{2} v^2 \qquad 1.24$$

Different from previous models, Celso evaluated the influence of screw rotation on the friction factor as well as the eccentricity effects. However, Celso didn't conduct experimental test. Hence, this model is still under verification with experimental data.

Xu [16] investigated the performance of a Bornemann MW-6.5zk-37 pump and a Flowserve LSIJS pump with very high GVF conditions. Xu also developed a model to predict the performance of multiphase twin screw pumps. This model predicts the multiphase performance for extreme high GVF according to the single phase water test data. Jian developed this model based on the previous work of Martin and Scott. Martin's model is able to predict the multiphase performance without knowing the dimensions of the clearances in the pump. Instead, he developed a concept, the effective clearance, which is used to predict performance at any operating conditions. In this model, the leakage flow is considered as single-phase flow. Hence, there is no gas slip in the clearance. However, Xu believed that this is not true at the extreme high GVF. Hence, both the liquid and the gas slip were taken into account in the new model. In this model, Lockhart-Martinelli parameter, X^2 is used to calculate the friction factor of two phase flow. The Lockhart-Martinelli parameter is defined as the ratio of pressure drop of liquid flow to that of gas flow,

$$X^2 = \left(\frac{\Delta p}{\Delta z}\right)_{F,SPL} \Big/ \left(\frac{\Delta p}{\Delta z}\right)_{F,SPG} \qquad 1.25$$

The pressure drop of two phase flow in this model is evaluated by two phase friction multiplier ϕ_L^2, which is defined as the ratio of pressure drop of two phase flow to that of liquid flow,

$$\phi_L^2 = \left(\frac{\Delta p}{\Delta z}\right)_{F,TP} \Big/ \left(\frac{\Delta p}{\Delta z}\right)_{F,SPL} \tag{1.26}$$

The value of ϕ_L^2 is related with X^2 by the following equation,

$$\phi_L^2 = 1 + \frac{C}{X} + \frac{1}{X^2} \tag{1.27}$$

Xu performed both isothermal and non-isothermal simulation for the leakage flow in this model. The prediction of the new model shows a good match with the experimental data with the GVF changing from 0% to 99%.

Rabiger *et al* [17, 18, 19, 20] published a series of research results on the twin screw pumps. Rabiger developed a thermo- and fluid dynamic model to investigate the multiphase twin screw pump. The chamber was considered as a thermodynamic open system. The chamber inflow and outflow were calculated separately. The two phase leakage flow was taken into account in the clearance. The authors proposed a homogeneous equilibrium model to simulate the multiphase leakage flow, which assumes the gas phase and liquid phase have the same pressure, velocity and temperature in the clearance. The mass, momentum and energy conservation equations are as follows,

$$\frac{\partial(\rho_H \cdot w \cdot s)}{\partial l} = 0 \tag{1.28}$$

$$\frac{\partial \rho}{\partial l} + \frac{1}{s} \cdot \frac{\partial(\rho_H \cdot w^2 \cdot s)}{\partial l} + \lambda \cdot \frac{\rho_H}{4s} \cdot w^2 = 0 \tag{1.29}$$

$$\frac{dT}{dl} + \frac{1}{c_{p,H}} \cdot w \cdot \frac{dw}{dl} = 0 \tag{1.30}$$

The heat transfer between the gas and the liquid in the chamber was investigated in this model. The author made a correlation of the heat transfer coefficients with different flow patterns. Both phases will have the same temperature after a time step. A simulation for an arbitrary operating point of a multiphase screw pump was presented in this study. The simulation results include the pressure distribution, the pressure and temperature distribution, the chamber gas densities and the convergence history of the volumetric efficiencies. The prediction shows the same trend with the experimental results.

Chan [6] investigated the multiphase performance of a twin screw pump under wet-gas conditions with GVF over 95%. Chan put forward two methods to improve pump performance under wet-gas conditions. One is to increase the viscosity of working liquid; another method is to inject liquid into specific pump chambers. It is found that pressure profiles become more linear with the through-casing injection. The injection increases as the GVF increases.

Chan investigated the effect of viscosity on the volumetric flow rate capacity. Experimental results shows that the leakage flow rate decreases with the increase of liquid viscosity for the single phase flow. The volumetric flow rate capacity increase with the increase of liquid viscosity as well. However, at extremely high GVF the

viscosity has an opposite effect on the volumetric flow rate capacity. The flow rate with higher viscosity liquid is lower than that of lower viscosity liquid. Chan attributes this phenomenon to the thinning behavior of the test oil and the loss of liquid sealing at high GVF conditions.

The Turbomachinery Lab of Texas A&M University has concentrated on the research of twin screw pumps. A series of performance tests have been conducted for various twin screw pumps.

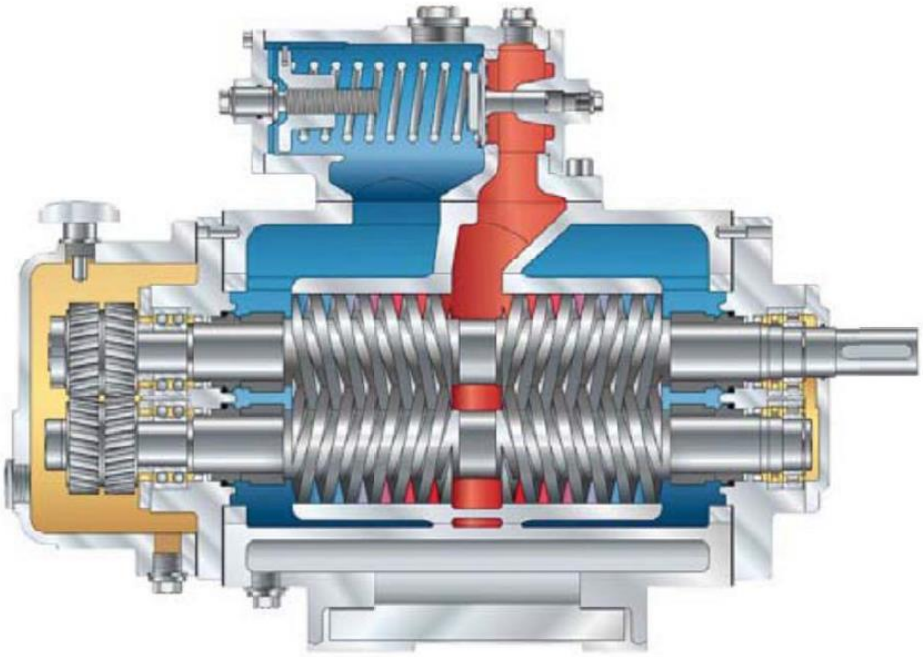

Figure 1.5 Sectional drawing of a twin screw pump [19]

Kroupa *et al* [21, 22] investigated the performance of a twin screw pump from Leistritz Corporation with high GVF conditions. The drawing of the pump is shown in Figure 1.5. The test was performed at the Turbomachinery Laboratory, Texas A&M University. With a liquid recirculation system, the pump was tested up to 100% GVF. Ryan compared the volumetric efficiencies with different GVFs and found that the maximum volumetric efficiency takes place at around 90% GVF. Kroupa also researched the effect of the inlet pressure and the operating speed on the performance of the Leistritz pump. The test results shows that the lower inlet pressure leads to better volumetric efficiency at the same differential pressure. However, the pump had higher mechanical efficiency with the higher inlet pressure. The liquid recirculation effect on the pump performance at extreme GVF operation was highlighted in the thesis. The liquid recirculation helps to seal the pump internal clearances and improve the pump's performance at high GVF conditions. However, as the re-circulated liquid is heated up during the repeating pumping process, it will lead to the temperature rise of the pump. Therefore, it is necessary to remove the heat stored in the recirculation fluid.

Patil *et al* [23, 24] evaluated a twin screw pump from Colfax with different GVFs, suction pressure and differential pressure. The pump was tested with GVF up to 100%. The pump performance was evaluated based on the leakage flow rate, mechanical efficiency and pump effectiveness. Transient analysis and flow visualization were performed to investigate the pump behavior at different working conditions. The effect of viscosity on the leakage flow was highlighted in this research. Patil found that the leakage flow doesn't always decrease as the viscosity increases. It is also found that

minimum seal flush should be provided when the twin screw pump work under high GVF conditions.

Patil performed 2D and 3D CFD simulation by ANSYS FLUENT for both single and two phase flows. The CFD simulation reflects the mixing process, heat transfer and the swirling of the two phase flow in the pump. In the 2D simulation, the pump was simplified to be a series of rotating disc with uniform speed and constant axial velocity. The 3D simulation was performed for 50% GVF at different working conditions. The bubble size has been studied and it is found that increasing bubble size leads to better separation of the multiphase flow in the pump.

Turhan [25] proposed different leakage models, each of which worked well for a specific flow case. At the low GVF conditions, the pipe flow model was built with Bernoulli equation as below,

$$\frac{p_{in}}{\rho_{in}} + \frac{1}{2} v_{in}^2 - \frac{p_{out}}{\rho_{out}} - \frac{1}{2}\, v_{out}^2 = \frac{1}{2} f \frac{L}{D} v_{in}^2 \tag{1.31}$$

Turhan assumed that the leakage flow in the clearance is homogenous. The mixture properties, such as density and friction factor, are calculated by the equations below,

$$\rho_m = \frac{\rho_g \cdot \rho_l}{x \cdot \rho_l + (1-x) \cdot \rho_g} \tag{1.32}$$

$$\mu_m = \frac{\mu_g \cdot \mu_l}{x \cdot \mu_l + (1-x) \cdot \mu_g} \tag{1.33}$$

Where x is the gas mass fraction. A software code was developed to calculate the leakage flow rate by solving the governing equation. At the high GVF conditions,

Turhan assumed that the leakage flow is choked in the first screw. Therefore, the velocity at the outlet will equal to the local speed of sound. The leakage flow rate was calculated based the GVF at the pump inlet and outlet separately. Turhan verified the model with the experimental results of Ryan Kroupa.

So far, all the previous research has concentrated on the performance of double-end twin screw pumps, which only has one-stage of pump elements. The performance characteristics of the multi-stage twin screw pump have never been investigated. Since the multi-stage twin screw pump has significant advantages compared with the double-end screw pump, it has a great potential utilization in the oil field. It is of great significance to investigate its performance characteristics.

1.2.2 Two Phase Flow

Brennen [26] summarized the performance characteristics of the two phase flow. The sonic speed of the homogeneous two phase mixture is derived with a homogeneous flow model. The sonic speed of the two phase mixture can be expressed with the following equation,

$$\frac{1}{c^2} = \left[\rho_l(1-\alpha) + \rho_g\alpha\right]\left[\frac{\alpha}{kp} + \frac{(1-\alpha)}{\rho_l c_l^2}\right] \tag{1.34}$$

It is found that the sonic speed of the two phase flow is much lower than that of the pure gas or the pure liquid. Brennen also synthesized the homogeneous multiphase flow in ducts and nozzles. The choked conditions in the ducts and nozzles can be derived with the given reservoir conditions P_0 and α_0 as well as the properties of the liquid and the gas.

2 OBJECTIVES

Previous research mainly concentrated on the performance of the “one-stage” screw pump. The multi-stage pump is a relatively new technology that raises lots of issues to investigate. It is of great significance to understand the performance of the multi-stage pump.

The objective of this research is to determine the multiphase performance of the multi-stage twin screw pump under various operating conditions. The effect of GVF, pressure rise and pump speed, and working fluid has been taken into consideration in the experiment. The pressure and the temperature distributions are recorded at different test conditions. Water and hydraulic oil have been selected as working liquid. The mechanical efficiency, the flow rate capacity, and the leakage flow are investigated.

The performance of multistage twin screw pump will be compared with that of the “one stage” pump. With more stages, the volumetric efficiency and the mechanical efficiency are different from that of the one stage pump, which need to be investigated to make it economically feasible for the petroleum industry.

The influence of viscosity is also investigated in this research. Hydraulic oil and water are selected as working fluid to specify the effect of viscosity. Pump performance with different working fluid viscosities was evaluated under different operating conditions.

The analytical prediction of the performance is a challenge for the multiphase twin screw pump as well. Until now, no universal model has been demonstrated valid to describe the performance of the multiphase twin screw pumps under various conditions. In this research, a new predictable model was developed by using MATLAB, which is able to predict the leakage flow under different operating conditions, such as variable GVF, pump speed, and differential pressure. Note that in the new model, the gas mass fraction was assumed to be uniform at every point in the chambers and clearances.

To verify that the analytical is able to work with different twin screw pumps, four twin screw pumps have been selected to test the model. The prediction has been compared with the experimental data to prove the validation of the model. The leakage flow conditions in the twin screw pump has also been analyzed by this model as well.

3 FUNDAMENTALS OF TWIN SCREW PUMP

This section highlights the internal construction and the working principle of the twin screw pump. Essential parameters, mechanical efficiency, pump effectiveness and volumetric efficiency, will be introduced to characterize the performance of the multiphase twin screw pumps.

As mentioned in the introduction, the twin screw pump is a type of positive displacement pump. It conveys fluids with the moving chambers created by two intermeshed threaded rotors. The twin screw pump is usually driven by an electrical motor, which is connected with one of the two rotors. The coupling of two rotors is accomplished by the timing gear. With the timing gear, the power can be transferred from one rotor to another without physical contact. This design significantly promotes the pump's life by avoiding the wear of screws. However, this design leads to the existence of the clearances between the screws, which have a significant effect on the pump performance.

For the double-end pump, the axial force on the rotors is balanced due to the reversed flow direction in the two pumping elements. However, the axial force is an issue for the single-end pump. As shown in Figure 1.2, a series of thrust bearings are arranged in the front part of the 425 ESTSP. These thrust bearings will keep the pump working safely, especially when the pump is operating with a large discharge pressure.

The core component of a twin screw pump is the two rotors, which will determine the pump's performance. In the following section, the detailed construction of the rotors will be highlighted.

3.1 The Geometry Parameters of the Screws

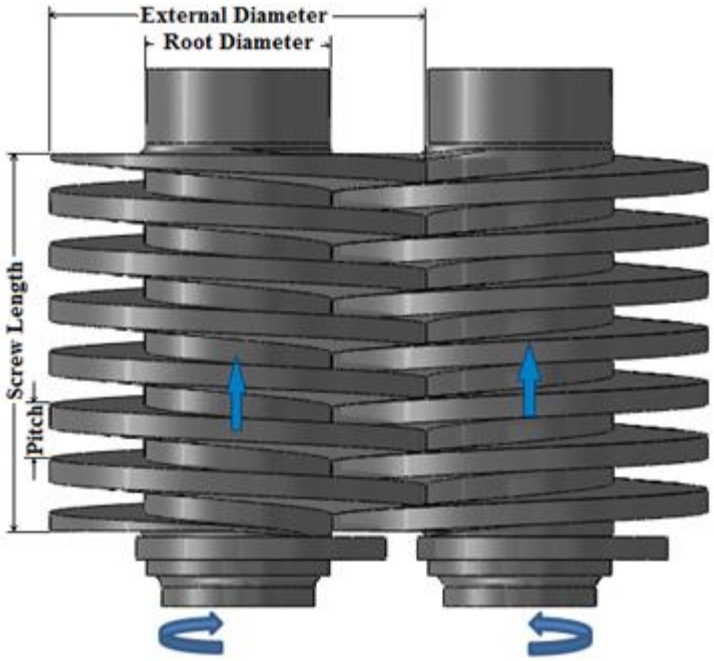

Figure 3.1 Geometric parameters of the twin screw pump [23]

Figure 3.1 shows two intermeshed screws. Pitch indicates the distance for one point on the screw periphery moves in one rotation. Screw length is the length of one screw. The screws are closely intermeshed with very small clearances. Thus, a series of closed

chamber are formed in the twin screw pump. The shape of a closed chamber is as shown in Figure 3.2. When the pump runs, the moving chamber will keep moving axially from the suction side to the discharge.

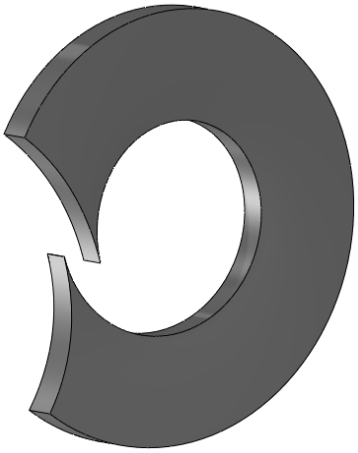

Figure 3.2 Fluid volume created by intermeshed screws [23]

With knowing the working principle of the twin screw pump, it is easy to understand that the volume displaced by one revolution for an ideal twin screw pump is constant. This volume can be defined as V_{rev}. Thus, the theoretical flow rate at the speed ω is defined as,

$$Q_{th} = V_{rev} \cdot \omega \tag{3.1}$$

However, the actual pump flow rate is always less than the theoretical flow rate, because the chambers can't be completely sealed in an actual pump. As mention in the beginning

of this chapter, there are clearances between the screws to avoid the wearing. Additionally, there are also clearances existed between the screws and the housings. These clearances are designed to promote the pump's life. However, they also lead to the degradation of the pump performance. Since they cause the leakage flow in the pump, which decreases the pump's actual flow rate. Especially with a high pressure rise, the pump flow rate capacity can decrease severely. Thus, the actual flow rate of the twin screw pump is the difference from the theoretical flow rate and the leakage flow rate. The actual flow rate is subject to operation conditions.

3.2 Volumetric Efficiency

The existence of internal clearances leads to the degradation of volumetric flow rate capacity of the twin screw pump. There are 3 types of clearances in the twin screw pump, circumferential clearance (CC), radial clearance (RC) and flank clearance (FC), which are detailed in Figure 3.3. The circumferential clearance is located between the periphery of the screws and the housing, while the radial clearance is located between the outer diameter of one rotor and the root diameter of the other rotor. The flank clearance is formed by two adjacent flanks. Previous researches show that the circumferential clearance accounts for about 80% of total leakage, while the radial clearance and the flank clearance account for 20% of total leakage. Hence, the circumferential clearance is the most important factor for the backflow.

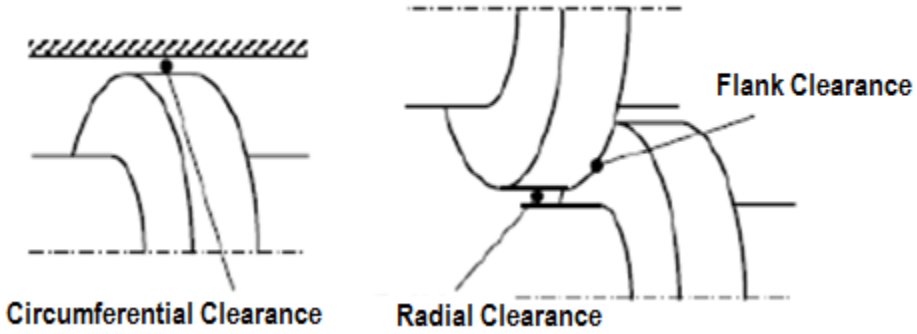

Figure 3.3 Clearance types of the twin screw pumps [21]

The leakage flow rate varies with the clearances dimensions and pump working conditions. Hence, the pump's actual flow rate is also influenced by the clearances and operating condition. The smaller clearances help to promote the pump's flow rate capacity, but it also leads to larger possibility of interior abrasion and friction loss. What's more, the actual flow rate is also subject to the pressure rise, GVF, fluid viscosity, etc. To compare the pump actual flow rate capacity with its theoretical flow rate capacity, it is necessary to define the parameter, volumetric efficiency (η_v). Volumetric efficiency is defined by the ratio of the actual volumetric flow rate to the theoretical flow rate of the pump.

$$\eta_v = \frac{Q_a}{Q_{th}} \tag{3.2}$$

Where Q_a represents the actual flow rate of the pump and Q_{th} is the theoretical flow rate of the pump. For the pump designer, it is a common goal to improve the pump's volumetric efficiency. Generally, increasing the pitch number is an effective method to

improve the volumetric efficiency. With more seals in the pump, the leakage flow will decrease. It is found that the volumetric efficiency can drop severely when the pump works at high GVF. In this case, it is necessary to introduce the sealflush recirculation. According to the research of Patil, the optimum sealflush recirculation to obtain the best volumetric efficiency is around 3% of the total flow rate.

3.3 Mechanical Efficiency

Mechanical Efficiency ($\eta_{mech}$is defined as the ratio of the power delivered to the fluid during the compression process to the power from the motor into the pump.

$$\eta_{mech} = \frac{P_{net}}{P_{drive}} \tag{3.3}$$

It represents friction losses incurred due to viscous and turbulence effect in the cavities as well as different clearances, mechanical losses due to friction inside bearings, seals, and gears.

The power transferred to the working fluid can be divided into two parts, the liquid power (P_l) and the gas power (P_g). As a result,

$$P_{net} = P_l + P_g \tag{3.4}$$

The P_l is the power transferred to the liquid. It can be calculated with the following equation,

$$P_l = Q_l \Delta p \tag{3.5}$$

When the twin screw pump runs at low GVF conditions, the temperature rise of the fluid is small. Thus the process can be considered as isothermal. Then the power delivered to the fluid can be calculated as:

$$P_{net,\ isothermal} = Q_l \Delta p + Q_g p_{in} \ln\left(\frac{p_{out}}{p_{in}}\right) \tag{3.6}$$

When a twin screw pump runs at high GVF conditions, the temperature rise is significant. Polytropic compression process is applied to calculate the power delivered into fluid.

$$P_{net,\ polytropic} = Q_l \Delta p + \frac{n}{n-1} Q_g p_{in} \left[\left(\frac{p_{out}}{p_{in}}\right)^{\frac{n-1}{n}} - 1\right] \tag{3.7}$$

Where n is the polytropic constant. The value of n can be obtained knowing the inlet and exit pressures and temperatures from the following equation,

$$n = \frac{In\left(\frac{p_{in}}{p_{out}}\right)}{In\left(\frac{p_{in}}{p_{out}} \cdot \frac{T_{out}}{T_{in}}\right)} \tag{3.8}$$

The polytropic constant varies from 1 to $\frac{c_p}{c_v}$ in the compression process. The polytropic constant equals to $\frac{c_p}{c_v}$ when the compression process is adiabatic.

3.4 Pump Effectiveness

Pump effectiveness (η_{eff}) represents the ratio of power imparted into the multiphase fluid to the power imparted into single liquid phase with same flow rate. [27] The pump effectiveness can be calculated as the following equation,

$$\eta_{eff} = \frac{P_{net}}{P_{hydraulic}} \quad 3.3$$

Where $P_{net} = P_{net,\ isothermal}$ or $P_{net,\ polytropic}$. The $P_{hydraulic}$ represents the power imparted into working fluid if the flow is incompressible. It is calculated by the equation below,

$$P_{hydraulic} = \left(Q_g + Q_l\right) \cdot \Delta p \quad 3.4$$

The pump effectiveness indicates the pump ability to compress the multiphase flow. Pump effectiveness decreases with an increase of the GVF.

In this chapter, the internal construction of the twin screw pump is highlighted. Essential parameters to evaluate the twin screw pump performance are introduced. In the following section, the experiment method will be presented. The test rig will also be detailed.

4 METHODOLOGY

This chapter highlights the establishment of the test rig and the details of the instruments. The pump was tested at the Turbomachinery Laboratory at Texas A&M University. The facilities at the Turbomachinery Lab make it very convenient to set up the test rig. Previous work generally chose water and air as the working fluids in the experiment. However, the fluid in the oil well is usually the mixture of water, oil and gas. To simulate the real working condition, the pump was tested with different working fluids. Water and oil are selected as the working liquid to test the pump with different water cuts: 100%, 80%, 50% and 0%. The compressed air was used as working gas to perform the multiphase test with 100% water cut, while nitrogen was chosen for the oil tests for safety. The water-air test was performed during August 2014, while the oil-water-nitrogen test was performed during April 2015.

4.1 Experimental Set Up

4.1.1 Test Rigs

Figure 4.1 illustrates the P&ID diagram for the water-air test. The water test was performed with an open loop. Only the liquid was recirculated in the test loop. Water was boosted into the flow loop by a charge pump. Pressure was held at 120 psig with a back pressure regulator. A water filter was installed in the water line to keep the water into the pump clean. Compressed air was supplied by oil free screw compressors with a common reservoir. The water and air flow rate was adjusted by the electro-pneumatic

valves and measured by the turbine flow meters. During the operation, the air was used to control the pump inlet pressure at 100 psig by adjusting an electro-pneumatic valve. The changing of GVF was accomplished by adjusting the water flow rate.

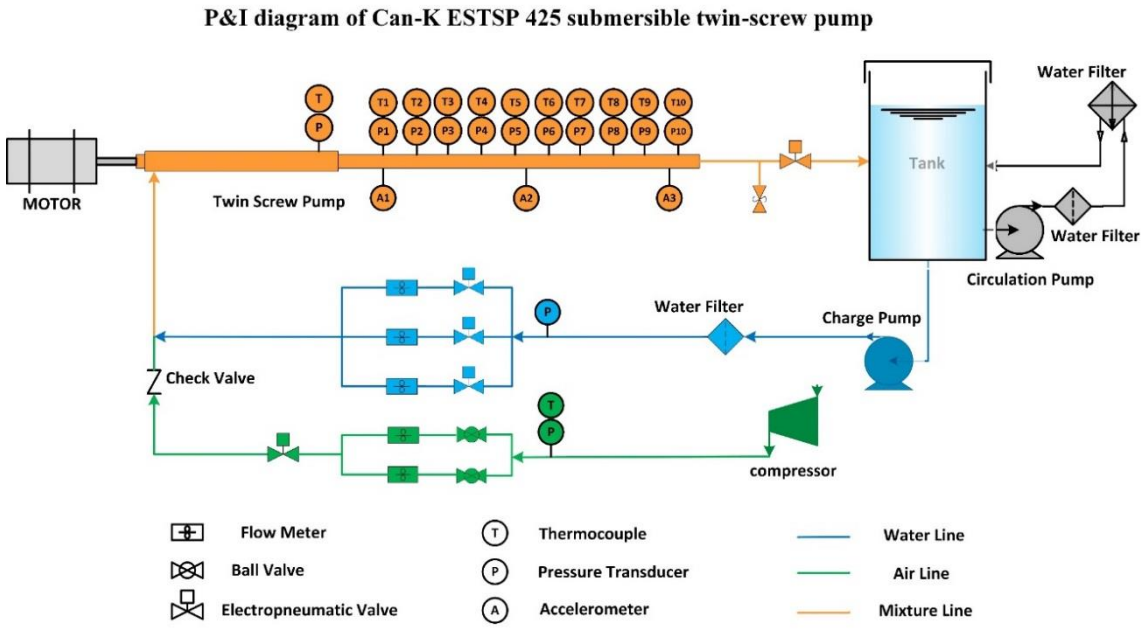

Figure 4.1 Flow loop diagram of water test

There are a series of water and air flow meters used to cover different flow ranges. Every flow meter has different working range. During the test, the proper flow meter was selected according to the water and air flow rate. Water and air were mixed in an intake manifold before the pump inlet. Pressure transducers and thermocouples were installed at the inlet and the exit of every stage. Three accelerometers were installed at the front, the middle and the rear of the pump to monitor the vibration level during operation.

At the discharge of the pump, a pressure relief valve was applied to ensure the safe operation of the pump. The control valve at the pump outlet was used to adjust the discharge pressure of the pump. The valve was controlled by 4-20 mA current.

Figure 4.2 Motor

The pump was driven by a 250 hp Hyundai motor as shown in Figure 4.2. The motor is controlled by VFD to change the speed stepless from 3000 rpm to 5000 rpm. An independent water circulation loop was set up to control the water temperature in the tank, since the water temperature will increase after a long period of running.

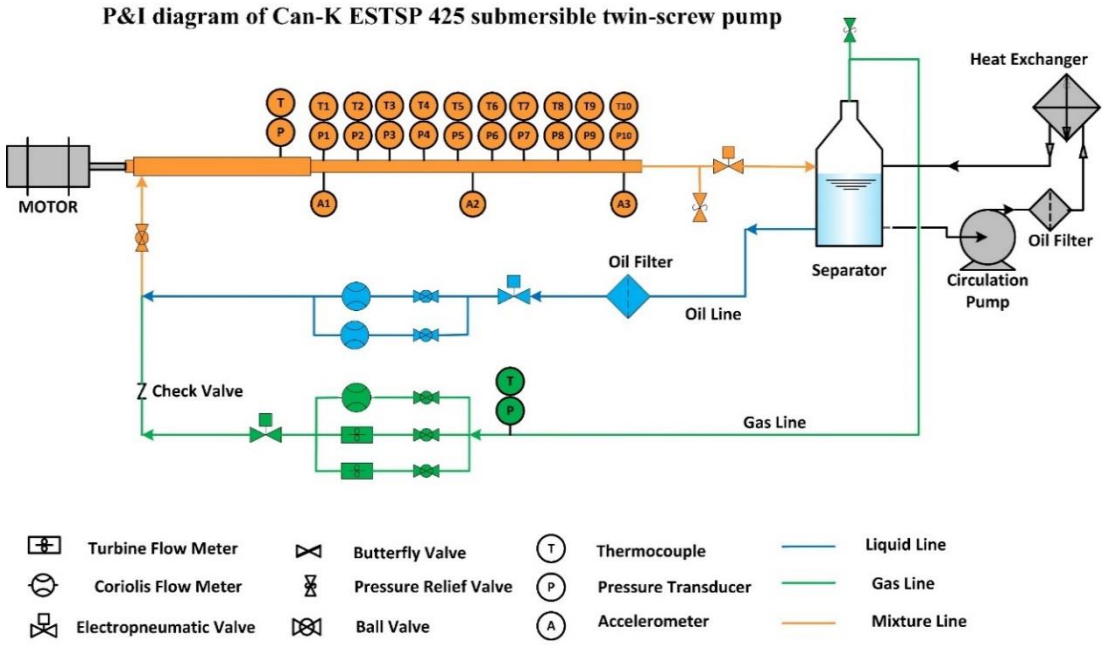

Figure 4.3 Flow loop diagram of oil test

Figure 4.3 shows the P&ID diagram of the test rig for the oil/water test. The oil/water test was performed with a closed loop. Both liquid and gas recirculated in the test loop. The Can-K pump was tested with pure oil, 50% water cut, 80% water cut and pure water in this facility. The liquid flow loop consists of two Coriolis flow meters which are connected in parallel, while the gas flow loop includes a Coriolis flow meter and two turbine flow meters. The flow meters work for different flow rate ranges, and proper flow meter combination were selected to use according to the flow rate. The liquid and the gas flow rates were controlled by the use of the electro-pneumatic valves operated by 4-20 mA current. A pressure transducer and a thermocouple were installed before the gas flow meters to monitor and record the gas pressure and temperature. A liquid filter was installed before the liquid flow meters to keep the liquid clean. An electro-

pneumatic valve was installed at the discharge side of the pump to control the outlet pressure as shown in Figure 4.4. The liquid and gas mixture discharged by the pump was sent to the separator where the oil, water and gas were separated. The valve control and data collection were accomplished by using a LabVIEW program. The separator is kept at 115 psig during the test.

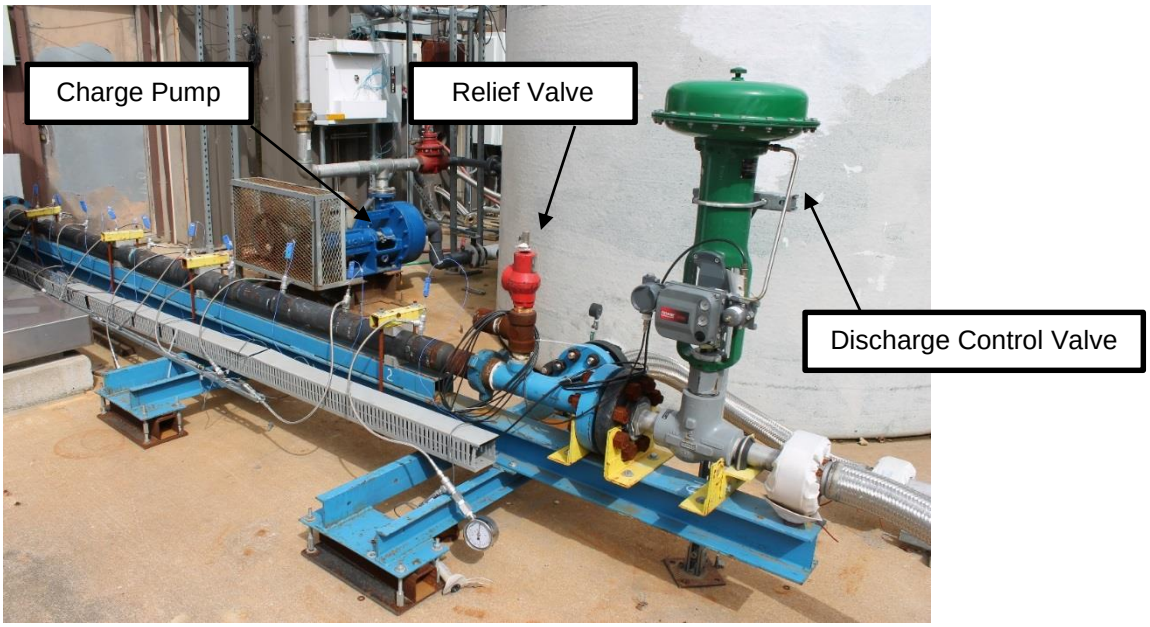

Figure 4.4 Can-K 425 ESTSP and discharge valve

An independent circulation loop was set up to maintain the oil/water temperature in the separator. It is found that the oil temperature increased rapidly in the experiment, since the heat capacity of oil/water is less than water and the capacity of the separator is much

smaller than the water tank. The oil/water temperature is controlled by the heat exchanger. Figure 4.5 shows the water tank, the heat exchangers and the separator.

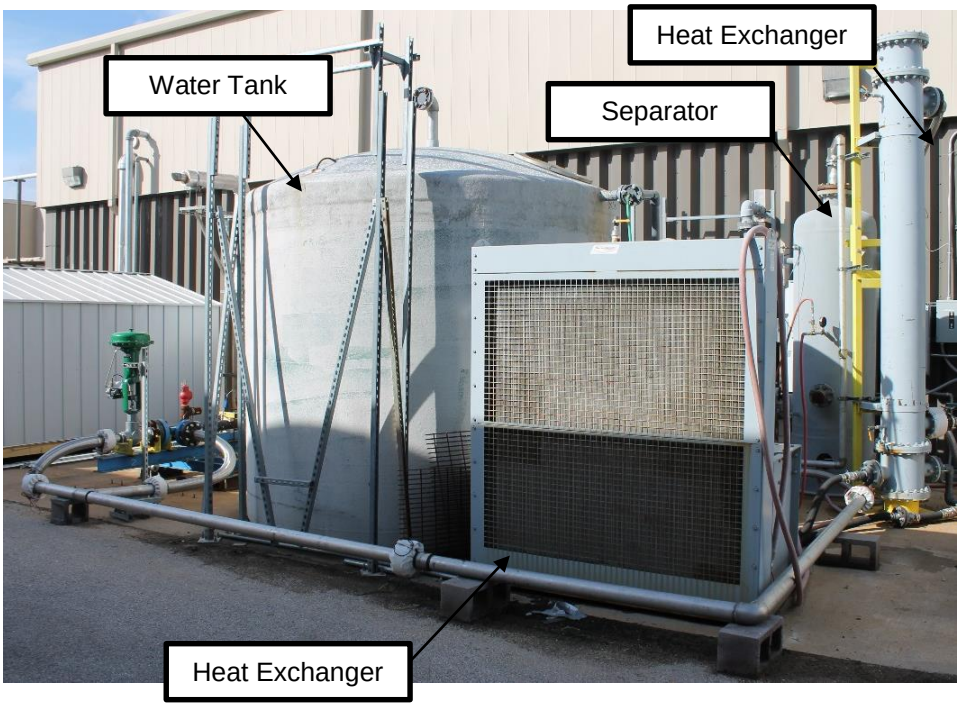

Figure 4.5 Water tank, heat exchanger and separator

The Can-K pump is 29 feet long, with the diameter 4.25 inches. The Can-K pump was coupled with the motor by a Lovejoy coupling. The pump-motor assembly is installed on the test bench as shown in Figure 4.6. The front part of the pump is timing gears, thrust module and centralizer. The pumping elements are located at the rear. There are 10 stages of pump modules in total.

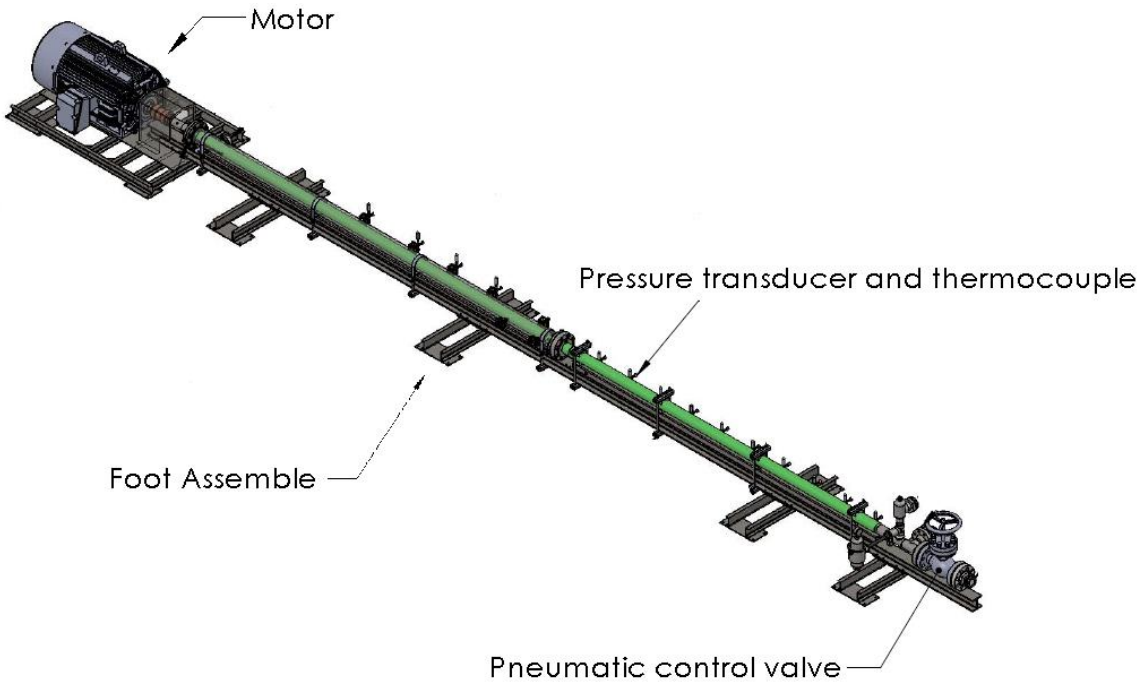

Figure 4.6 Pump and motor assembly (Klayton, 2013)

4.1.2 Instrumentations

Solid state pressure transducer of Omega PX-429 series were used to measure the pressure. Detailed information of the pressure transducers are shown in Table 4.1. The pressure transducer was connected with a resistance and a 20V power supply. The resistance of the pressure transducer varied with the measured pressure. The pressure can be calculated by measuring the voltage on the pressure transducer.

T-type thermocouples from Omega were used to measure the temperature. They were integrated into data acquisition system with NI 9213. The accuracy of the thermocouple

is 0.75%. The temperature at the exit of every stage and the temperature at the inlet of the gas flow meters were recorded.

Table 4.1 Pressure transducers used in experimental testing

Location	Principle	Manufacturer	Accuracy	Range
Air Inlet	Solid State	Omega	0.08%BFSL maximum	0-150 PSI
Pump Inlet				0-150 PSI
1st stage				0-250 PSI
2nd stage				0-500 PSI
3rd stage				0-1000 PSI
4th stage				0-1000 PSI
5th stage				0-1000 PSI
6th stage				0-1500 PSI
7th stage				0-1500 PSI
8th stage				0-2500 PSI
9th stage				0-2500 PSI
10th stage				0-2500 PSI

For the water-air test, three turbine flow meters were used to measure the water flow rate. Two turbine flow meters and a Coriolis flow meter were used to measure the air flow rate. Table 4.2 details the flow meters used to measure water and air flow rate. For the oil/water test, two Coriolis flow meters were used to measure the liquid flow rate and the water cut. Two turbine flow meters and a Coriolis flow meter were used to measure the gas flow rate. Table 4.3 details the flow meters used to measure the liquid and gas

flow rate in the oil test. Table 4.4, Table 4.5 and Table 4.6 present the accuracy of the Coriolis flow meter used in the measurement of gas and liquid. The Coriolis flow meter is more accurate and can be used to measure the flow rate and density of any liquid, while the liquid turbine flow meters are designed to be used with only water.

Table 4.2 Flow meters for water test

Type	Manufacturer	Accuracy	Repeatability	Range
Air flow meters	Micro Motion CMFS015M	0.25%	0.2%	0-2 ACFM
	Omega FTB-935	1%	0.25%	1-10 ACFM
	Omega FTB-938	1%	0.25%	8-250 ACFM
Water flow meters	Daniel Industries	0.25%	0.02%	25-250 gpm
	Omega FTB-1425	1%	0.1%	5-50 gpm
	Omega FTB-1422	1%	0.1%	0.75-7.5 gpm

Table 4.3 Flow meters for oil/water test

Type	Manufacturer	Accuracy	Repeatability	Range
Gas flow meters	Micro Motion CMFS015M	0.25%	0.2%	0-1.5 ACFM
	Omega FTB-935	1%	0.25%	1-10 ACFM
	Omega FTB-938	1%	0.25%	10-100 ACFM
Liquid flow meters	Micro Motion CMF200M	0.1%	0.05%	18-200 gpm
	Micro Motion CMFS075M	0.1%	0.05%	5-20 gpm

Table 4.4 Micro Motion CMFS015M accuracy and repeatability (Gas)

Performance Specification	Accuracy	Repeatability
Mass flow rate	0.25%	0.2%
Temperature	1%	0.25%

Table 4.5 Micro Motion CMFS075M accuracy and repeatability (Liquid)

Performance Specification	Accuracy	Repeatability
Mass/volume flow rate	0.1%	0.05%
Density	0.5 kg/m^3	0.2 kg/m^3
Temperature	0.5%	0.2 °C

Table 4.6 Micro Motion CMF200M accuracy and repeatability (Liquid)

Performance Specification	Accuracy	Repeatability
Mass/volume flow rate	0.1%	0.05%
Density	0.5 kg/m^3	0.2 kg/m^3
Temperature	0.5%	0.2 °C

A TOSHIBA P9 adjustable speed drive (ASD) was used to control the motor's speed. The output power and output current of the ASD were automatically recorded by the data acquisition system. The adjustment of motor's speed during the test was accomplished by the P9 ASD Electronic Operator Interface. A Hyundai motor was installed to drive the pump, which can be operated continuously from 3000 RPM to 5000 RPM providing a maximum 250 HP power.

4.1.3 Data Acquisition System

A NI-based data acquisition and control system was developed to operate the pump and record the experimental data. A variety of sensors, flow meters and control valves were all integrated into this system with NI data acquisition modules. Data acquisition and PID control of the pump could be achieved by the Graphical User Interface of LabVIEW as shown in Figure 4.7 and Figure 4.8.

Figure 4.7 LabVIEW front panel

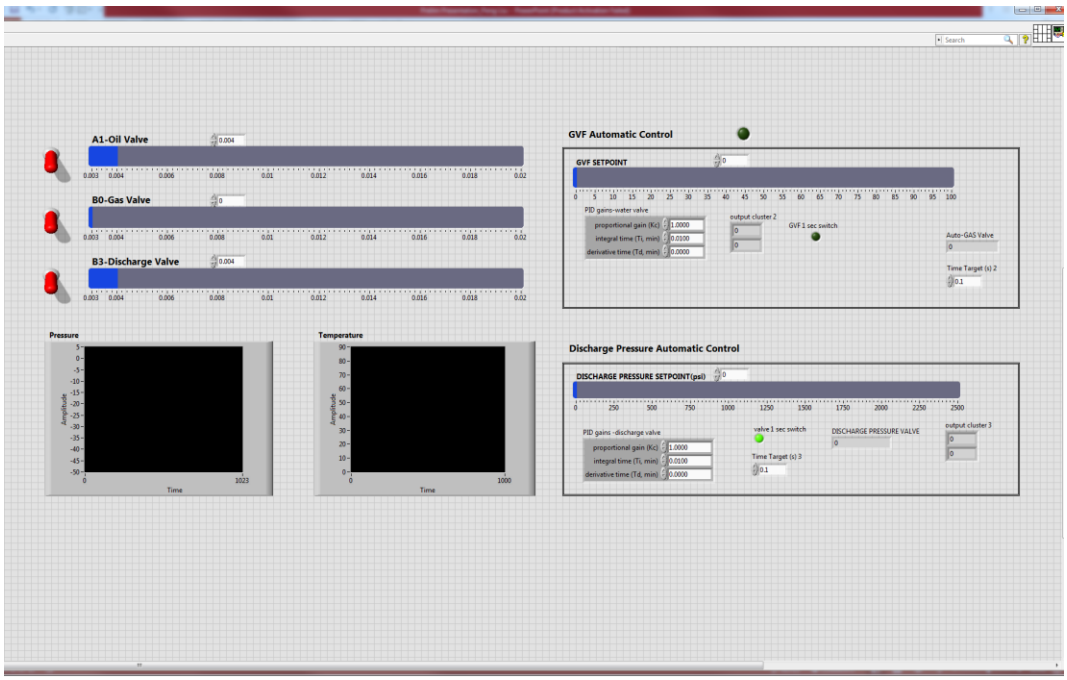

Figure 4.8 LabVIEW front panel (continue)

NI Module 9205 was used to collect data of pressure transducers, Coriolis flow meters, and VFD. NI Module 9213 was used to collect data of thermocouples. Module 9265 was used to control electro-pneumatic valves with 4-20 mA current. NI Module 9205 and 9213 were integrated with NI 9074 chassis which transmitted the signals to the computer program. The output data of the turbine flow meters are transmitted by three iServer Microservers from OMEGA. The specifications of the NI Modules and iServer are shown in Table 4.7.

Table 4.7 Specifications of the NI Modules and iServer Microserver

Instrument	Accuracy	Range
NI 9205	±1.00%	±10 V
NI 9213	±0.30%	±10 V
NI 9265	±2.50%	0-20 mA
iServer Microservers	±0.30%	1Hz-100KHz

4.2 Test Matrix

Before starting to record data, the pump was operated at no choke at 3000 RPM for 20 minutes and at 3550 RPM for 130 min. Then, the pump was tested with various GVF at different speeds and discharge pressures. At each test point, the pump was run for 5 minutes to be stable, and then the average of all the data in a time interval of 8 seconds was recorded. Table 4.8 shows the water test matrix for the Can-K ESTSP 425 submersible twin screw pump. For 3000 RPM, only 0% GVF and 10% GVF were tested. For 3550 RPM and 4000 RPM, the pump was tested from 0% GVF to 65% GVF.

Table 4.8 Test matrix of water test

Speed(rpm)	dP(psig)	GVF (%)
3000	200	0
3550	400	10
4000	600	20
	800	30
	1000	40
		50
		60
		65

The Can-K pump was tested with pure oil for all the low GVF points first, then switched to the test with 20% oil and 50% oil for low GVF test. After the low GVF test, the pump was operated at high GVF with 50% oil, 20% oil and pure oil separately. At last, the pump was tested with pure water for low and high GVF to compare with the test results of last year. At every test point, the pump was fixed and then the averages of all the data in a time interval of 8 seconds were recorded. Table 4.9 and Table 4.10 show the oil-water test matrix for the ESTSP.

It was found that for the 100% oil test the liquid density read from the Coriolis flow meter during the test was lower than the real density, which means the liquid flow through the flow meter contained some gas bubbles. This is because the separator can't totally separate the oil and gas. As a consequence, the pump was not able to be tested with 0% GVF. A LabVIEW program was imbedded in to the main program to calculate

the correct GVF in the pump inlet considering the effect of the gas bubbles in the liquid flow.

Table 4.9 Test matrix of oil test, low GVF

Oil	Speed(rpm)	dP(psig)	GVF (%)
100	3000	100	10
50	3550	200	20
20	4000	400	30
		600	40
		800	50
		1000	60
			70

Table 4.10 Test matrix of oil test, high GVF

Oil	Speed(rpm)	dP(psig)	GVF (%)
100	3550	100	75
50	4000	200	80
20		400	85

For 3000 RPM, only 10% GVF was tested. For 3550 RPM and 4000 RPM, the pump was tested from 10% GVF to 70% GVF.

In this chapter, the test rig and the instruments are detailed. Test method and the experiment content are also presented. In the next chapter, the test results will be

presented. The pump performance will be analyzed and compared with that of the double-end pump.

5 PERFORMANCE EVALUATION OF EXPERIMENTAL RESULTS

This chapter will discuss the experimental results. First, the multiphase performance of the Can-K pump will be presented and discussed. Experimental results of water test, oil test and water/oil test are analyzed. Then, the performance of the Can-K pump will be compared with that of the single-stage twin screw pump. In this study, the test data of a Colfax pump is selected to make the comparison.

The Can-K pump was tested with 100% water cut twice, the first time was tested with the open loop in Aug. 2014 and the second time was tested with the closed loop in Apr. 2015. The water test data of the Apr. 2015 is selected to evaluate the pump performance in the discussion. The two sets of 100% water cut test data are compared in this chapter as well.

5.1 Power Consumption

Power consumption is defined as the power required by the motor to maintain the pump speed. The power transferred to motor was recorded by the LabVIEW program for each test point.

Figure 5.1 shows the variation of power consumption of the 100% water cut test with different differential pressures at 10% GVF. Power consumption increases nearly linearly as the differential pressure increases. Power consumption generally can be divided into two components, one component is to pressurize the working fluid and another component is to overcome the viscous and friction losses in the pump. The

increase of pump speed leads to the increase of flow rate which require increased power input, and the viscous and friction losses are increased at higher speed as well. Thus, the power consumption increases with an increase of the pump speed.

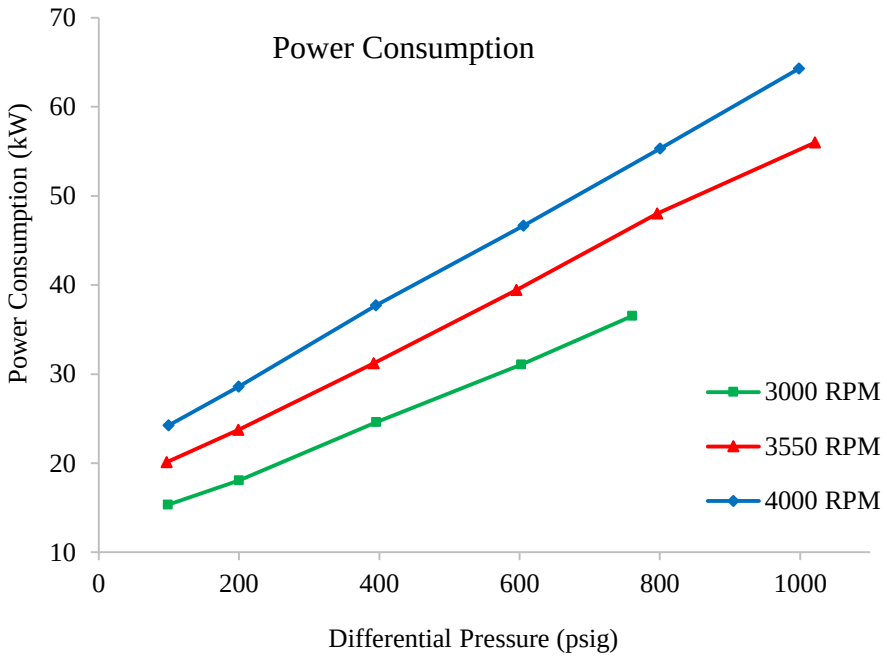

Figure 5.1 Effect of different speeds on power consumption at 10% GVF, 100% water test

Figure 5.2 represents the effect of GVF on the power consumption for 100% water cut test at 4000 RPM. Power consumption generally decreases with an increase in the GVF. This phenomena is due to the decrease of the liquid flow rate. The decrease of liquid flow rate leads to significant decrease of the component to pressurize the liquid. While the increase of the component to pressurize the gas is much less, which leads to the

decrease of the total power to pressurize the fluids. Also with the GVF increasing, there is more gas in the clearances, which will decrease the viscous friction losses. As a result, both these two reasons lead to the decrease of the power consumption with an increase of the GVF.

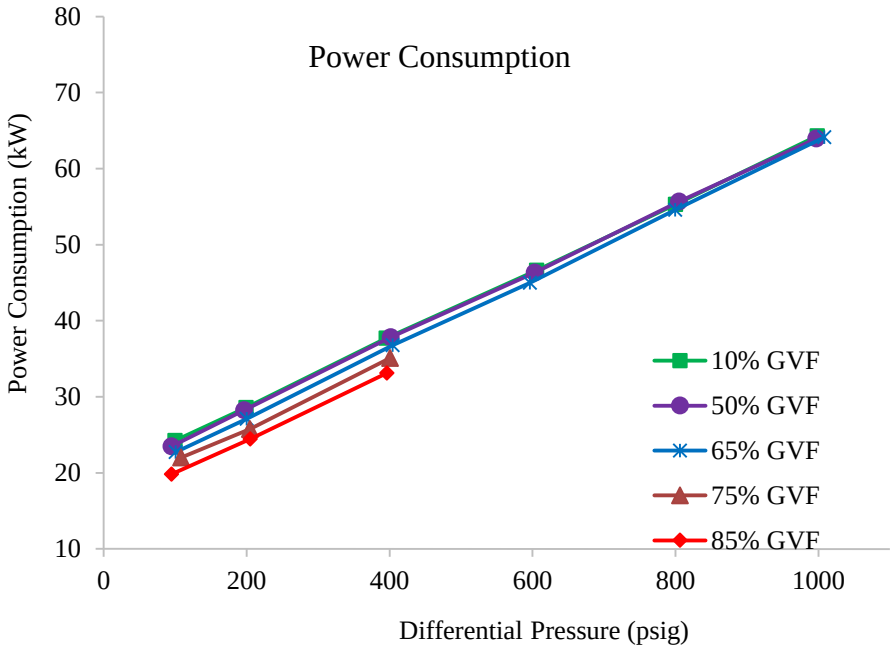

Figure 5.2 Effect of GVF on power consumption at 4000 RPM, 100% water cut test

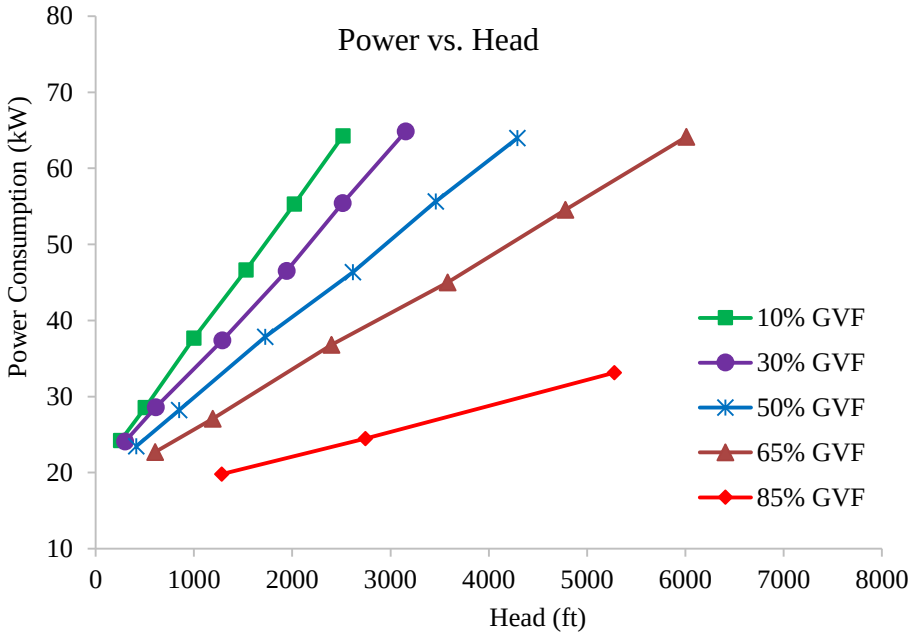

Figure 5.3 Effect of GVF on power consumption at 4000 RPM, 100% water cut test

As shown in Figure 5.3, the larger pump head leads to larger power consumption. With the same power consumption, the pump head increases with an increase of the GVF. This is because the density of the working fluid decreases with an increase of the GVF. Thus, the same power consumption can produce a larger pump head.

Water cut has an essential influence on the power consumption as well. As shown in Figure 5.4, the power consumption decreases with the increase of water cut. The viscosity of the working fluid decrease with the increase of water cut. The friction losses generally increase with the viscosity. However, in this study, the oil viscosity is about 2 ct, which is very close with that of water. Thus, the effect of viscosity isn't the

dominant factor. In this research, the 100% water test shows the largest total flow rate capacity. According to equation 3.4, the higher flow rate requires more power to pressurize the fluid. The increase of power imparted into the fluid counteracts the decrease of power to overcome the friction losses. As a consequence, the power consumption increase with water cut.

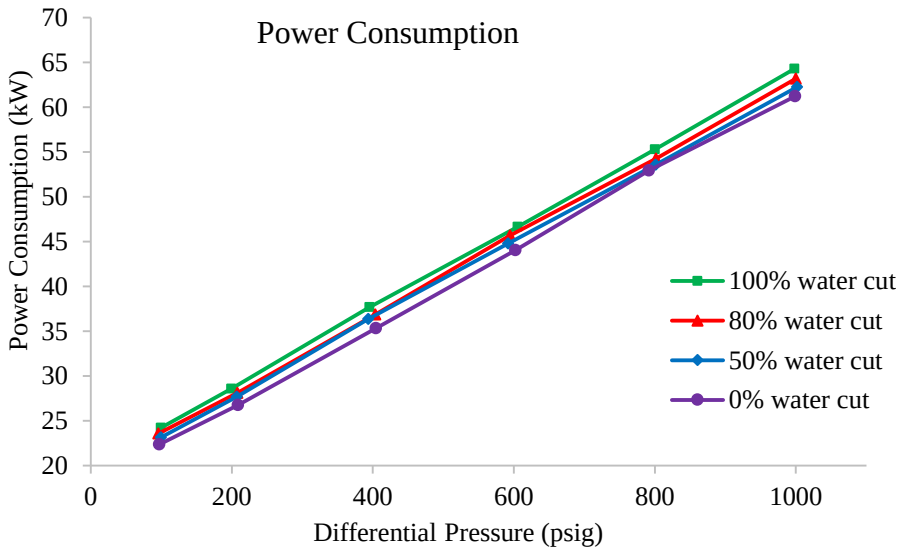

Figure 5.4 Effect of water cut on power consumption at 4000 RPM, 10% GVF

5.2 Pressure and Temperature Distribution

In this research, pressure and temperature at the end of each stage are measured for each test point. Pressure and temperature recorded is the mean value within a time period of 8 seconds, since the pressure and the temperature kept changing during the experiment.

The pressure and temperature distributions help to understand the compression process of the working fluid in the pump.

Figure 5.5 shows the pressure distribution stage by stage along the pump at 4000 RPM for 100% water cut test. The pressure transducers are located at the inlet and the outlet of every stage. Using the pressure distribution it is convenient to find the pressure rise cross a certain stage. The pressure distribution is affected by the GVF of the working fluid. As shown in Figure 5.6, at the low GVFs, the shape of the pressure distribution is concave-down. However, with an increase of the GVF, the shape of the pressure distribution changes to concave-up. The pressure changes the largest at the last stage.

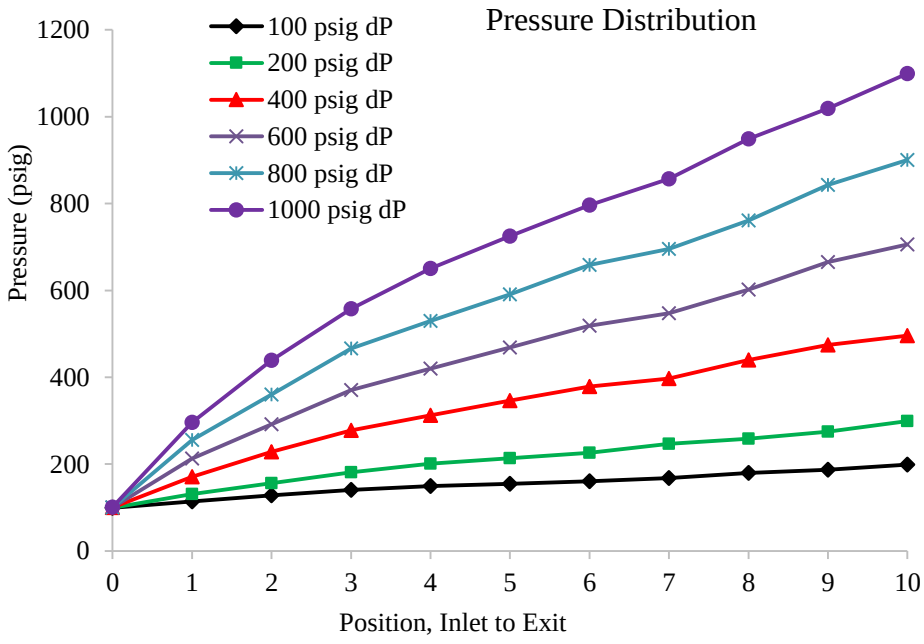

Figure 5.5 Pressure distributions at 4000 RPM, 100% water cut, 10% GVF

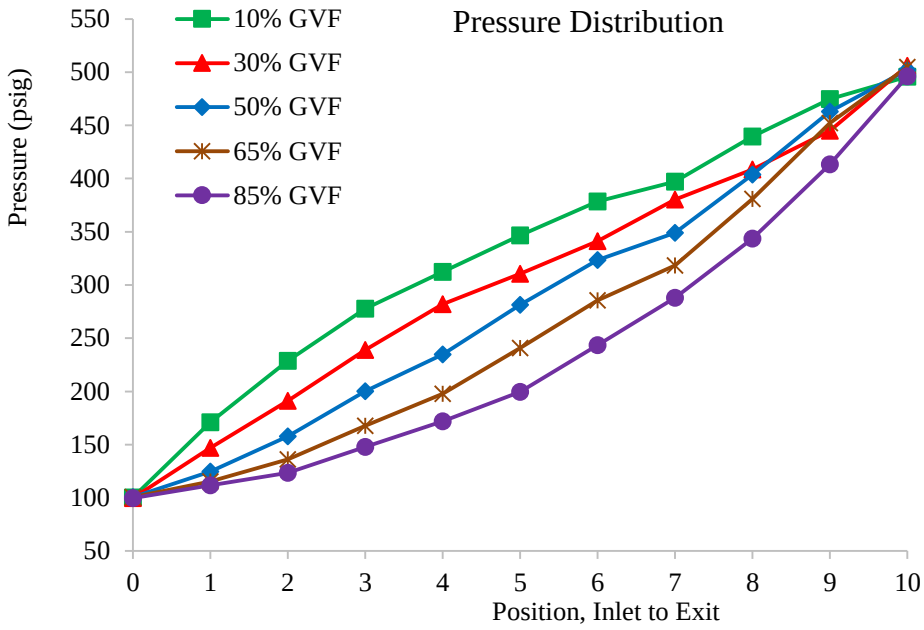

Figure 5.6 Effect of GVF on pressure distribution at 4000 RPM, 100% water cut, 400 psig differential pressure

The temperature distribution along the pump is shown in Figure 5.7. Due to the viscous friction and the compression processes in the pump, the temperature rises from the suction side to the discharge side. Since the heat capacity of the liquid is much larger than that of the gas, the temperature rise is very small at the low GVFs. In this condition, the compression process is close to isothermal process. However, with the increase of GVF, there is insufficient liquid in the pump to absorb the heat produced by internal frictions and compression process. As a result, the temperature rise increases with the increase of GVF. In consequence, the compression process can be considered as polytropic process at the extremely high GVF conditions. The variation of temperature

rise with different water cut is shown in Figure 5.8. Compared with water, the oil has the lower heat capacity. As a result, the temperature rise is larger for the oil test. At 1000 psig differential pressure and 10% GVF, the temperature rise for pure oil test is about 8 °F higher than that of pure water test.

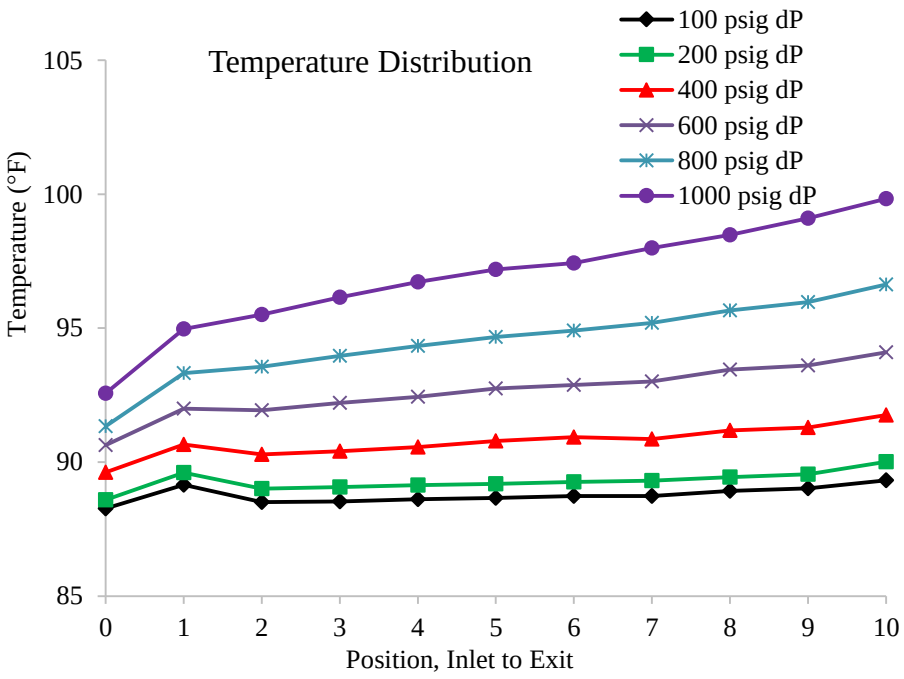

Figure 5.7 Temperature distributions at 4000 RPM, 100% water cut, 10% GVF

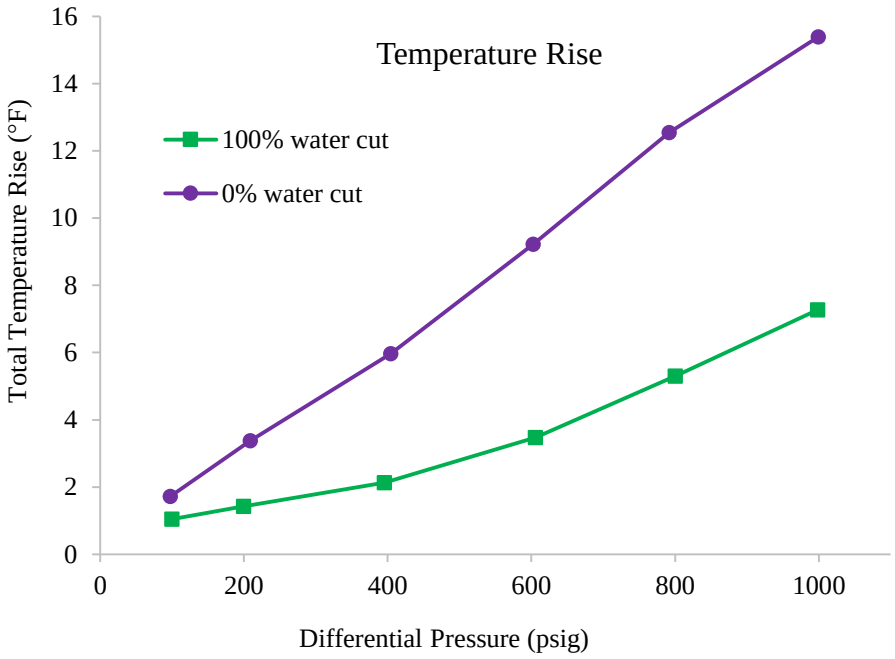

Figure 5.8 Effect of water cut on total temperature rise at 4000 RPM, 10% GVF

The polytropic coefficient is an essential parameter to indicate the compression process in the twin screw pump. In the compression process, the polytropic coefficient varies from 1 to $\frac{c_p}{c_v}$, indicating the compression process varied from isothermal to adiabatic. As shown in Figure 5.8, the polytropic coefficient in this research is around 1.0 even for 85% GVF. As a result, the compression process in this research is very close to isothermal process.

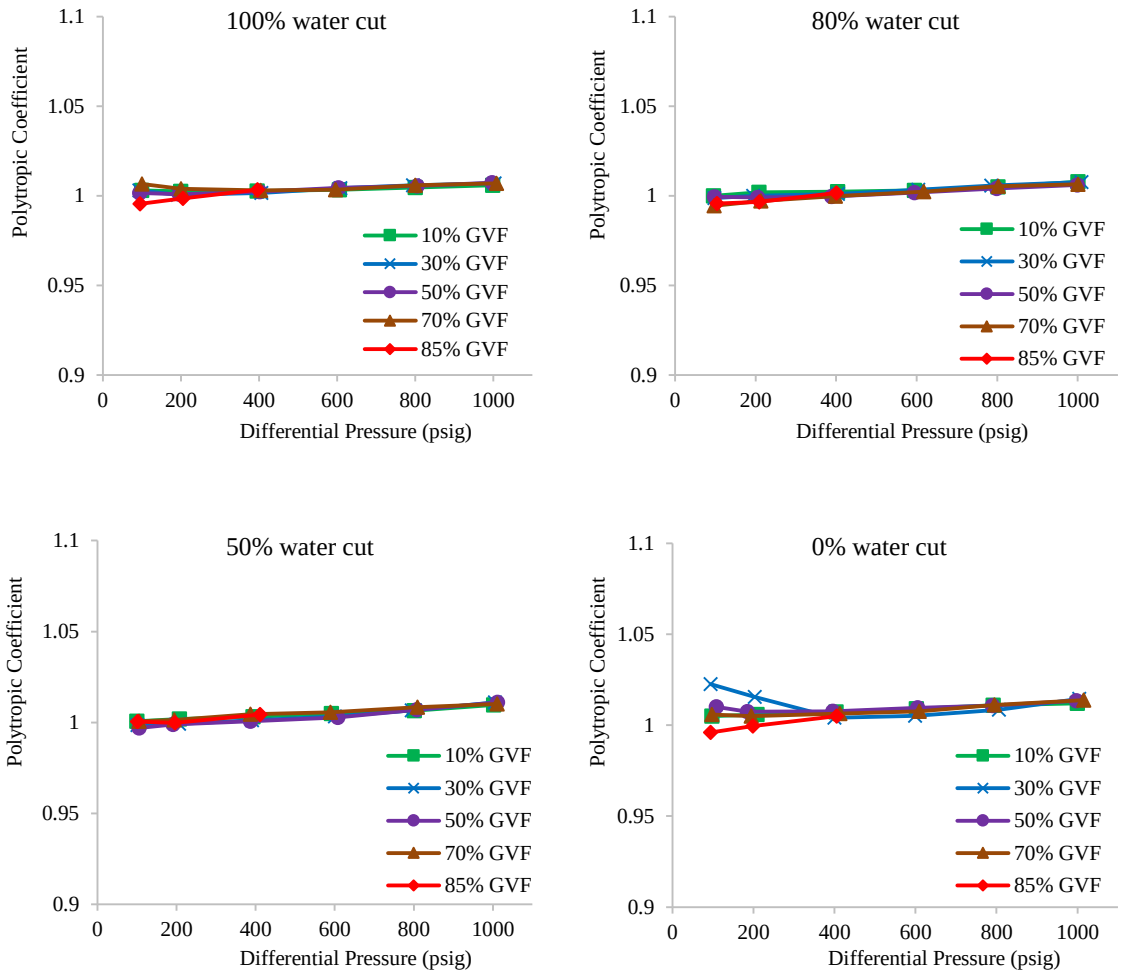

Figure 5.9 Polytropic coefficient of different water cuts, 4000 RPM

Figure 5.10 shows the effect of water cut on the polytropic coefficient. Polytropic coefficient of 0% water cut test is higher than that of 100% water cut test. This is because the temperature rise of 0% water cut test is higher due to the lower heat capacity of the oil. Compared with the 0% water cut test, thus the 100% water cut test is more close to the isothermal process.

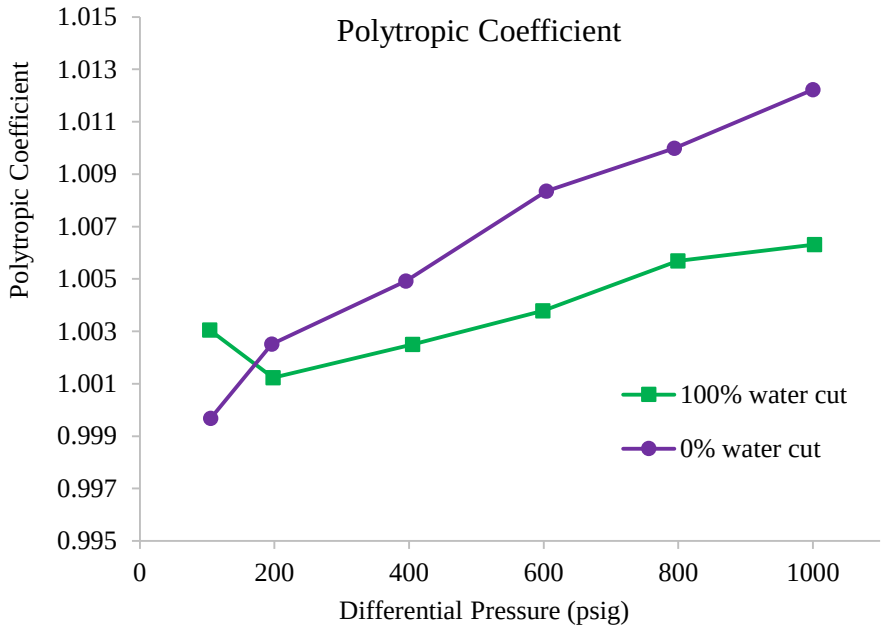

Figure 5.10 Effect of water cut on polytropic coefficient at 4000 RPM, 20% GVF

5.3 Volumetric Flow Rate Capacity

Volumetric flow rate capacity refers to the total flow rate flowing into the pump inlet. As mentioned in the previous section, theoretical flow rate capacity of the twin screw pump is only a function of geometrical parameters and pump speed. However, the actual volumetric flow rate capacity is affected by various factors, such as differential pressure, GVF, viscosity, et al. In this section, the characteristics of total flow rate capacity of the Can-K pump will be investigated.

Figure 5.11 shows the volumetric flow rate capacity at 3550 RPM and 4000 RPM with different GVF. At 4000 RPM, the theoretical volumetric flow rate is 113.5 gpm. But the

actual flow rate capacity is less than the theoretical flow rate due to the internal leakages. The actual flow rate capacity varies with differential pressure and GVF. As shown in Figure 5.11, the volumetric flow rate decreases with the increase of differential pressure. With the increase of differential pressure, there is more leakage flow from discharge side back to suction side. Thus, the total flow rate entering pump inlet is decreased. It is also found that the volumetric flow rate increases with an increase of the GVF at the same differential pressure. As shown in Figure 5.12 and Figure 5.13, the volumetric flow rate capacity becomes the largest at 85% GVF with the same differential pressure. The effect of GVF on the volumetric flow rate has been researched previously. Both Patil [23] and Kroupa [21] found that the volumetric flow rate capacity increases with GVF first then decreases. Patil found that the maximum volumetric flow rate capacity occurs when the pump operated at around 90% GVF. In this research, the pump was tested with the GVF up to 85%. The total flow rate capacity keeps rising with the increase GVF. With more gas injected into the clearance, the two phase flow performs the seal function. Since the sonic velocity of the two phase flow decreases as the GVF increases, and then increases as the GVF increases. Thus, the sonic velocity of the two phase flow is lower than that of pure liquid or pure gas. As a result, the two phase flow is more inclined to be choked in the clearance, which means the two phase flow is able to provide a better seal function.

Water cut shows an essential effect on the total flow rate. As shown in Figure 5.14, the 100% water test presents the largest total flow rate capacity. With the decrease of water cut, there is a slight drop of total flow rate capacity, especially at high differential pressures. Chan [6] investigated the effect of viscosity. For the pure-liquid test, it is

found that increase in viscosity leads to the decrease of leakage flow. While for the high GVF operation, viscosity isn't a dominant role to determine the total flow rate. Patil [23] also found that total flow rate capacity decreases with the increase of viscosity at the high GVFs, especially when the viscosity increases from 1 cp to 10 cp. Patil [23] concluded that there is insufficient liquid to seal the gas in the clearance at the high GVF conditions due to the decreased fluidity. In this research, it is found that flow rate capacity decreases with the increase of viscosity for all GVFs. As shown in Figure 5.14, the flow rate capacity of the water test is always higher than that of oil test.

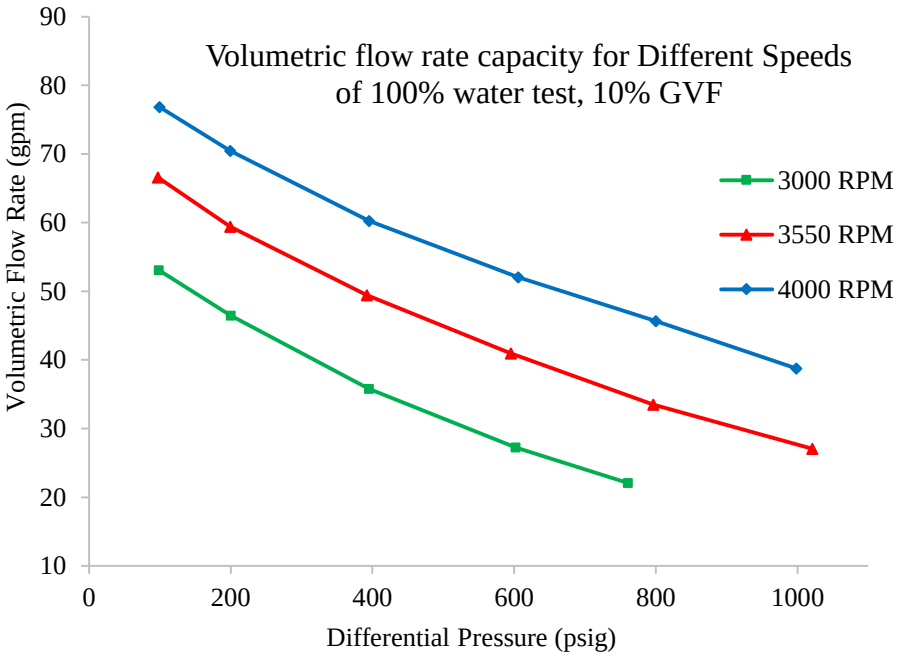

Figure 5.11 Effect of pump speed on volumetric flow rate capacity at 10% GVF, 100% water cut test

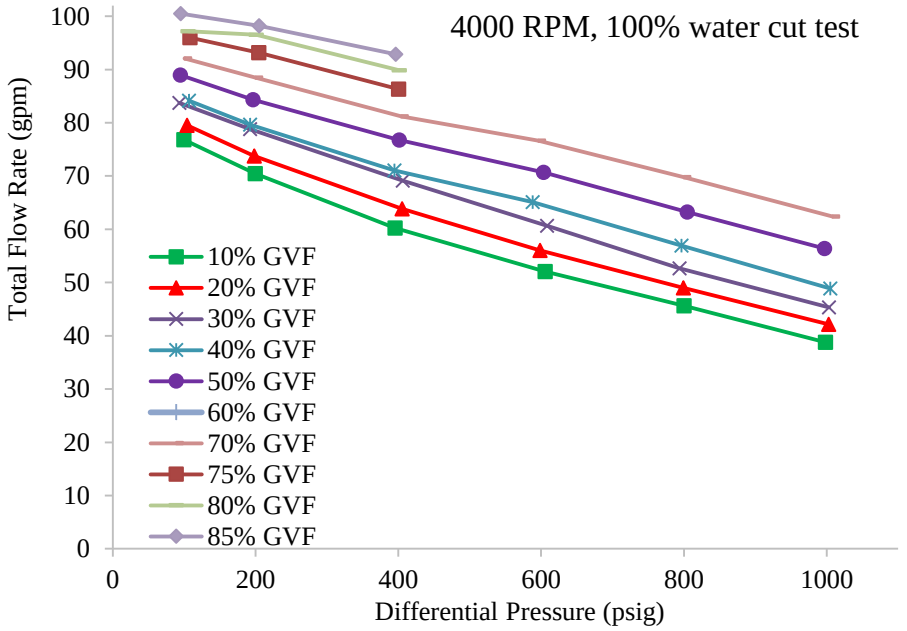

Figure 5.12 Volumetric flow rate capacity at 4000 RPM, 100% water test

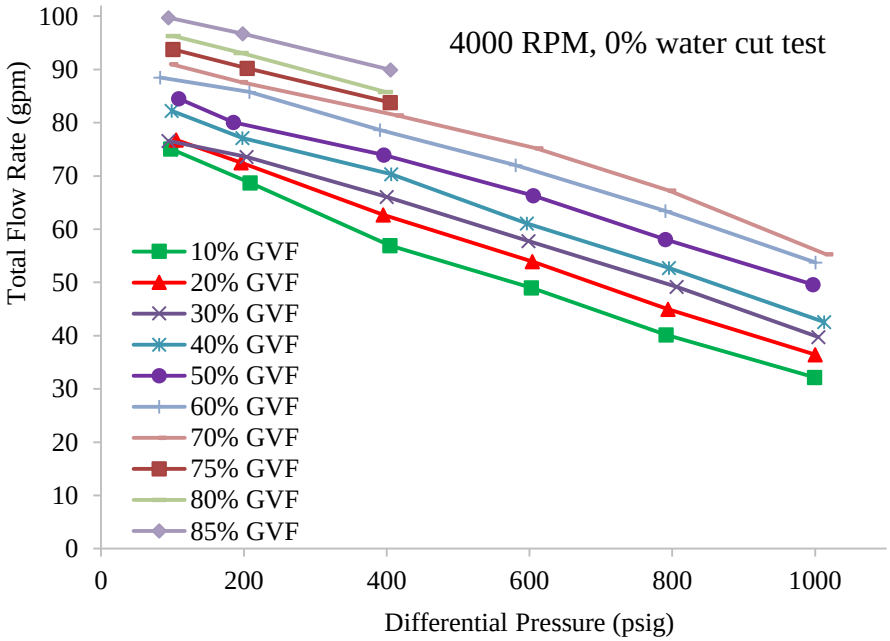

Figure 5.13 Volumetric flow rate capacity at 4000 RPM, pure oil test

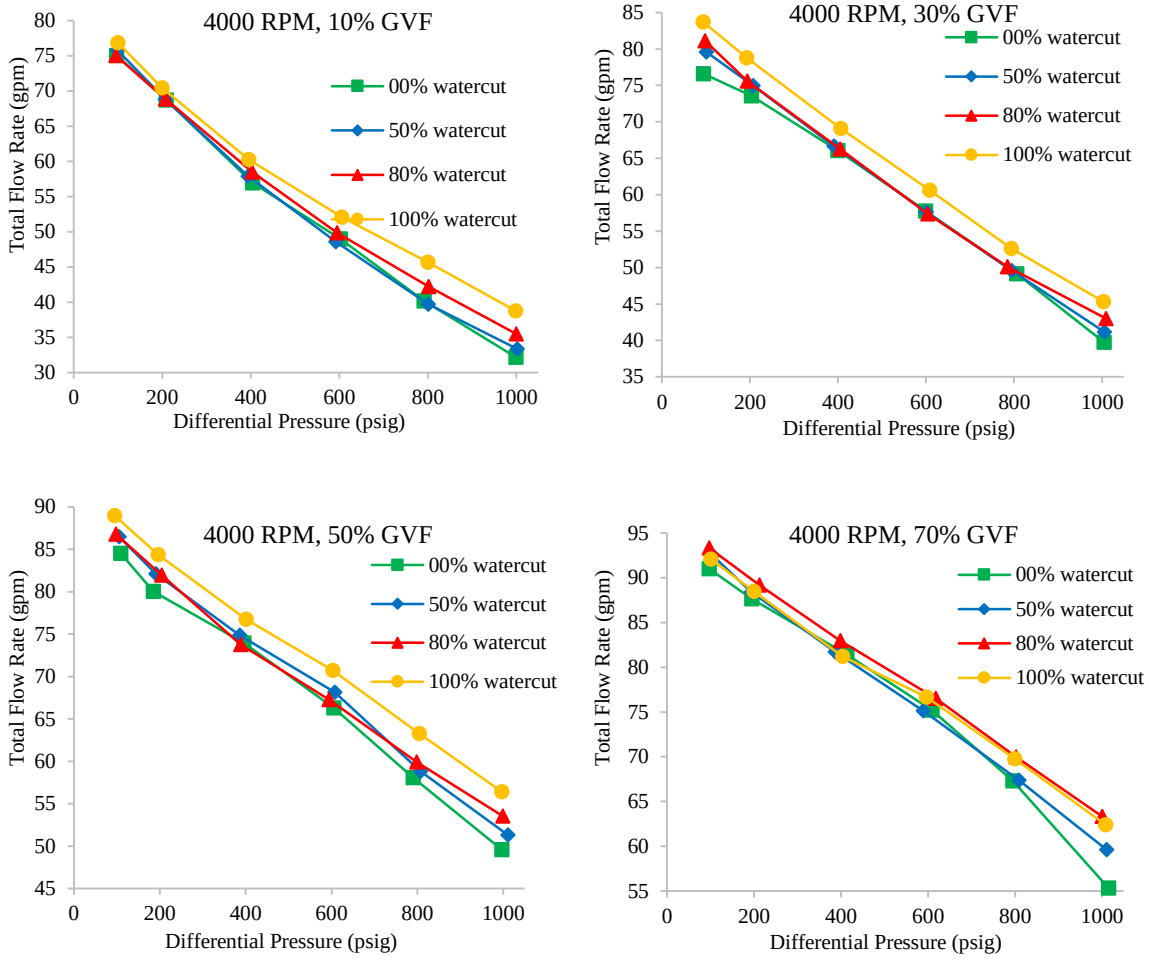

Figure 5.14 Effect of water cut on volumetric flow rate capacity

5.4 Volumetric Efficiency

Volumetric efficiency indicates the ratio of actual flow rate capacity to theoretical flow rate capacity. Figure 5.15 shows the variation of volumetric efficiency with different GVF at 4000 RPM for 100% water cut test. Figure 5.16 shows the variation of volumetric efficiency with different GVF at 4000 RPM for 100% oil test. Since the

theoretical flow rate capacity is constant at 4000 RPM, the curve of volumetric efficiency shows the same trend with that of volumetric flow rate capacity. Volumetric efficiency decreases with the increase of differential pressure due to the leakage flow. Volumetric efficiency becomes the maximum with 100 psig differential pressure. Volumetric efficiency increases with the increase of GVF. At 85% GVF volumetric efficiency shows the maximum with the same differential pressure. As shown in Figure 5.15, the volumetric efficiency at 85% GVF and 100 psig differential pressure is about 88%. While the volumetric efficiency at 10% GVF and 1000 psig differential pressure is only about 34%.

Figure 5.17 shows the effect of pump speed on the volumetric efficiency. As the pump speed increases, the volumetric efficiency increases. It has been found that the leakage flow rate doesn't change significantly with pump speed, while theoretical flow rate increases linearly with the pump speed. As a result, volumetric efficiency increases with an increase in pump speed. It is also found that with the increase of differential pressure, the effect of pump speed becomes more important. At 100 psig different pressure, there is no significant difference of volumetric efficiency. While at 800 psig differential pressure, the volumetric efficiency of 4000 RPM is about 40.2% and that of 3000 RPM is only about 25.9%. This is because the leakage flow rate increases with an increase in the differential pressure. Since the theoretical flow rate at 3000 RPM is the least. The volumetric efficiency at 3000 RPM decreases faster though the leakage flow doesn't have a significant difference between different speeds.

Figure 5.18 shows the effect of water cut on volumetric efficiency, which presents the same trend with the curve of volumetric flow rate capacity. At the low differential pressure, water cut has no evident effect on volumetric efficiency. With the increase of differential pressure, 100% water cut test shows the highest volumetric efficiency.

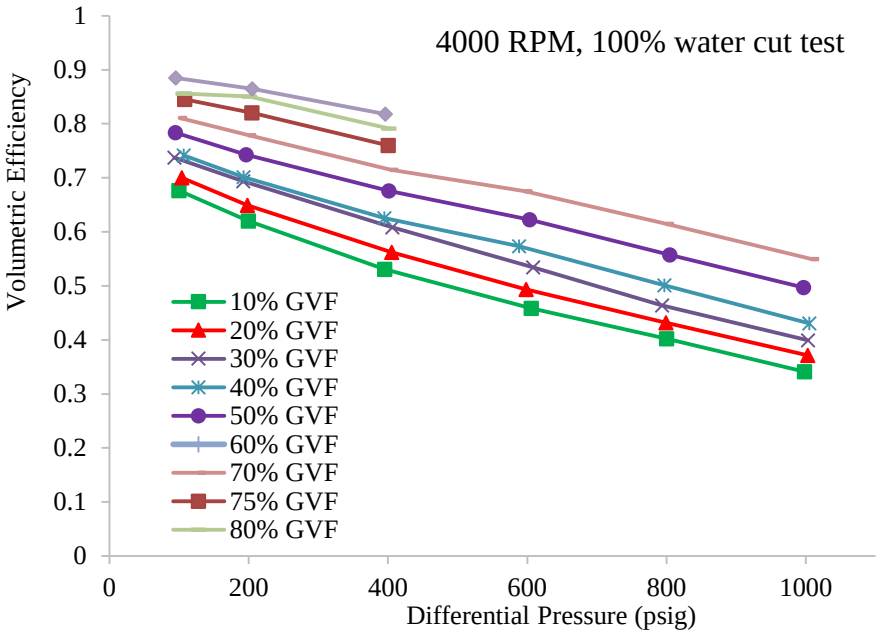

Figure 5.15 Volumetric efficiency at 4000 RPM, 100% water cut test

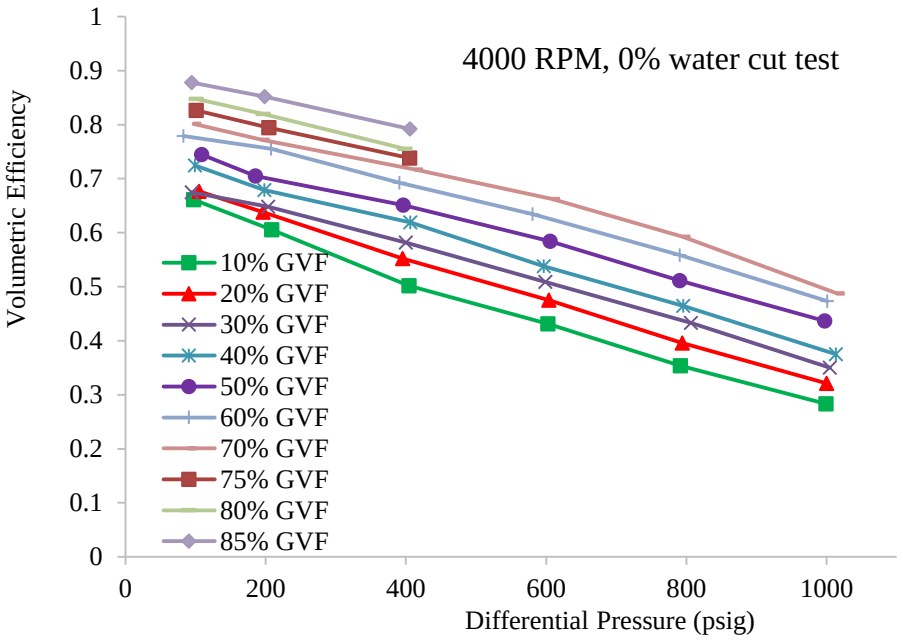

Figure 5.16 Volumetric efficiency at 4000 RPM, 0% water cut test

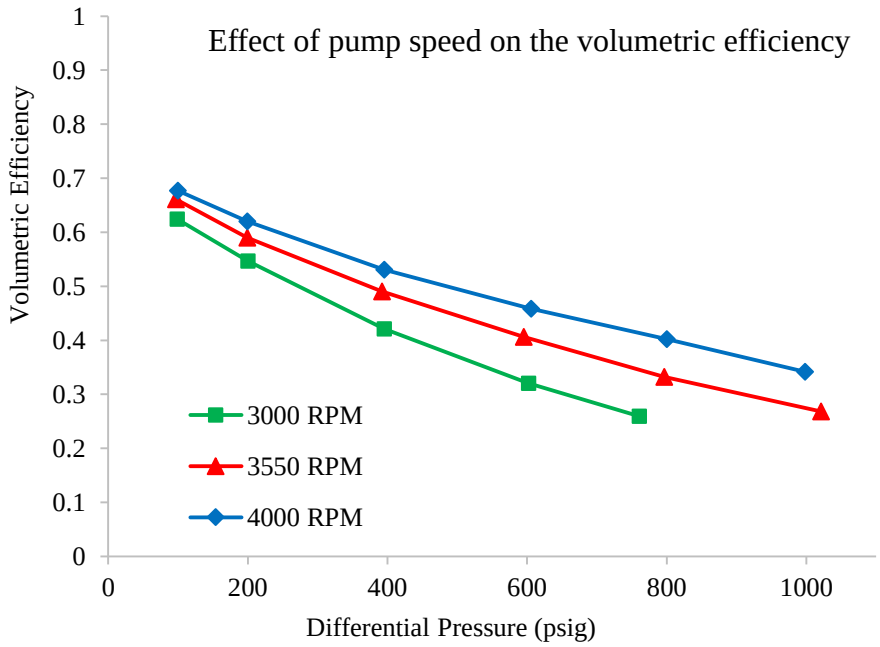

Figure 5.17 Effect of speed on volumetric efficiency at 10% GVF, 100% Water Test

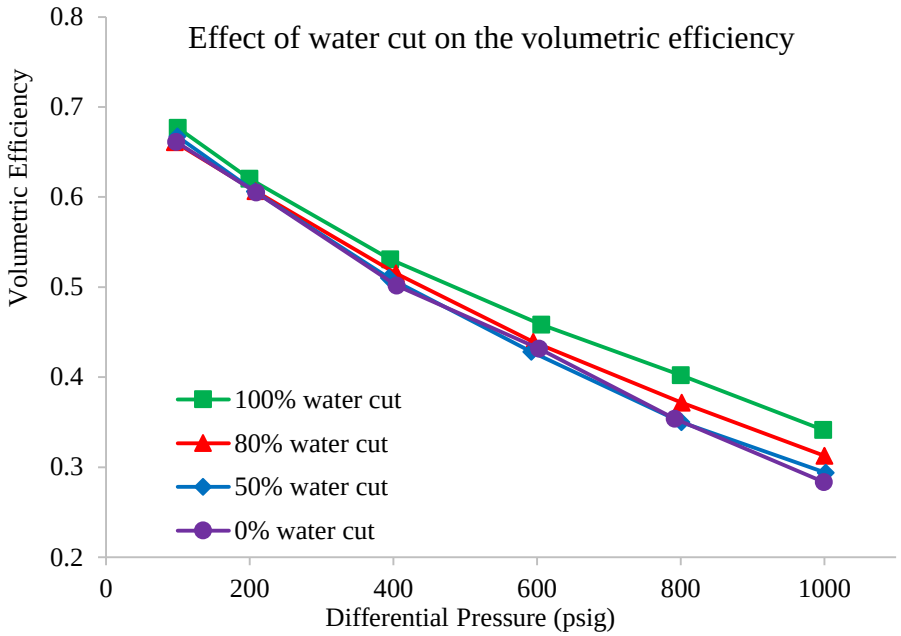

Figure 5.18 Effect of water cut on volumetric efficiency at 4000 RPM, 10% GVF

5.5 Mechanical Efficiency

Mechanical efficiency indicates the ratio of the power delivered to the fluid to the power transferred from the motor to the pump. As shown in Figure 5.9, the polytropic coefficient is nearly equal to 1.0 at all test conditions, which means that the compression is very close to an isothermal process.

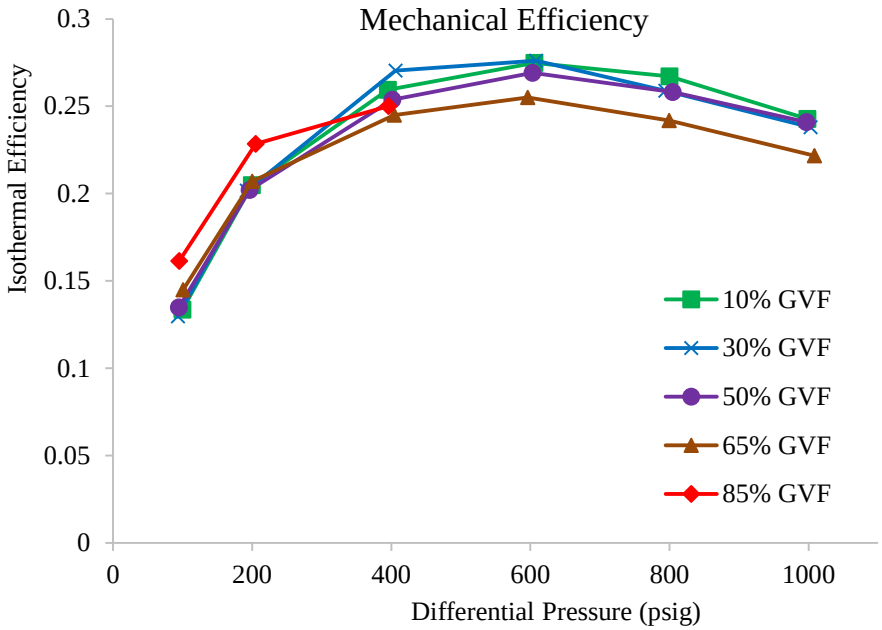

Figure 5.19 Mechanical efficiency (isothermal) for 100% water cut test at 4000 RPM

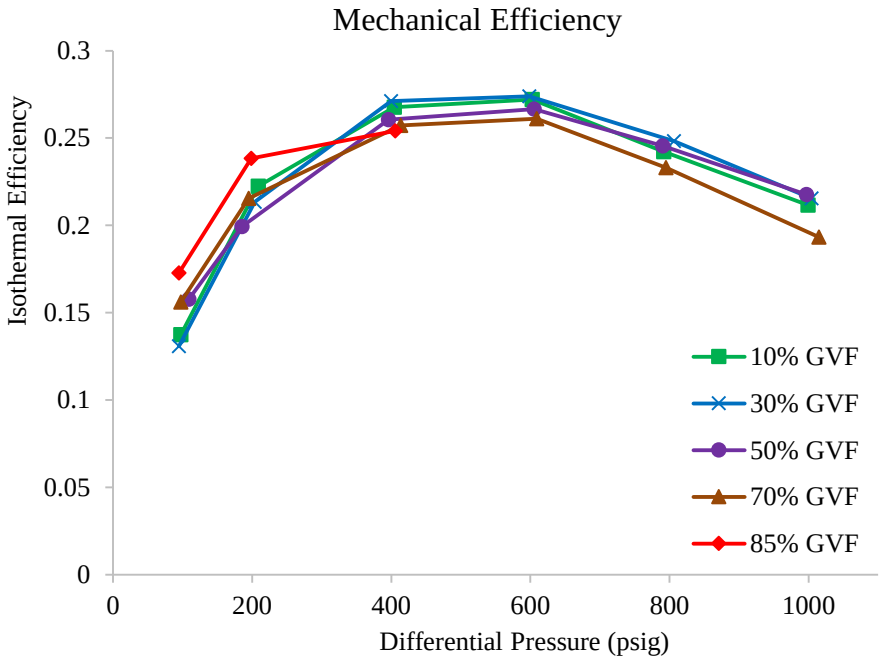

Figure 5.20 Mechanical efficiency (isothermal) for 0% water cut test at 4000 RPM

Figure 5.19 presents the mechanical efficiency of the 100% water test. Figure 5.20 presents the mechanical efficiency of the 100% oil test. With the increase of differential pressure, mechanical efficiency increases first, and then decreases with the increase of differential pressure.

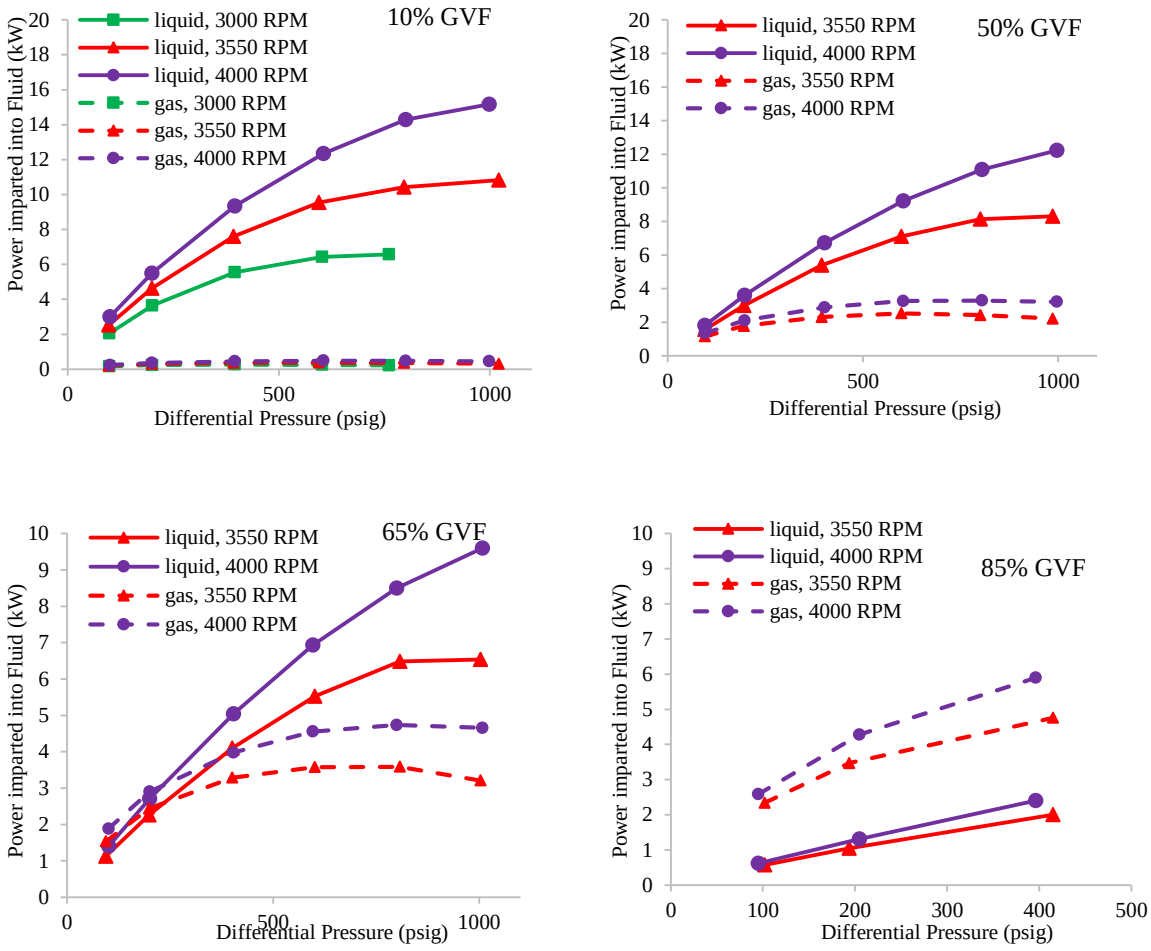

Figure 5.21 Power imparted into liquid and gas at different GVF of 100% water cut test

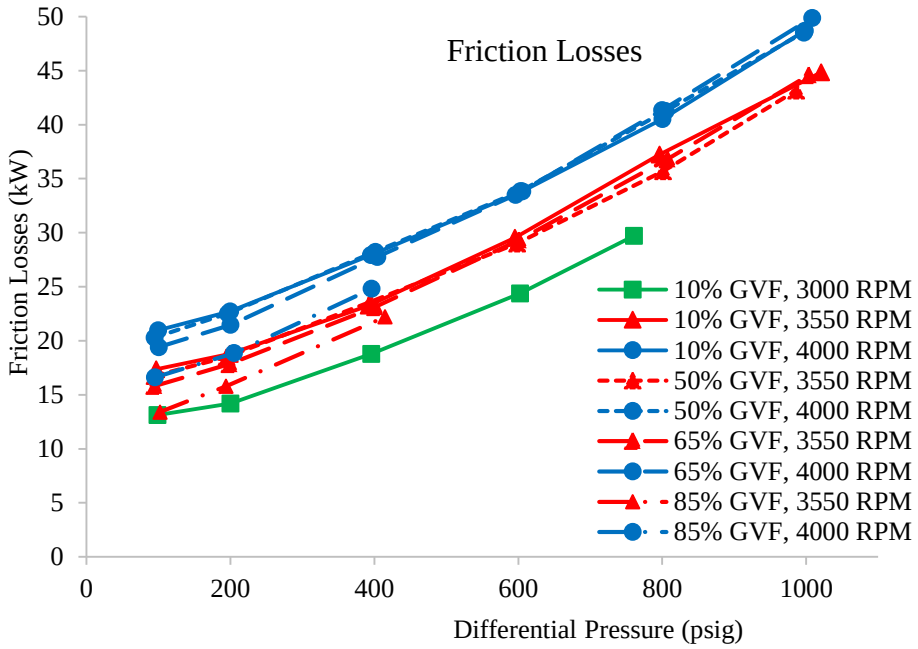

Figure 5.22 Friction losses of 100% water cut test

The power imparted into the pump can be divided into two components, one is to pressurize the fluid and another one is to overcome the friction losses. To understand the variation of mechanical efficiency, it is necessary to investigate the variation of the two components at different operating conditions. Figure 5.21 shows the variation of power imparted into liquid and gas at different operating conditions for the 100% water cut test. Figure 5.22 illustrates the variation of power component to overcome the viscous and friction losses. At the low differential pressure, the component to pressurize the fluid increases rapidly with the increase of differential pressure. Thus, the mechanical efficiency increases at the low differential pressure. At the high differential pressure, the rapid decrease of flow rate leads to the decrease of the component to pressurize the fluid

while the component to overcome the friction losses increases rapidly. As a result, the mechanical efficiency decreases at the high differential pressure.

With the differential pressure higher than 400 psig, mechanical efficiency decreases with the increase of GVF. Figure 5.21 shows the variation of power imparted to the liquid and the gas with different differential pressures. It is found that the power imparted in to the liquid is dominant with the GVF up to 65%. Since compared with the power imparted into the liquid and the power component to overcome the friction losses, the power imparted into the gas is relatively small. However, the power imparted into the liquid drops dramatically with the increase of GVF, which leads to the decrease of total power imparted into the fluid. As mentioned in the previous section, the power consumption changes little with the increase of GVF. Thus, the mechanical efficiency drops with the increase of GVF.

As shown in Figure 5.23, the pump speed has an essential effect on the mechanical efficiency. With the differential pressure less than 200 psig, the mechanical efficiency doesn't have big difference between different pump speeds. However, mechanical efficiency increases with the increase of pump speed when differential pressure is larger than 200 psig. As mentioned in the section of volumetric flow rate, volumetric flow rate increases with the increase of pump speed. Thus, with the increase of pump speed, the power imparted into the fluid increases faster than the power to overcome the fraction losses. As a consequence, it shows higher mechanical efficiency at higher pump speed.

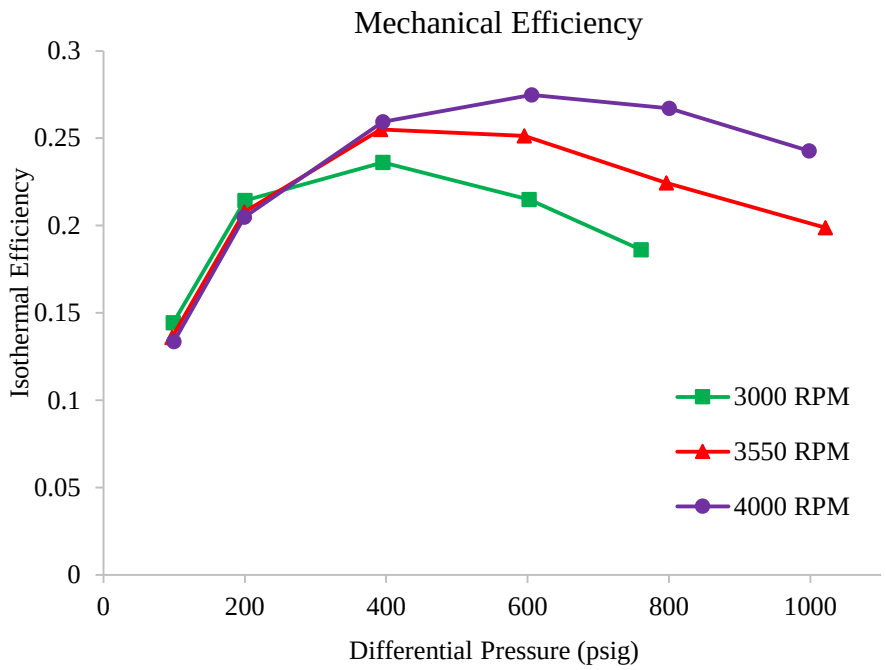

Figure 5.23 Effect of pump speed on mechanical efficiency (Isothermal) at 10% GVF, 100% water test

Figure 5.24 shows the effect of water cut on the mechanical efficiency. The mechanical efficiency of different water cuts only shows the difference at the high differential pressures. Since 100% water cut test shows the highest volumetric flow rate in this research especially at high differential pressure, the power imparted into the fluid increases with the increase of water cut. It is found the viscous and friction losses don't change much with different water cuts. As a result, the mechanical efficiency increases with the increase of water cut.

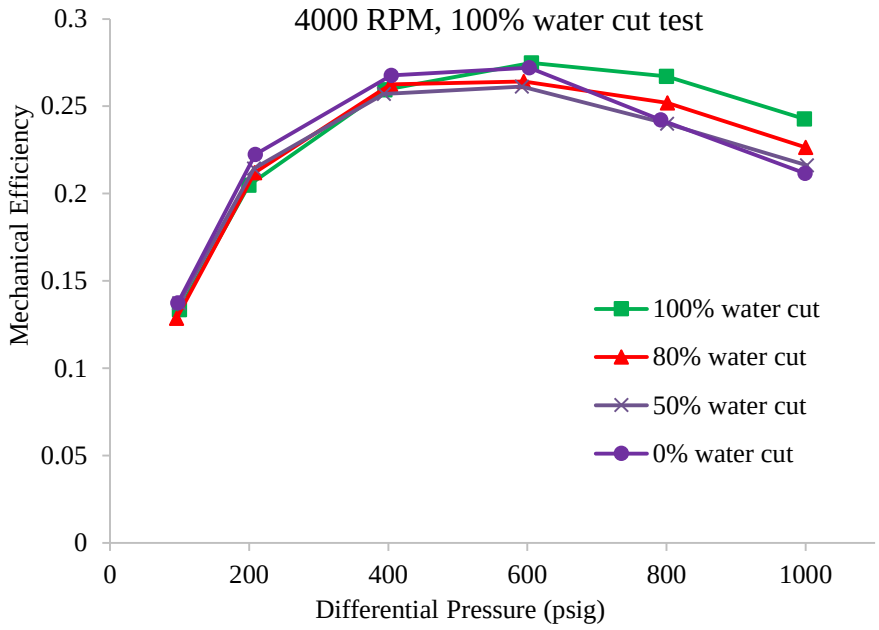

Figure 5.24 Effect of water cut on mechanical efficiency at 4000 RPM, 10% GVF

5.6 Pump Effectiveness

Pump effectiveness reflects the pump ability to compress multiphase flow. Figure 5.25 and Figure 25 illustrates the effect of GVF on the pump effectiveness for 100% and 0% water cut test. Pump effectiveness decreases with the increase of differential pressure. With the increase of GVF, pump effectiveness decreases faster due to the increasing gas fraction in the multiphase flow. Pump effectiveness decreases rapidly with the increase of GVF.

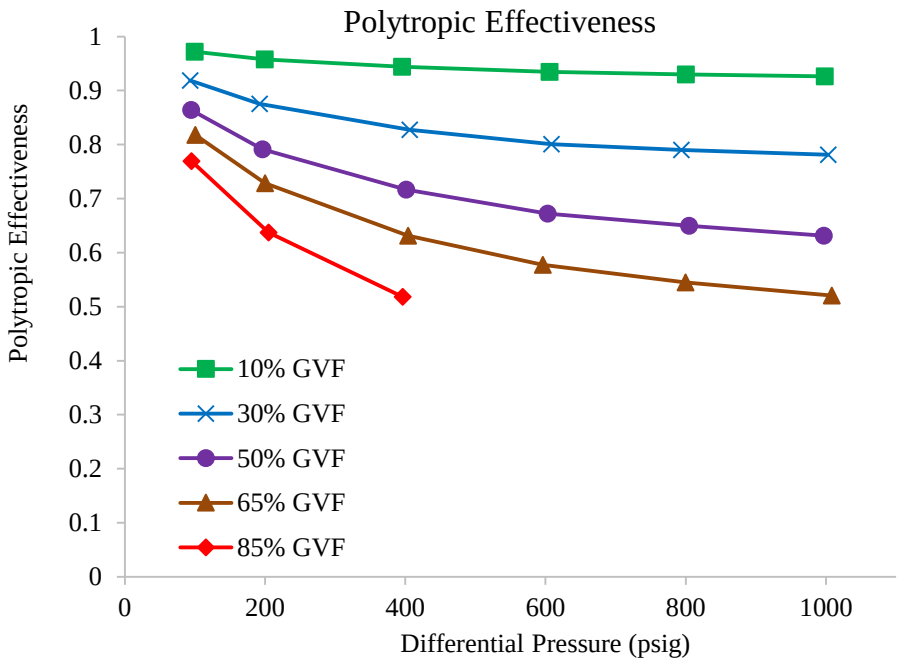

Figure 5.25 Polytropic effectiveness for 100% water test at 4000 RPM

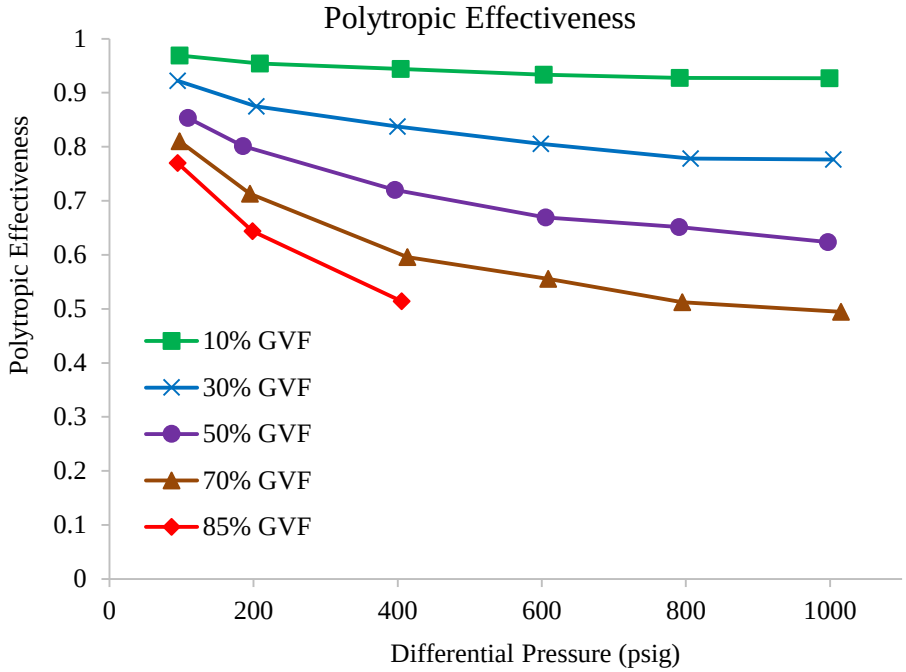

Figure 5.26 Polytropic effectiveness for 0% water cut test at 4000 RPM

5.7 Leakage Flow Rate

As discussed in the previous section, the non-contact design of pump rotors results in the existence of internal clearances in the pump. Due to the internal clearances, there is leakage flow from discharge to inlet in the pump. Leakage flow rate is the difference of the theoretical flow rate and the actual flow rate, which can be expressed as,

$$Q_l = Q_{th} - Q_a \tag{5.1}$$

Where the actual flow rate, Q_a, is the flow rate of fluid entering the inlet of the pump. The leakage flow rate is generally a function of differential pressure, GVF, and pump speed. It is influenced by the property of working fluid as well. In this research, the leakage flow of the Can-K pump will be evaluated under different working conditions.

Pump speed has an important effect on the leakage flow rate. Figure 5.27 shows the effect of pump speed on the leakage flow rate. It is found that as the pump speed increases, the leakage flow rate increases at 10% GVF. However, with an increase of the GVF the leakage flow rate is lower at 4000 RPM than that at 3550 RPM.

The leakage flow is typically composed by two components: one is due to the differential pressure and one is due to the rotation,

$$Q_l = Q_{dP} + Q_r \tag{5.2}$$

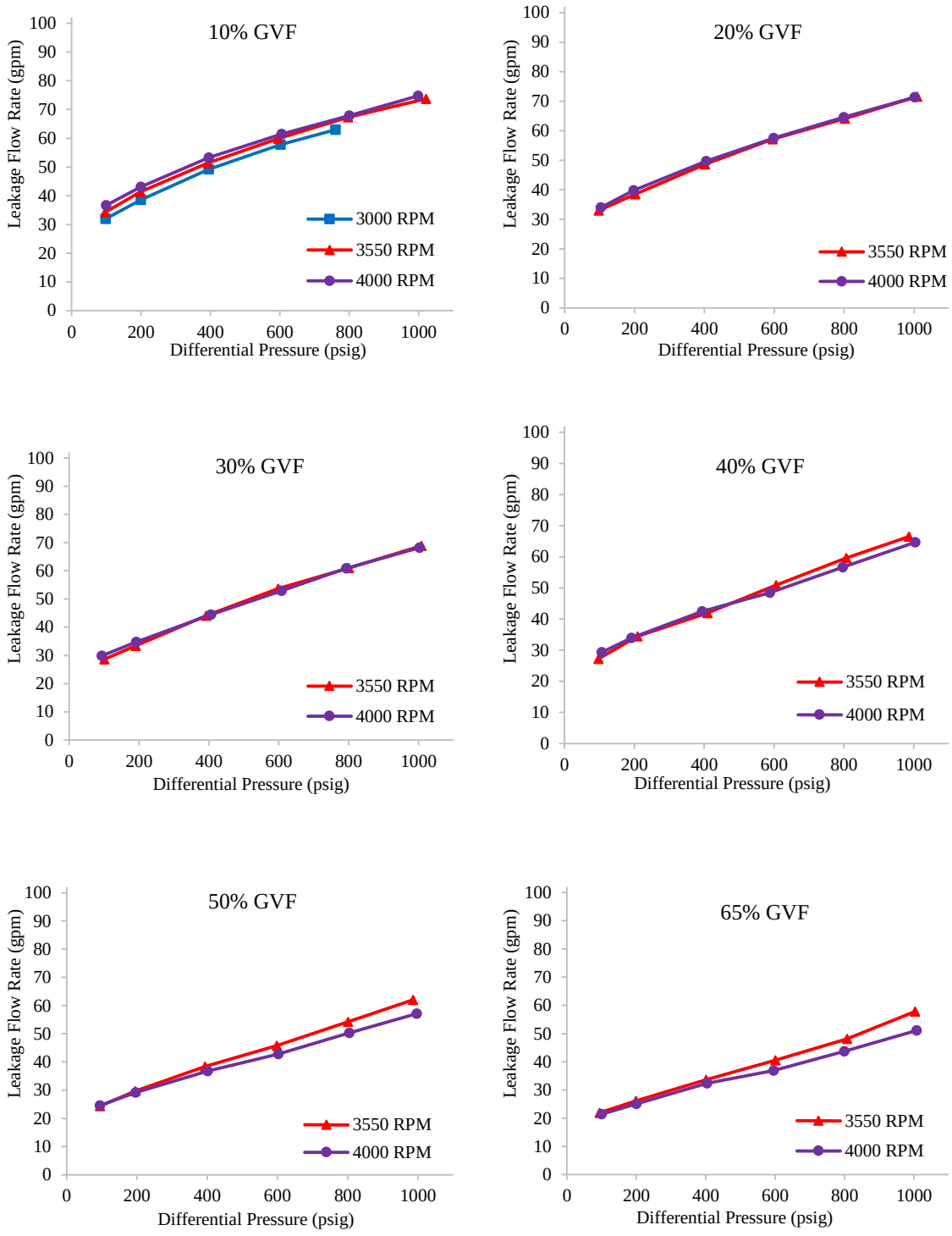

Figure 5.27 Effect of pump speed on leakage flow for 100% water cut test

As the pump speed increases with constant differential pressure, the leakage flow of differential pressure component remains the same, while the rotation component increases with the increase of pump speed at the low GVF conditions. At the low GVF conditions, the rotation component increases with the increasing pump speed. However, with an increase of the GVF, the effect of centrifugal effect becomes the dominant reason to determine the leakage flow rate. More gas is injected into clearance at high pump speed, which helps to seal the clearances. But generally the pump speed doesn't have a significant influence on the leakage flow for the Can-K pump.

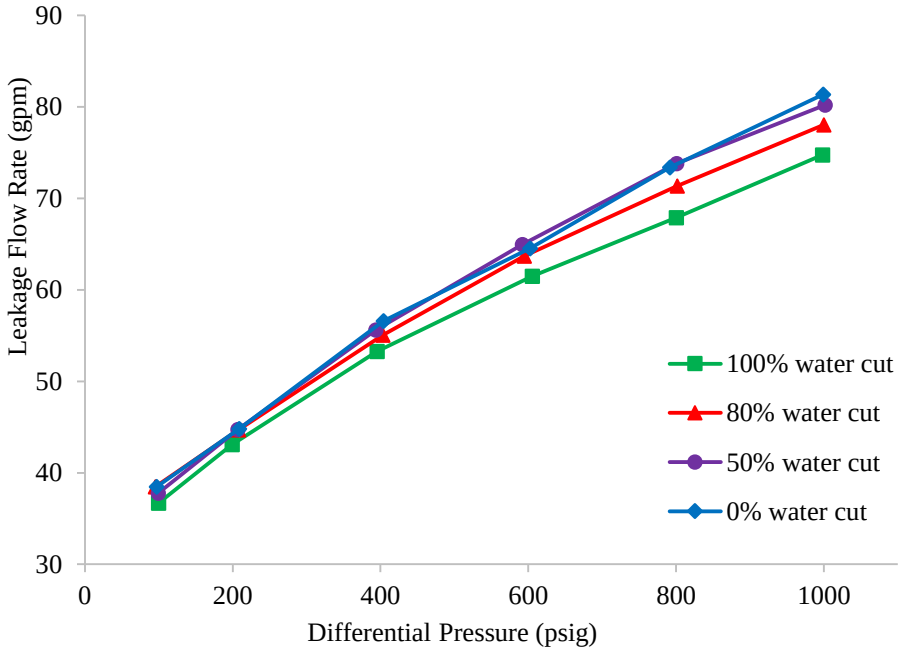

Figure 5.28 Effect of water cut on leakage flow at 4000 RPM, 10% GVF

Water cut has an essential effect on the leakage flow rate as shown in Figure 5.28. The water and gas mixture shows better seal function for the Can-K pump.

5.8 Comparison of the Water Tests

100% water cut test was performed with the open loop in 2014 and with the closed loop in 2015. The total flow rate capacity measured by the second test is lower than that measured by the first test. Figure 5.29 presents the comparison of the test data of 3550 RPM. Figure 5.30 shows the comparison of the test data of 4000 RPM. It is found that the largest difference occurs at 10% GVF. It is also found that with the increase of differential pressure, the flow rate reduction increases. With the increase of GVF, the flow rate difference decreases.

The reduction of flow rate capacity is subject to various potential factors. One possible reason that may lead to the difference is the measurement error of the instrumentations. To eliminate the effect of measurement error, the consistency of the flow meters used in the two times is investigated. The water flow rate of Can-K pump varies from around 15 gpm to 75 gpm with the GVF increasing from 10% to 65%. As a result, data were recorded when water flow rate varied from 10 gpm to 80 gpm. The measurement of the Coriolis flow meter and the turbine flow meter was saved simultaneously by LabVIEW when the flow rate is stable. The test result shows that the difference between Coriolis flow meter and turbine flow meter is less than 1% within the flow range 10 gpm to 80 gpm. Consequently, the measurement error of flow meter should not be the dominant reason that leads to the difference.

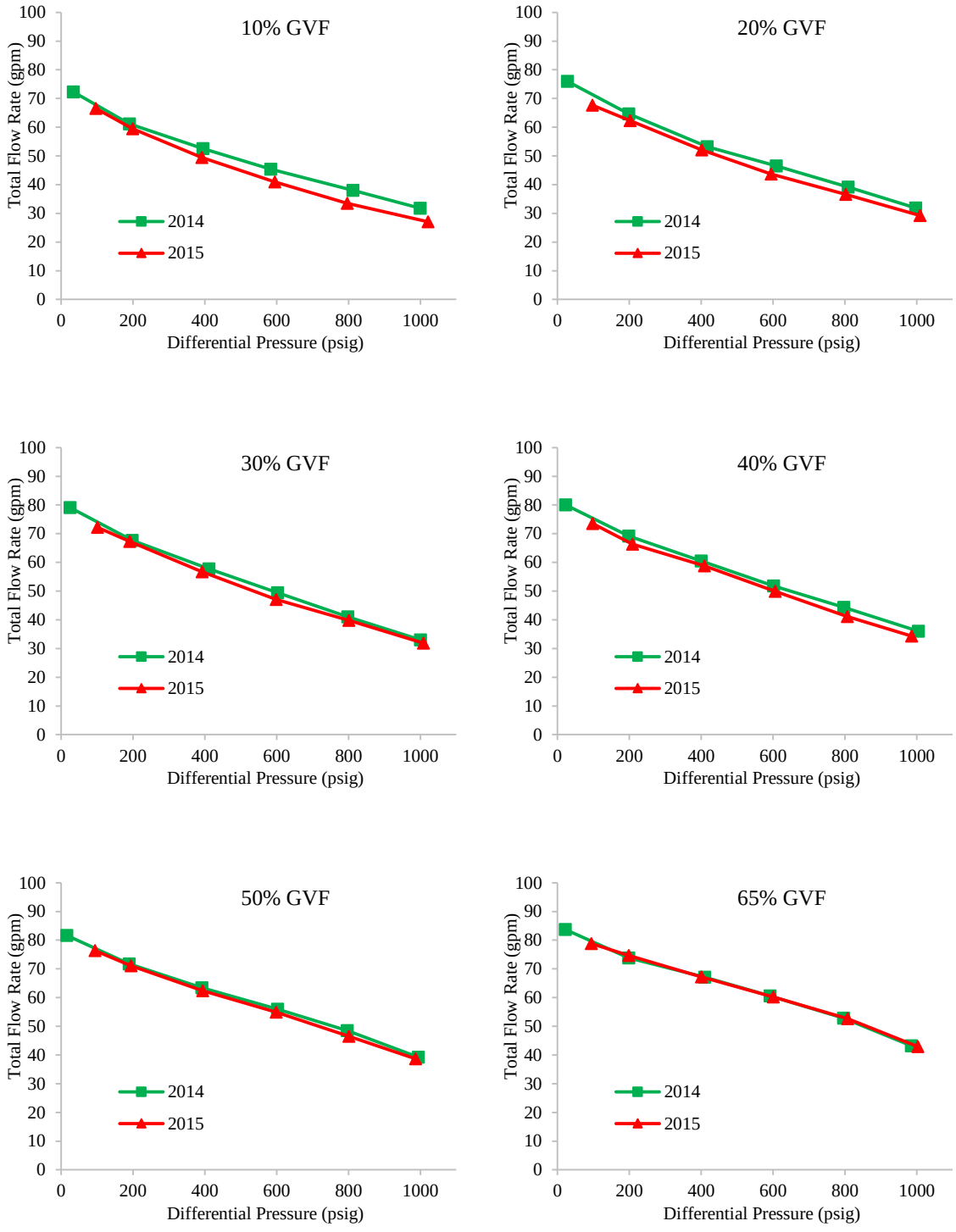

Figure 5.29 Comparison of volumetric flow rate capacity for 100% water test, 3550 RPM

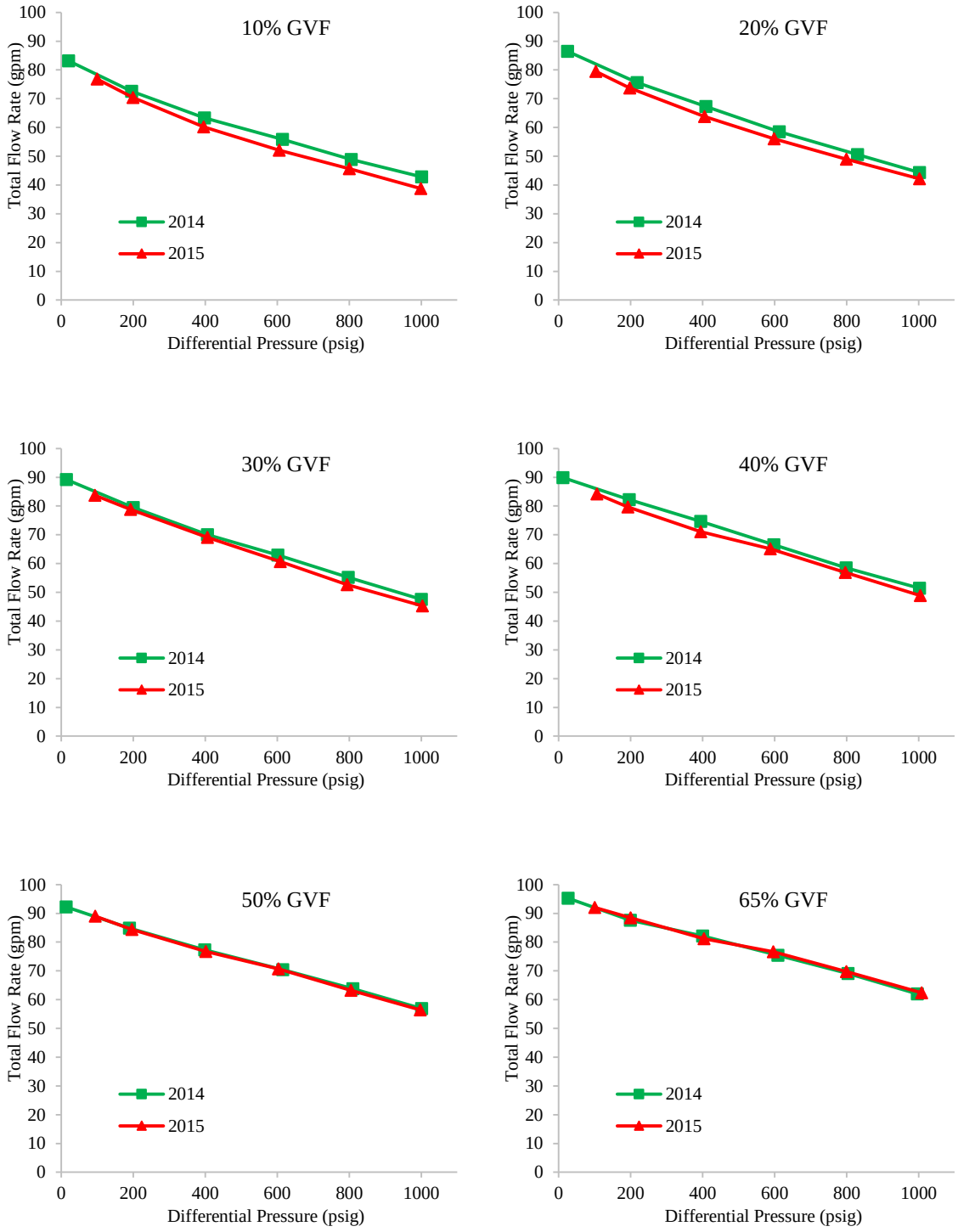

Figure 5.30 Comparison of volumetric flow rate capacity for 100% water test, 4000 RPM

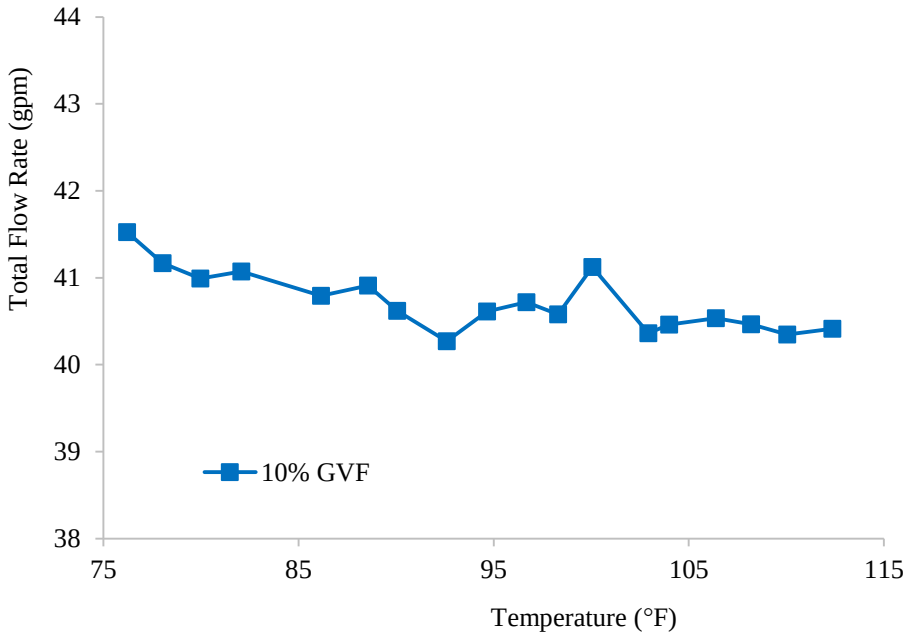

Figure 5.31 Effect of temperature on volumetric flow capacity

The flow rate capacity is also significantly affected by the inlet pressure and the outlet pressure. As a result, pressure transducers were recalibrated. It is found that measurement error of the pressure transducer at the pump inlet is less than 0.6 psig, and the error at the pump outlet is less than 5 psig. From the curve of flow rate capacity, it can be conclude that the error of the pressure transducer can't be the dominant reason of the difference.

The temperature may also be a potential effect on the pump performance. To confirm the effect of temperature, the pump was operated with different inlet temperatures at 3550 RPM, 10% GVF and 600 psig differential pressure. As shown in Figure 5.31, the temperature has little effect on the flow rate capacity.

Instruments have been demonstrated to work well. Thus, it is necessary to investigate the pump itself. Since the change of certain parameter of pump can have an important effect on the pump performance. As a result, it is highly possible that there is something different in the pump between the two tests. However, there is no way to have an internal investigation of the dimensions of the Can-K pump in the lab. This is can only feasible when it ships back to the manufactory.

5.9 Performance Comparison of Colfax Pump and Can-K Pump

Patil [23] investigated the multiphase performance of a MR-200 Colfax twin screw pump. Experimental tests were performed with GVF ranging from 50% to 100% at different differential pressures. The pump was operated with various speeds and suction pressures. In this section, steady state performance was analyzed for the two twin screw pumps with different design. Since the Colfax pump was only tested with water, only the 100% water cut test data of Can-K pump is selected in the following analysis.

5.9.1 Volumetric Flow Rate Capacity

Since the Colfax pump is a double-end pump, its flow rate capacity drops dramatically when differential pressure increases to 250 psig. The Maximum working pressure of the Colfax pump is rated 490 psig. However, the Can-K pump can work with differential pressure up to 1000 psig. The Can-K pump owns much more seals than the Colfax pump, which enable it to maintain the performance at extreme high differential pressure. The Colfax owns a larger flow rate capacity due to its larger sizes. The theoretical flow

rate capacity of the Colfax pump is 651 gpm at 1800 RPM, while the theoretical flow rate capacity of the Can-K pump is 113.5 gpm at 4000 RPM.

5.9.2 Leakage Flow Rate

The Colfax pump has a larger volumetric flow rate capacity while the flow rate capacity of Can-K pump is relatively smaller since the size of Can-K pump has to be designed to fit in the oil well. As a result, the double-end pump is generally used as a surface multiphase pump, while the Can-K pump can be used as a subsurface pump.

The leakage flow of Colfax pump shows the same pattern with that of Can-K pump. For the single phase test, the leakage flow increases with the increase of pump speed. For the two phase test with the GVF above 50%, the leakage flow decreases with the increase of pump speed. However, it is found that the leakage flow rate of Colfax pump is more subject to pump speed, especially at high differential pressure. As shown in Figure 5.32, the leakage flow rate increases rapidly as the pump speed increases.

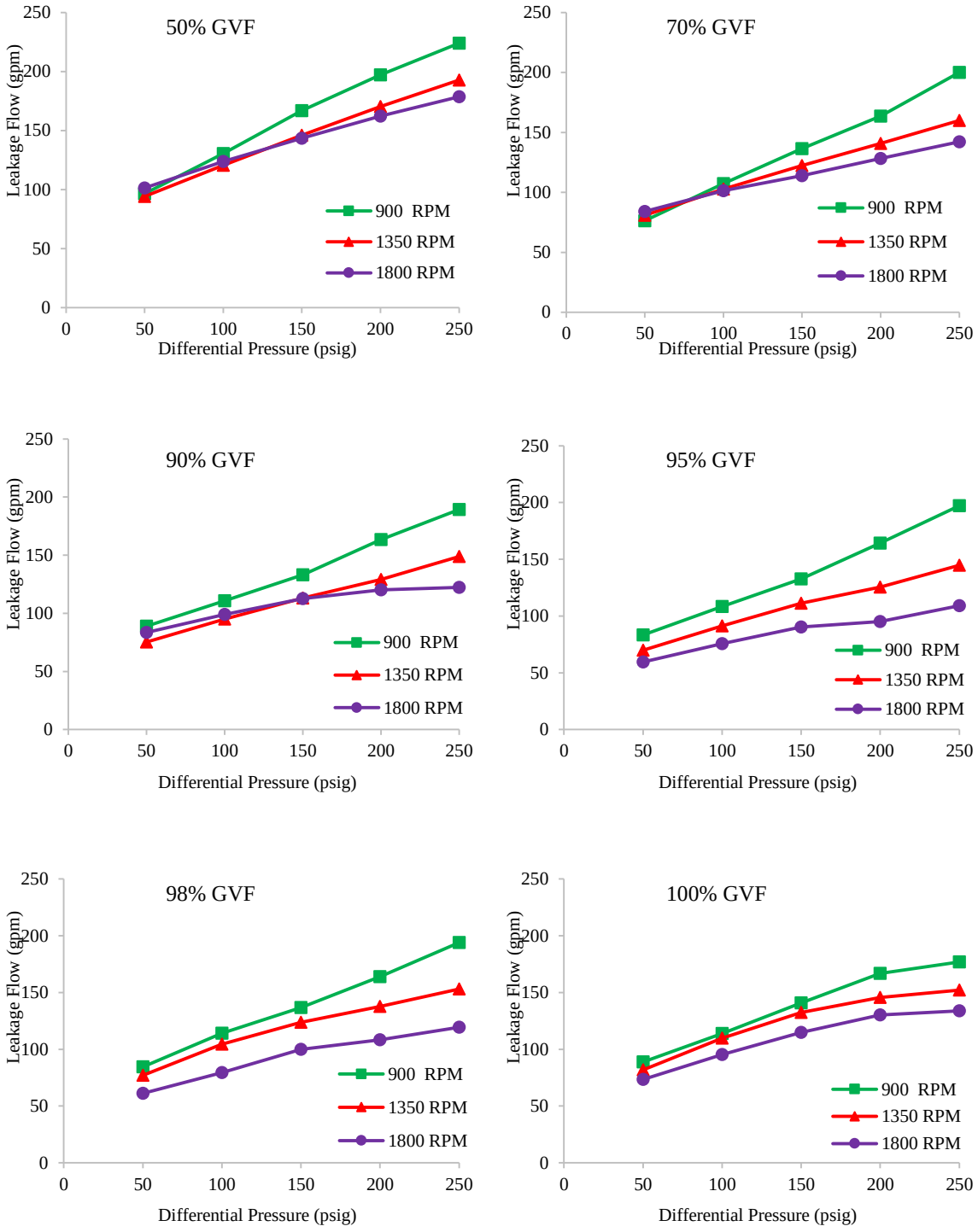

Figure 5.32 Effect of speed on leakage flow for different GVF at 100 psig inlet pressure, Colfax pump

5.9.3 Volumetric Efficiency

Figure 5.33 shows the comparison of volumetric efficiency. Volumetric efficiency of Colfax pump is consistently higher than that of Can-K pump. Note that the pump speed of Colfax pump is less than that of Can-K pump. It can be expected that the volumetric efficiency of Colfax pump is even higher than the Can-K pump if they can be operated at the same speed. Information of the clearance size is not available for the Can-K pump. The size of circumferential clearance of Can-K pump can be estimated with the analytical model of Vetter. It is found that the circumferential clearance of Can-K pump is around 0.5 mm, which is much larger than that of Colfax pump. However, the rotor diameter and the displacement per revolution of Colfax pump are much larger than that of Can-K pump. Thus, the leakage of Colfax pump may has less effect on the volumetric efficiency.

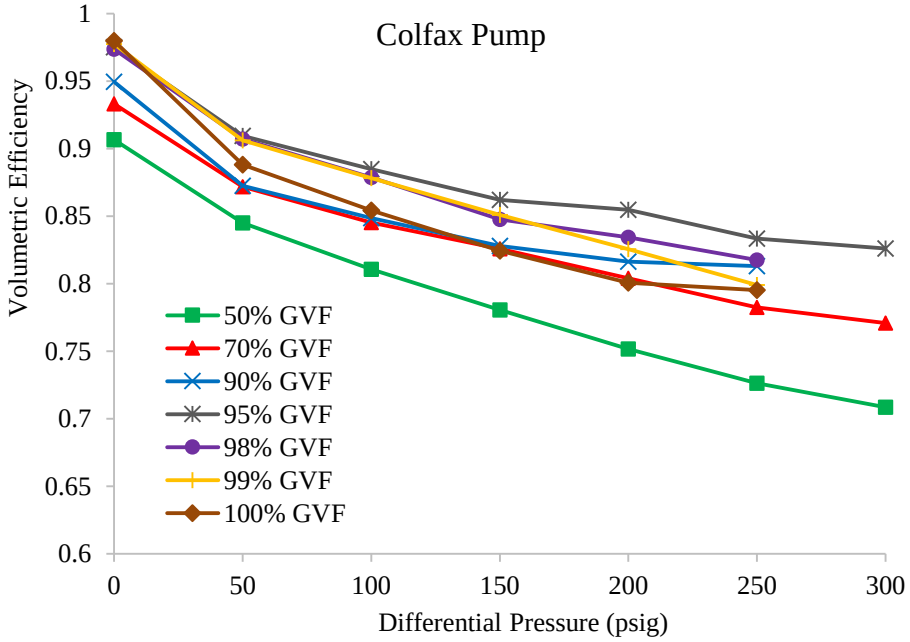

Figure 5.33 Volumetric efficiency of Colfax pump at 100 psig inlet pressure, 1800 RPM

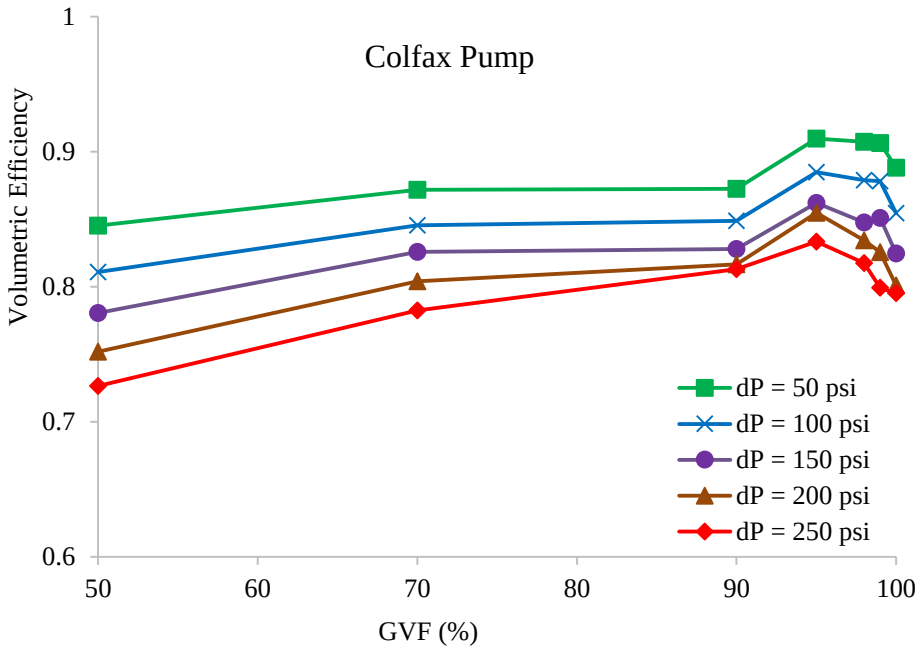

Figure 5.34 Volumetric efficiency for Colfax pump at 100 psig inlet pressure, 1800 RPM

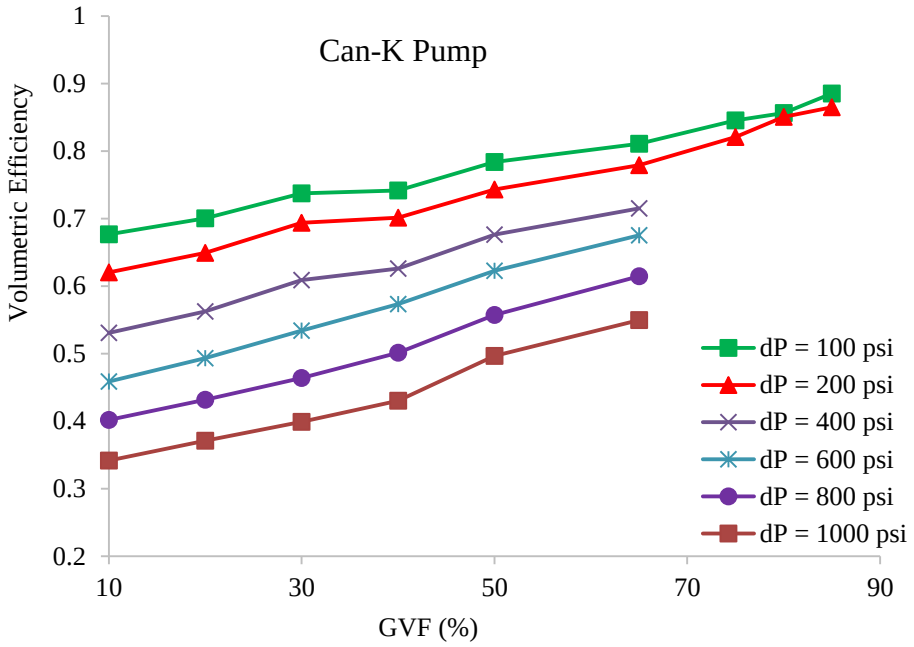

Figure 5.35 Volumetric efficiency for Can-K pump at 100 psig inlet pressure, 4000 RPM

As shown in Figure 5.34, the volumetric efficiency of Colfax pump maximizes around 95% GVF. The Colfax pump has a liquid recirculation system which is used to inject a specific amount of liquid into the pump to seal the clearance at extremely high GVF operation. As a result, the Colfax pump can be operated with extremely high GVF flows. Note that the GVF for Colfax pump is skid based data, which is calculated by the following equation,

$$GVF = \frac{Q_g}{Q_l + Q_g} \tag{5.3}$$

As a result, this GVF doesn't reflect the real GVF at the entrance of the Colfax pump, since the skid based GVF doesn't include the effect of the recirculation. The real GVF is also referred to as pump based GVF, which can be calculated by the following equation,

$$GVF = \frac{Q_g}{Q_l + Q_g + Q_r} \tag{5.4}$$

In this section, the GVF of Colfax pump is skid based data. The skid based GVF is generally larger than the real GVF as shown in Figure 5.36, since it doesn't include the recirculation flow.

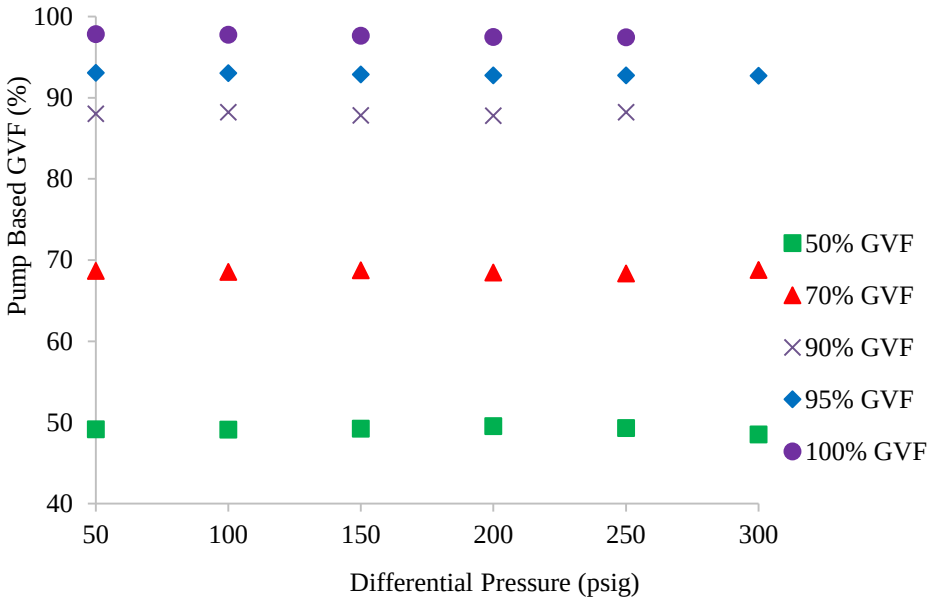

Figure 5.36 Comparison of skid based GVF and pump based GVF

For the Can-K pump, the volumetric efficiency always increases with the increase of GVF. However, since there is no recirculation system for the Can-K pump, it was only tested to 85% GVF. But it can be expected that the volumetric efficiency will begin to decrease with the increase of GVF above this GVF.

5.9.4 Mechanical Efficiency

Figure 5.37 shows the comparison of the mechanical efficiency. It is found that the mechanical efficiency of Colfax pump is much higher than the Can-K pump. As shown in Figure 5.37, the mechanical efficiency of the Colfax pump is generally higher than 50% within the test conditions. However, mechanical efficiency of Can-K pump is less than 30%. Since the Can-K pump is a multistage pump, there are many more seals in the Can-K pump. The design of the Can-K pump results in more internal friction losses.

As shown in Figure 5.37, the mechanical efficiency of Colfax pump is more dependent upon GVF. With the 200 psig differential pressure, the mechanical efficiency at 50% GVF is about 58%, while it is only 25.6% at 100% GVF. However, the GVF has little effect on the Can-K pump. Additionally, the maximum mechanical efficiency for the Colfax pump occurs at about 150 psig differential pressure, while the maximum mechanical efficiency for the Colfax pump occurs at about 600 psig.

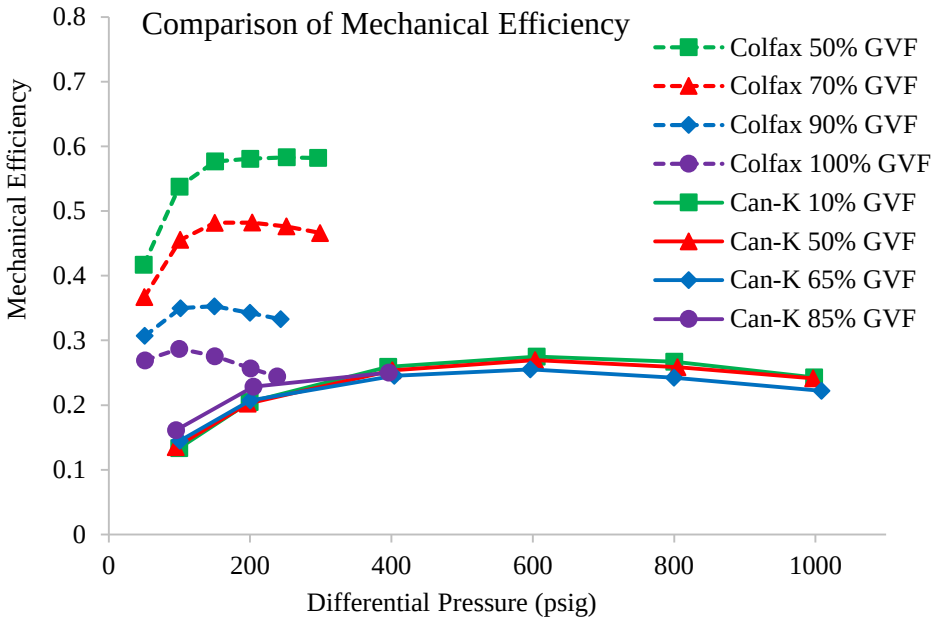

Figure 5.37 Comparison of mechanical efficiency

6 MULTIPHASE TWIN-SCREW PUMP MODEL

This chapter represents the development of an analytical model to predict the multiphase performance of the twin screw pumps. As mentioned in the literature review, previous research of the analytical model is still insufficient to reflect the flowing condition in the twin screw pump. Most of the previous models didn't consider the compressibility of the leakage flow. Besides, none of the previous models try to predict the performance of the multistage pump. Hence, a new model is necessary to be created to model the leakage flow in the twin screw pump.

In this model, the compressibility of leakage flow will be investigated. It is assumed that the gas mass fraction is uniform at an arbitrary position in the chambers and clearances at the low GVFs. At the high GVFs the gas mass fraction in the clearance is smaller than the gas mass fraction in the chamber due to centrifugal force. In this model, the gas mass fraction in the clearance is assumed to be 80% of the gas mass fraction in the chamber. The leakage flow is considered as compressible flow in the clearances. The choked flow condition may have an essential effect on the leakage flow rate. In this research, the possibility of the choked flow condition at the exit of clearance will be investigated.

Previous models are mainly applied on the single-stage pump. In this research, a new model is proposed to predict the multiphase performance of a multi-stage twin screw pump. The pressure distribution along the stages is modeled by an empirical equation.

6.1 Simplification of Twin Screw Pump Working Process

The working process of a real twin screw pump is too complex to analyze by an analytical method. It is necessary to make requisite simplifications and assumptions before the simulation. In this model, the twin screw pump is simplified to a series of the chambers divided by discs which moving axially from the suction side to the discharge side. The fluids enter and exit the chambers through the clearances. It is assumed that the liquid and the gas are fully mixed at an arbitrary point in the pump.

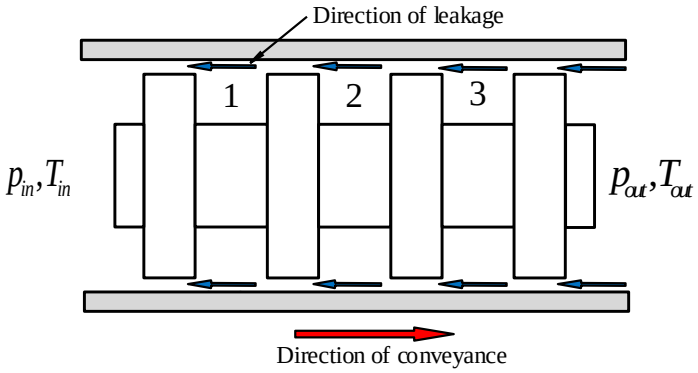

Figure 6.1 Simplification of the twin screw pump

The model is established with the assumptions and simplifications below:

- The gas is considered as ideal gas
- The leakage flow is assumed as two phase compressible flow
- The circumferential leakage accounts for 80% of the total leakage
- Division of one revolution into small time segments

- Chamber pressure and temperature remain constant in one time segment
- Leakage flow is one-dimensional compressible flow; flow in the circumferential direction is neglected
- At the end of one rotation, the i^{th} chamber become the $i+1^{th}$ chamber; the last chamber vanished; a new chamber is created at the pump inlet

During the operation, the closed chambers move continuously from the suction side to the discharge side. The pressure and temperature keep changing all the time as well. Hence, the period of one revolution is divided into multiple time steps in this model. And the distance the chamber moved forward in one revolution is also divided into appropriate distance. During one time step, the discs remain stationary. The pressure and the temperature in the chambers are assumed to be constant. At the next time step, the discs jump to the next corresponding positions. Thus, the working process is largely simplified. It is only necessary to find the conditions during the time steps. Since the pressure and temperature in the chamber remain constant during one time step, the leakage flow rate can be calculated by an analytical method.

6.2 Geometric Parameters

With these simplifications and assumptions, an analytical model can be proposed to present the working process of twin screw pump. However, to start the simulation, the following geometric parameters of pump is requisite to import into the computer program,

- Screw outer diameter
- Screw root diameter

- Screw pitch
- Screw length
- Thickness of the screw threads
- Displacement per revolution
- Size of circumferential clearance

Typically the geometric parameters are provided by the manufacturer. However, sometimes the actual size of circumferential clearance is not available or the manufacturer doesn't want to disclose the information. In this circumstance, the size of the circumferential clearance can be estimated based upon pure water experimental performance data. Assuming the leakage area can be represented with a hydraulic diameter, so the Bernoulli's Equation for a pipe flow can be used.

$$\frac{p_{in}}{\rho_l} + \frac{1}{2} v_{in}^2 - \frac{p_{out}}{\rho_l} - \frac{1}{2}\, v_{out}^2 = \frac{1}{2} f \frac{l}{d_h} v_{in}^2 \qquad 6.1$$

Since for pure liquid flow $V_{in}^2 = V_{out}^2$. Thus,

$$\Delta p = \frac{1}{2} f \frac{l}{d_h} \rho_l v_{in}^2 \qquad 6.2$$

Since $d_h = 2c$, the size of circumferential clearance can be solved by the following equation,

$$c = \frac{f L \rho_l v_{in}^2}{4\Delta p} \qquad 6.3$$

For the laminar flow,

$$f = \frac{96}{Re} \tag{6.4}$$

For the turbulent smooth clearance,

$$f = \frac{0.316}{Re^{0.25}} \tag{6.5}$$

In this research, the sizes of circumferential clearance for Can-K pump and Colfax pump are estimated.

6.3 Leakage Flow in the Clearance

To predict the behavior of twin screw pump, it is important to model the leakage flow in the clearance. As shown in Figure 6.2, the circumferential clearance connects two adjacent chambers. In this model, the chamber is regarded as a reservoir where the fluid is static. When the fluid is injected into the clearance due to differential pressure between two adjacent chambers, the fluid will be accelerated from static at the entrance as shown in Figure 6.3. If the pressure at the clearance entrance is known, the clearance inlet GVF, density and velocity can be solved with equation 6.6 - 6.8 by Brennen [26].

$$\alpha = \frac{p_0 \alpha_0 (1-\alpha)}{p + \alpha_0 (p_0 - p)} \tag{6.6}$$

$$\rho = \frac{1-\alpha}{1-\alpha_0} \cdot \rho_0 \tag{6.7}$$

$$u^2 = \frac{2p_0\alpha_0}{\rho_0}\left[\frac{1-\alpha_0}{\alpha_0} - \frac{1-\alpha}{\alpha} + In\left(\frac{(1-\alpha_0)\alpha}{\alpha_0(1-\alpha)}\right)\right] \tag{6.8}$$

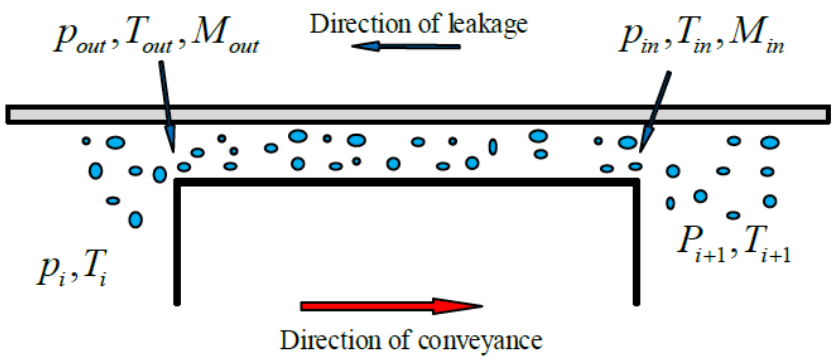

Figure 6.2 Leakage flow in the circumferential clearance

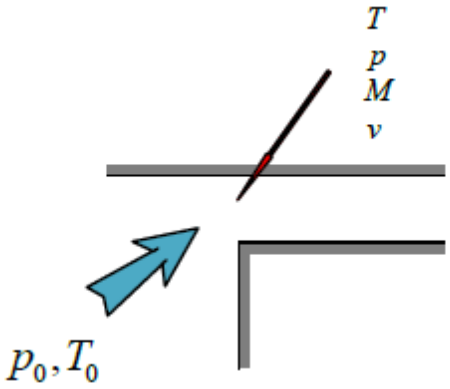

Figure 6.3 Fluids acceleration in the entrance of clearance

However, the pressure at the clearance entrance is typically unknown in the beginning of calculation. Instead, only the pressure and temperature in the upstream and downstream chambers are known. Hence, the inlet velocity must be found by iteration. To start calculation, an initial inlet pressure is assumed at the beginning of calculation. Then the

flow conditions in the clearance can be calculated with a Fanno flow model. The inlet pressure is adjusted according to the condition at the exit of clearance until the exit pressure equals to the downstream chamber pressure or the leakage flow is choked at the exit. Figure 6.4 shows the computer algorithm to calculate the leakage flow.

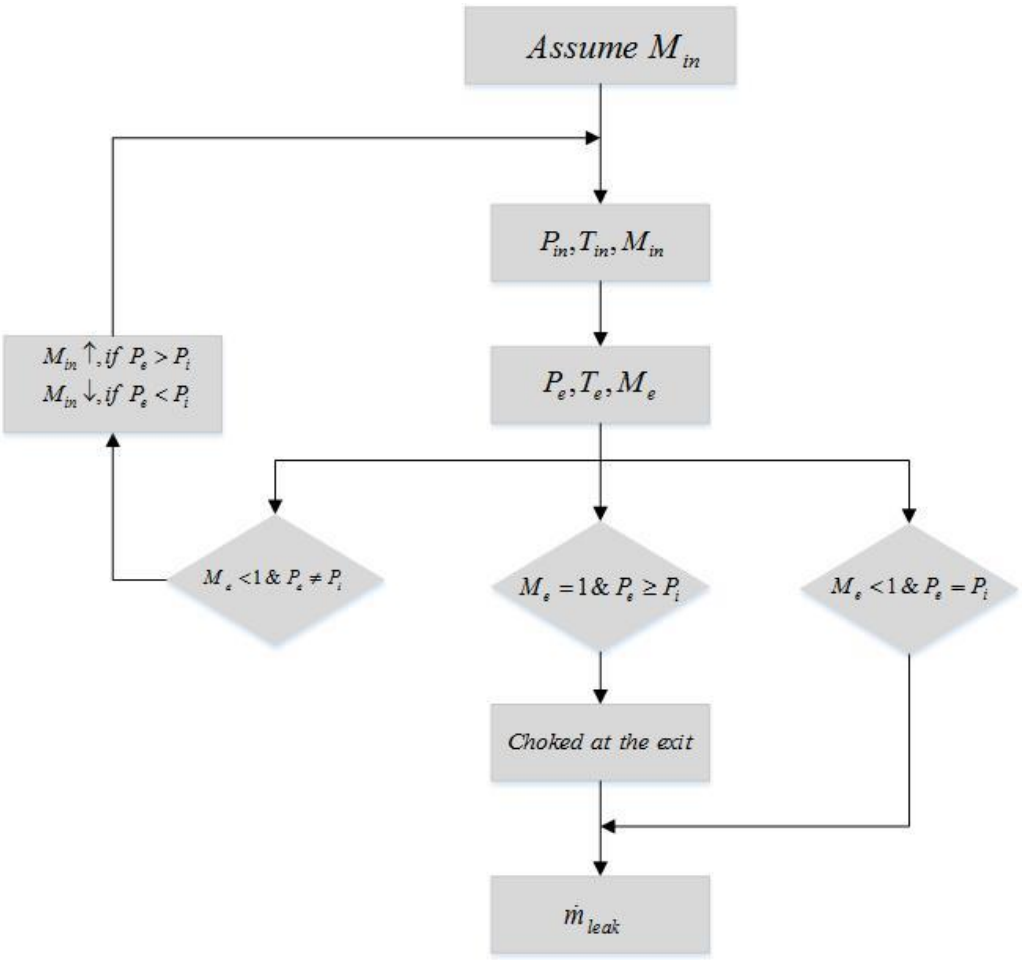

Figure 6.4 Computer program algorithm

The flow in the clearance is solved using a two phase Fanno flow model. Since the size of the clearance is much smaller than the length of the clearance and the perimeter of the screw, the leakage flow through the circumferential clearances can be simplified to a one-dimensional adiabatic flow in a duct, which can also be referred to as Fanno flow. With knowing the inlet conditions, the downstream conditions can be calculated with the following differential equations. The change of Mach number is related with a small distance by the following differential equation,

$$\frac{f}{D_h}dx = 2\frac{(1-M^2)}{\left(1+\frac{k-1}{2}M^2\right)\cdot kM^2}\frac{dM}{M} \tag{6.9}$$

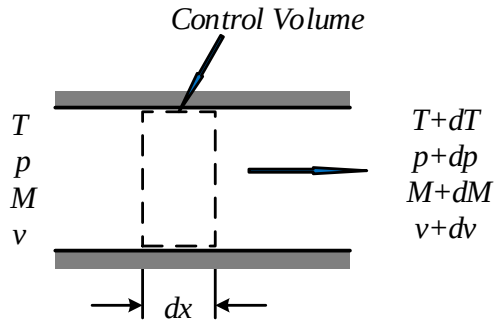

Figure 6.5 Control volume of fanno flow in the duct

With the local Mach number, the change of the pressure and temperature can be calculated with the following equations,

$$\frac{dT}{T} = -\frac{(k-1)MdM}{1+\frac{k-1}{2}M^2} \tag{6.10}$$

$$\frac{dP}{P} = -\frac{dM}{M} + 0.5\frac{dT}{T} \tag{6.11}$$

For the two phase flow, the fluid properties are different from single component flow. In this model, the density and the viscosity of the mixture are the weighted averages of liquid and gas.

$$\rho_m = \alpha\rho_g + (1-\alpha)\rho_l \tag{6.12}$$

$$\mu_m = \alpha\mu_g + (1-\alpha)\mu_l \tag{6.13}$$

The friction factor is calculated according to local Re number. For the laminar flow,

$$f = \frac{96}{Re} \tag{6.14}$$

For the turbulent smooth clearance,

$$f = \frac{0.316}{Re^{0.25}} \tag{6.15}$$

Due to the intensive mixing process in the pump, the heat and momentum transfer process is so rapid that the leakage flow can be treated as homogenous flow. The velocity and the temperature of the two phases are considered to be the same.

$$Re = \frac{\rho v D}{\mu} \tag{6.16}$$

Where $v = Mc$, and c is the speed of sound in the mixture. The viscosity of gas can be obtained through the Sutherland's formula,

$$\mu = \mu_0 \frac{a}{b}\left(\frac{T}{T_0}\right)^{1.5} \tag{6.17}$$

Where a, b, μ_0 and T_0 are constants.

Until now, the leakage flow has been modeled during one time step. Therefore, the mass balance in the chamber can be calculated with the leakage flow rate. The change of pressure and temperature in the chamber can also be found with energy conservation.

6.4 Sonic Speed of Homogeneous Two Phase Flow

In a constant area duct, the speed of compressible flow can't exceed the local speed of sound. As a result, the maximum Mach number is 1 at the exit of the clearance. In this case, the leakage flow velocity will not increase even with lower downstream pressure. In this circumstance, the leakage flow velocity is largely affected by the sonic speed of the two phase flow. As a result, it is necessary to discuss the characteristics of the sonic speed of homogeneous two phase flow. Sonic speed of homogeneous two phase flow represents distinguished property compared with single phase flow. The sonic speed of a two phase liquid/gas flow can be expressed with the following equation, [26]

$$\frac{1}{c^2} = \left[\rho_l(1-\alpha) + \rho_g\alpha\right]\left[\frac{\alpha}{kp} + \frac{(1-\alpha)}{\rho_l c_l^2}\right] \tag{6.18}$$

In many applications, $\frac{\alpha}{kp} \gg \frac{(1-\alpha)}{\rho_l c_l^2}$ thus equation 6.3 can be simplified to, [26]

$$\frac{1}{c^2} = \frac{\alpha}{kp} \cdot \left[\rho_l(1-\alpha) + \rho_g\alpha\right] \tag{6.19}$$

Figure 6.6 shows the variation of sonic speed for the two phase water/air flow with different GVF at 100 psig. It is found that the sonic speed of homogenous two phase flow becomes the minimum with GVF around 60%. The sonic speed at 60% GVF is about 68 m/s, which is much lower that of pure water or pure air.

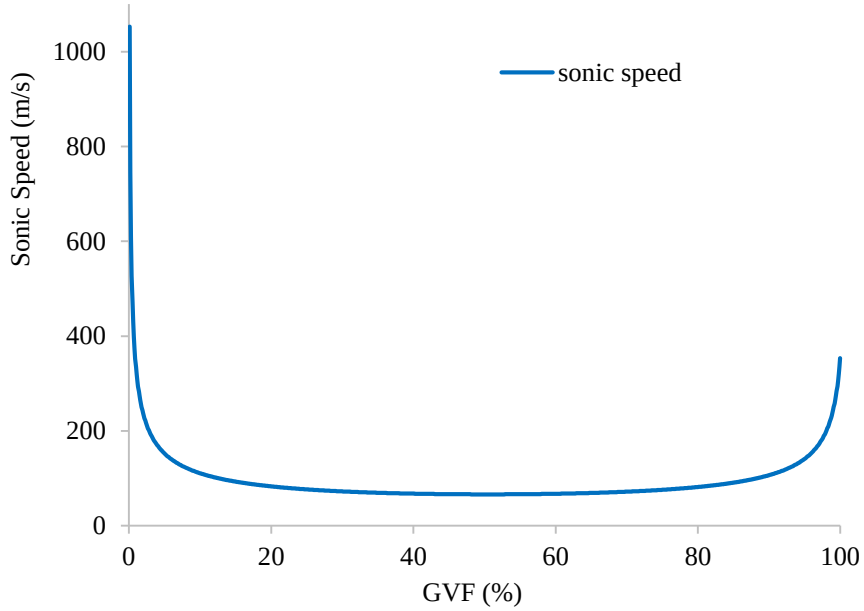

Figure 6.6 Sonic speed of two phase water/air flow at 100 psig

6.5 Mass Balance in the Chambers

According to Vetter, the circumferential gap flow contributes 80% percent of the total leakage, 15% of the total leakage is through the radial clearance, and another 5% is due to the flank leakage. As a result, the prediction of the circumferential gap flow is

dominant to determine the accuracy of the new leakage model. In this model, only circumferential leakage flow is calculated in the computer program. The radial leakage and the flank leakage are assumed to be 15% and 5% of total leakage separately.

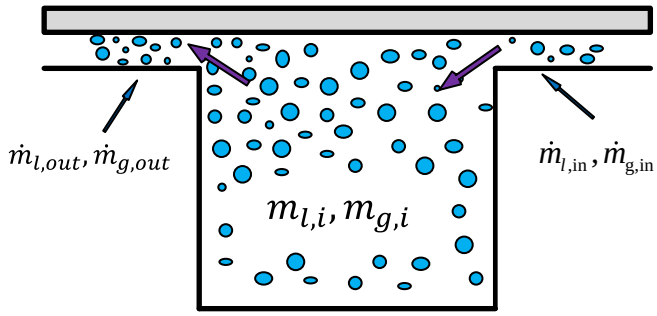

Figure 6.7 Mass balance in one closed chamber

Figure 6.7 shows the liquid and the gas flow in and out of a chamber from the circumferential clearance. The mass balance for the chamber can be calculated by the following differential equations,

$$\frac{dm_{l,i}}{dt} = \frac{dm_{l,in}}{dt} - \frac{dm_{l,out}}{dt} \tag{6.20}$$

$$\frac{dm_{g,i}}{dt} = \frac{dm_{g,in}}{dt} - \frac{dm_{g,out}}{dt} \tag{6.21}$$

The rapid rotating of rotors leads to intensive mixing between the liquid and the gas. Therefore, the pressure and the temperature can be considered to be uniform in the chamber. The liquid and the gas is assumed to be fully mixed. As a result, it is assumed that the flow in the clearance is homogenous.

It is assumed that the chamber is adiabatic. According to the energy balance equation,

$$\frac{dU_i}{dt} = \left(\frac{dm_{l,in}}{dt} \cdot h_{l,in} + \frac{dm_{g,in}}{dt} \cdot h_{g,in}\right) - \left(\frac{dm_{l,out}}{dt} \cdot h_{l,out} + \frac{dm_{g,out}}{dt} \cdot h_{g,out}\right) \quad 6.22$$

With knowing the condition of the entering and leaving leakages, the temperature in the next time step can be calculated.

Therefore, the chamber pressure in the next time step can be calculated by the following equation,

$$p_{i,\, t+\Delta t} = \rho R T_{i,\, t+\Delta t} \quad 6.23$$

6.6 Solution Methodology

The computer algorithm is shown in Figure 6.8. To start the simulation, an arbitrary initial pressure and temperature distribution need to be entered into the computer program. With the initial pressure and temperature distribution, the leakage flow rate can be calculated within one time step. Then the mass and pressure distribution in the chamber will be modified according to leakage flow rate, which will be used as initial condition in the calculation of the next time step.

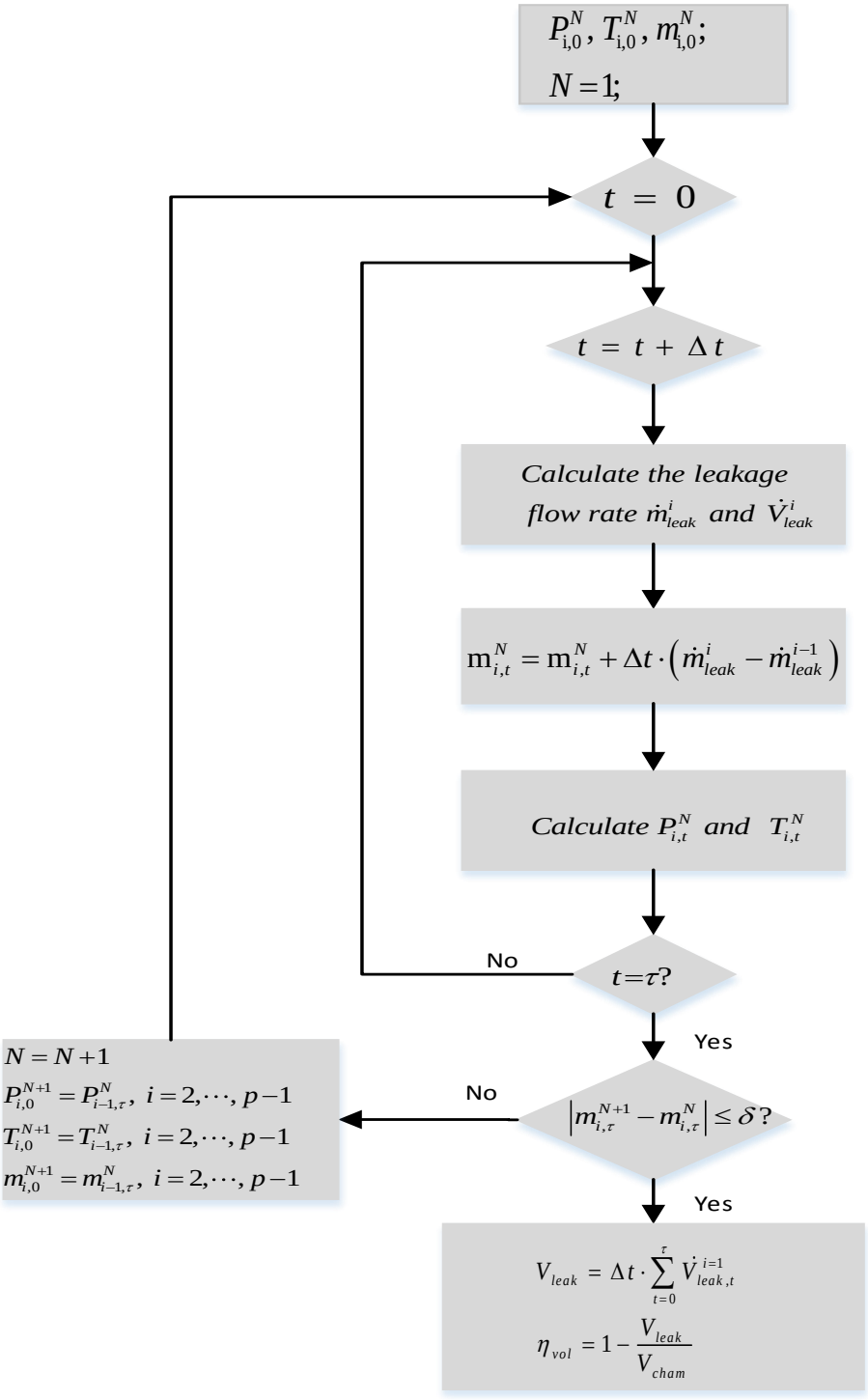

Figure 6.8 Computer program algorithm

After one revolution, the i^{th} chamber will be the $i+1^{th}$ chamber, the chamber condition at the end of last revolution are set to be the initial condition for the calculation of next revolution.

$$p_{1,0}^{N+1} = p_{in}, p_{i,0}^{N+1} = p_{i-1,\tau}^{N} \quad 6.24$$

$$T_{1,0}^{N+1} = T_{in}, T_{i,0}^{N+1} = T_{i-1,\tau}^{N} \quad 6.25$$

The pump is considered to be steady state when the flow rate of one revolution is equal to that of last revolution. In this case, the program will stop and predictions of steady state condition will be saved.

6.7 Modeling of Multistage Twin Screw Pump

Multistage twin screw pump consists of more than one stage, and each stage can be considered as a single stage pump. The model isn't able to be applied directly on the multistage twin screw pump. Since only the pressure and temperature at the pump inlet and the outlet is known, it is necessary to find the pressure and temperature distribution along the stages. Based on the experimental data, the following empirical equation of pressure distribution has be developed,

$$\frac{p_i - p_{in}}{p_{out} - p_{in}} = \left(\frac{i}{N}\right)^{2\alpha} \quad 6.26$$

The temperature is assumed to be linearly distributed along the stages. To prove the validation of an analytical model, it is necessary to make comparisons between the predicted and experimental results. In the next chapter, experimental data will be selected to verify the prediction of this model.

7 MULTIPHASE TWIN-SCREW PUMP MODEL VALIDATION

To verify the validation of this model, the model will be used to predict the behavior of twin screw pumps in this chapter. The predictions of volumetric efficiency will be compared with experiment data to determine the model's accuracy. The validation procedure utilizes experimental data for the following pumps:

- Leistritz L4MG Twin Screw Pump
- Colfax MR-200 Multiphase Twin Screw Pump
- Flowserve MP1 Twin Screw Pump
- Can-K 425 ESTSP

In addition, the pressure distribution and flow status in the pump will be presented. The choked condition and its effect on the pump performance will also be investigated.

7.1 Prediction of Pressure Distribution in the Twin Screw Pump

Pressure distribution in the twin screw pump of two phase flow represents unique characteristics compared with the pressure distribution of single phase flow. Typically, the pressure is linearly distributed along the pump screws from the suction side to discharge side for the single phase flow. However, the shape of the pressure distribution changes from linear to concave up when the pump is operated with two phase flow.

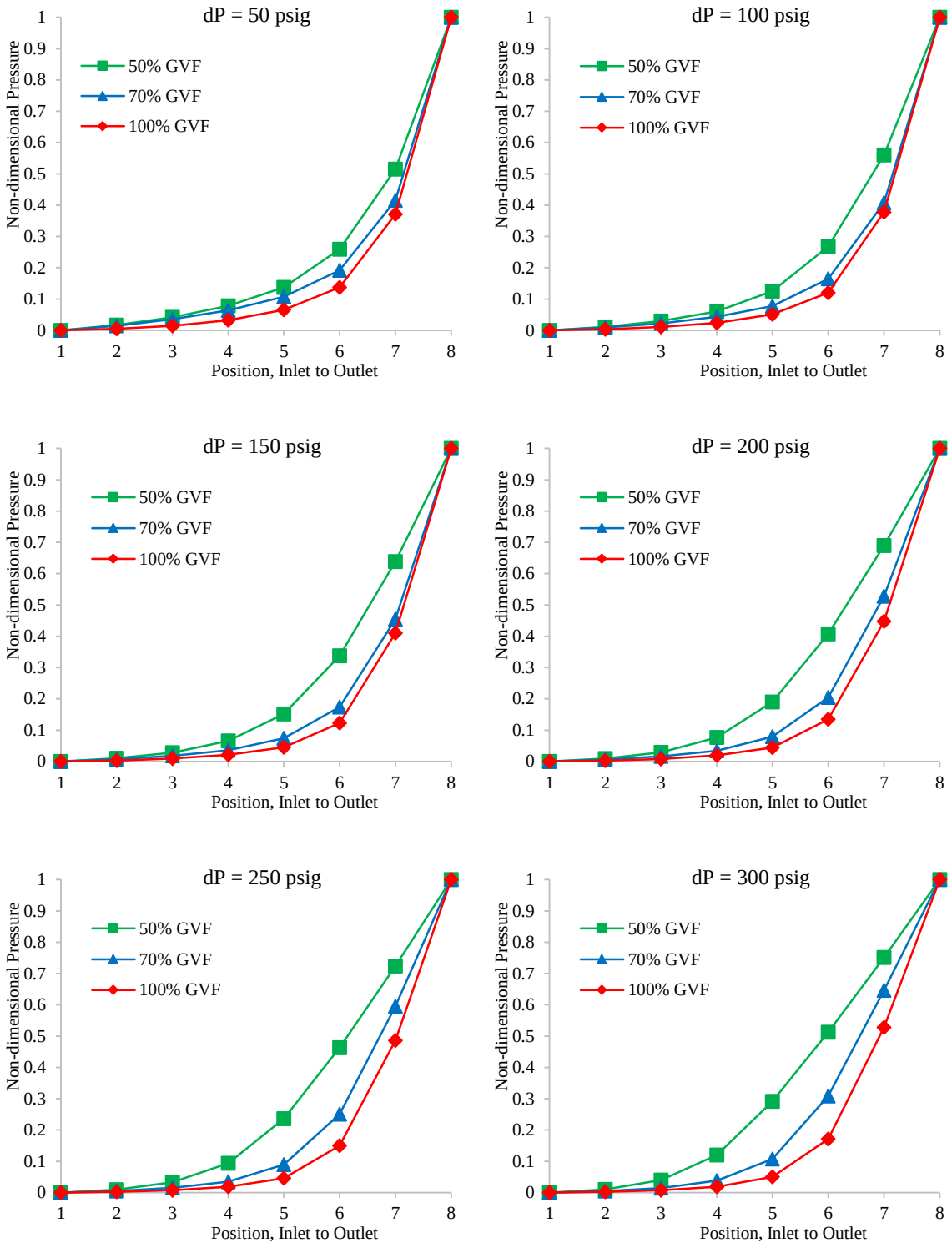

Figure 7.1 Non-dimensional pressure distribution of Colfax pump with 15 psig suction pressure

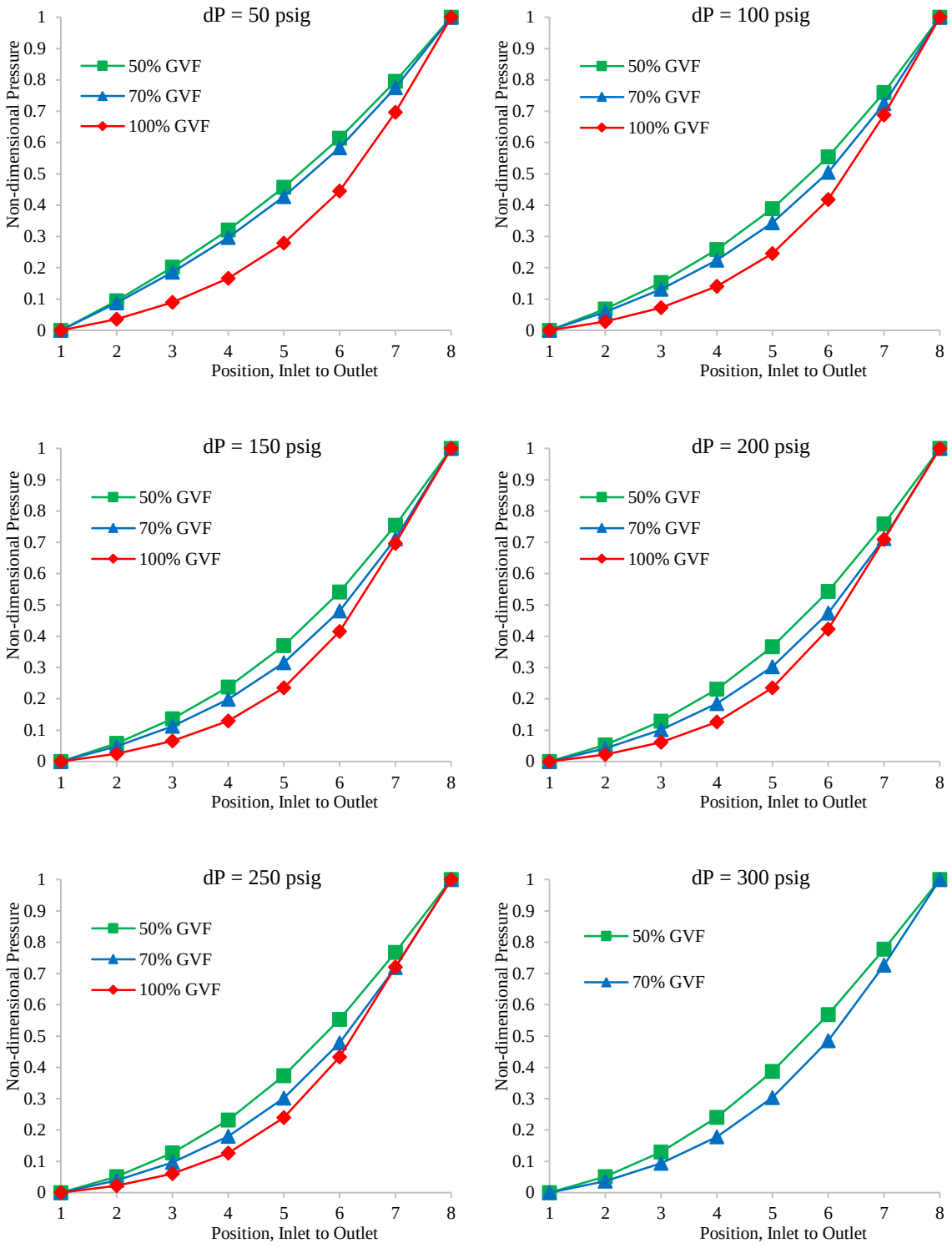

Figure 7.2 Non-dimensional pressure distribution of Colfax pump with 100 psig suction pressure

Steady state pressure distribution of the Colfax pump are presented by Figure 7.1 and Figure 7.2. Obviously GVF has a significant influence on the pressure distribution. With the increase of GVF, the pressure rise becomes steeper near the discharge side.

7.2 Volumetric Efficiency Prediction of Colfax Pump

The Colfax pump was tested by Patil [23] with two phase flow. Water and air were selected as testing fluids. The pump was tested with different suction pressure, GVF, and differential pressure. Steady state and transient pump performance were investigated. In this section, the experimental data of steady state is selected to compare with simulation results. The comparison of simulation and experimental results is shown in the Figure 7.3 and Figure 7.4. The simulation results show the same trends as the experimental data within the test conditions.

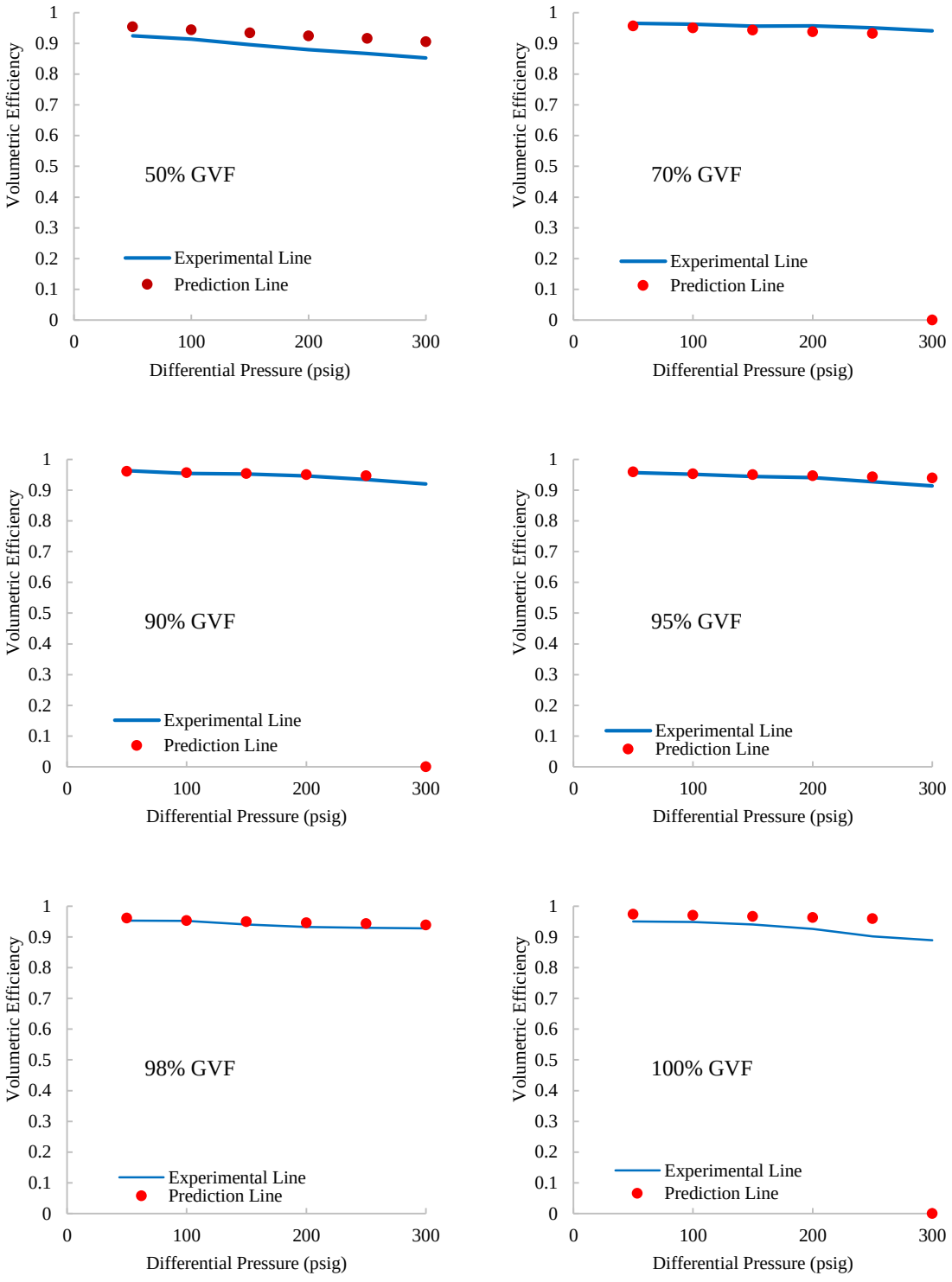

Figure 7.3 Comparison of prediction and experimental results of Colfax pump with 15 psig suction pressure

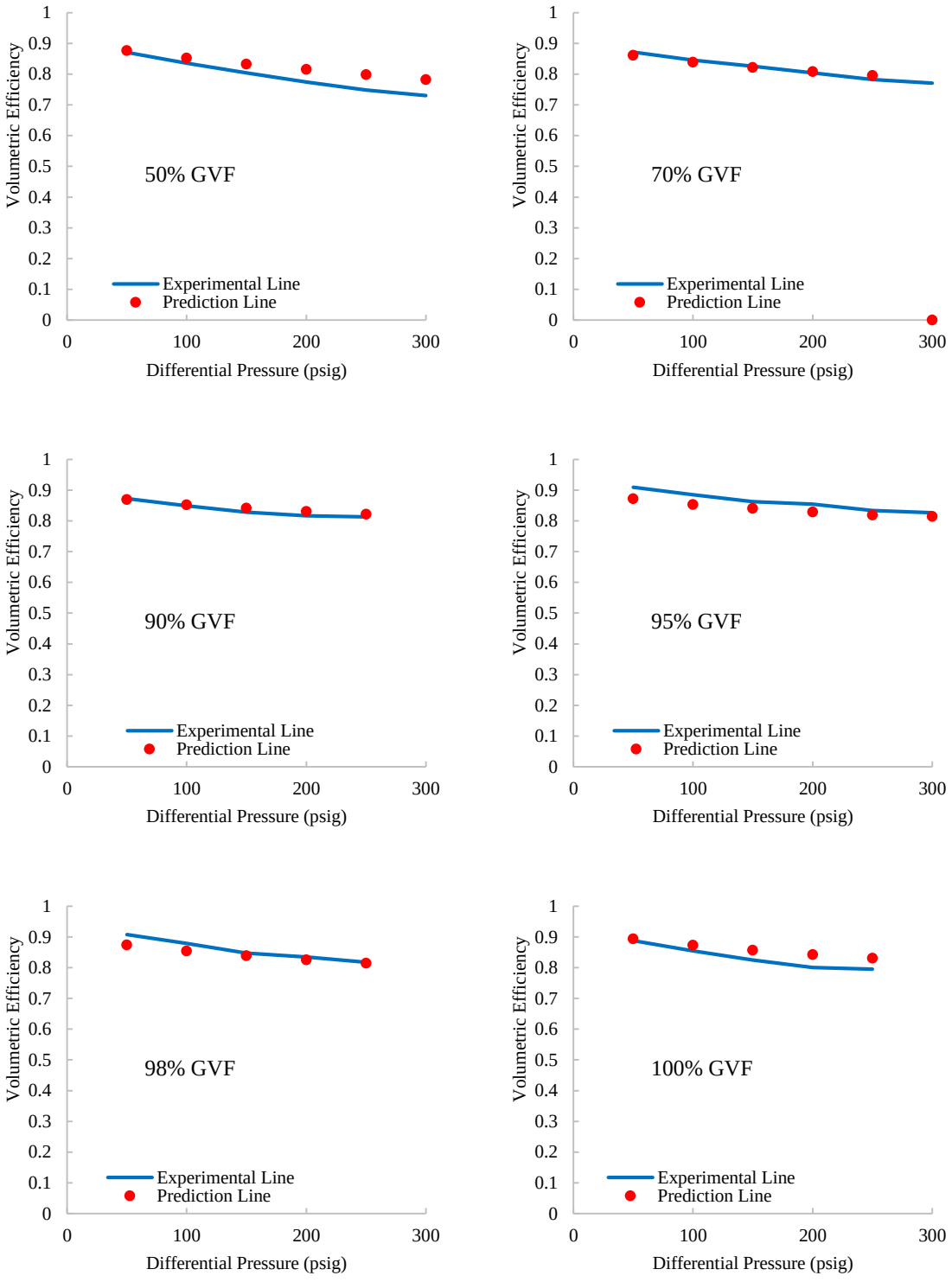

Figure 7.4 Comparison of prediction and experimental results of Colfax pump with 100 psig suction pressure

7.3 Volumetric Efficiency Prediction of Can-K Pump

For the Can-K pump, the exit pressure of the first stage is obtained by the empirical equation. Only the first stage was selected to perform the simulation, which largely reduces the complexity of modeling multistage pump. The simulation has been performed for both water test and oil test. As shown in Figure 7.5 to Figure 7.8, the simulation results represent good agreement with experimental data.

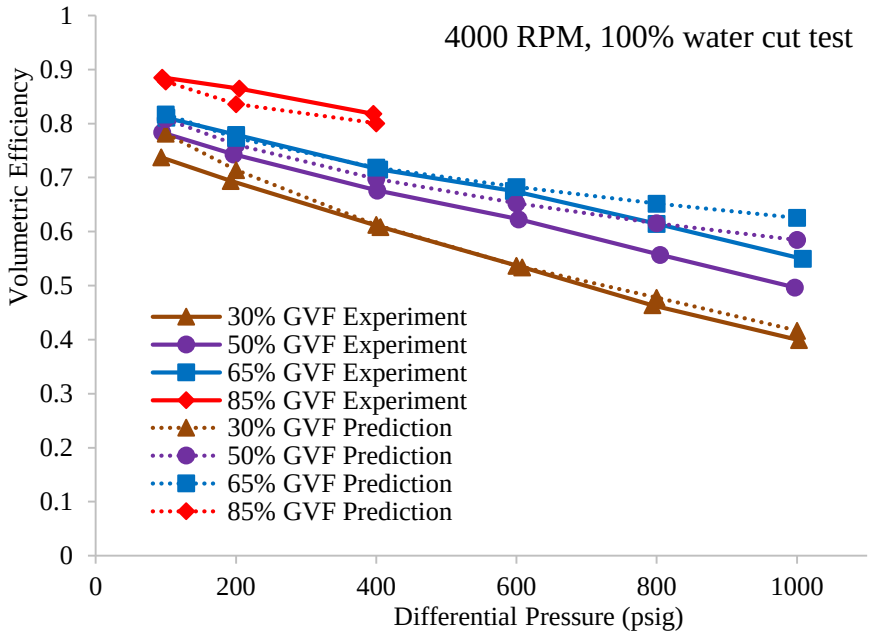

Figure 7.5 Comparison of prediction and experimental results of Can-K pump for water test at 4000 RPM

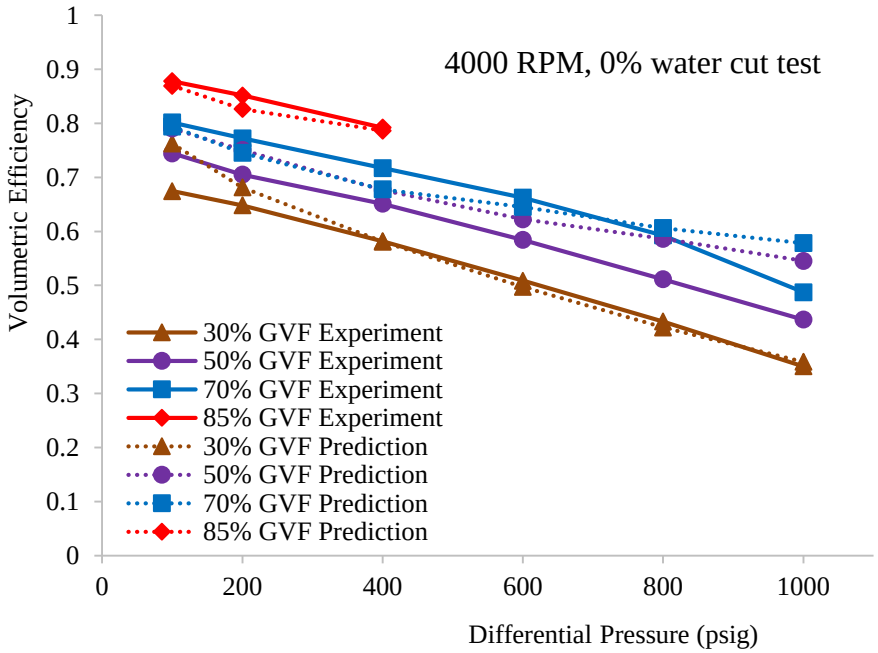

Figure 7.6 Comparison of prediction and experimental results of Can-K pump for oil Test at 4000 RPM

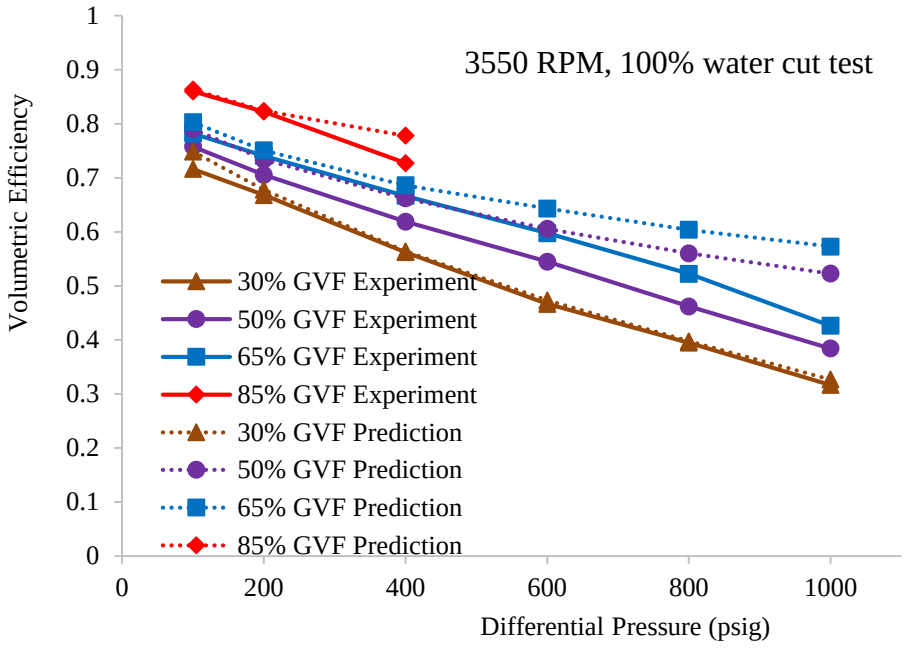

Figure 7.7 Comparison of prediction and experimental results of Can-K pump for water test at 3550 RPM

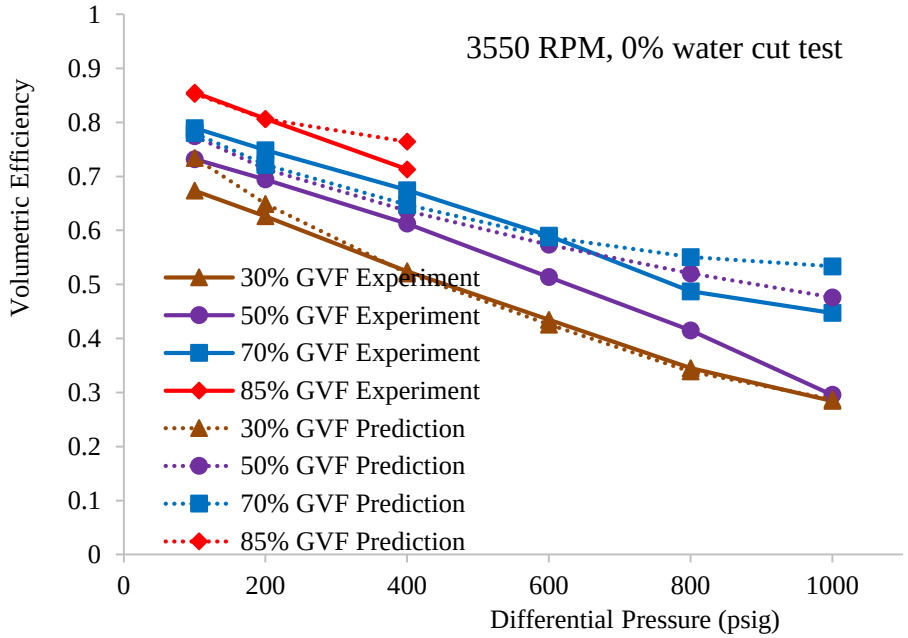

Figure 7.8 Comparison of prediction and experimental results of Can-K pump for oil test at 3550 RPM

7.4 Volumetric Efficiency Prediction of Leistritz Pump

The Leistritz pump was tested by Kroupa [21] with two phase flow. Water and air were selected as testing fluids. Steady state pump performance was investigated with GVF ranging from 50% to 100%. The effect of liquid recirculation loop was studied at high GVFs. In this section, only the steady state performance data is selected to make the comparison with simulation results. The comparison of prediction and experimental results are shown in Figure 7.9. The prediction shows good agreement with experimental results with GVF less than 90%. The prediction of volumetric efficiency is larger than experimental data at 95% GVF and 100% GVF.

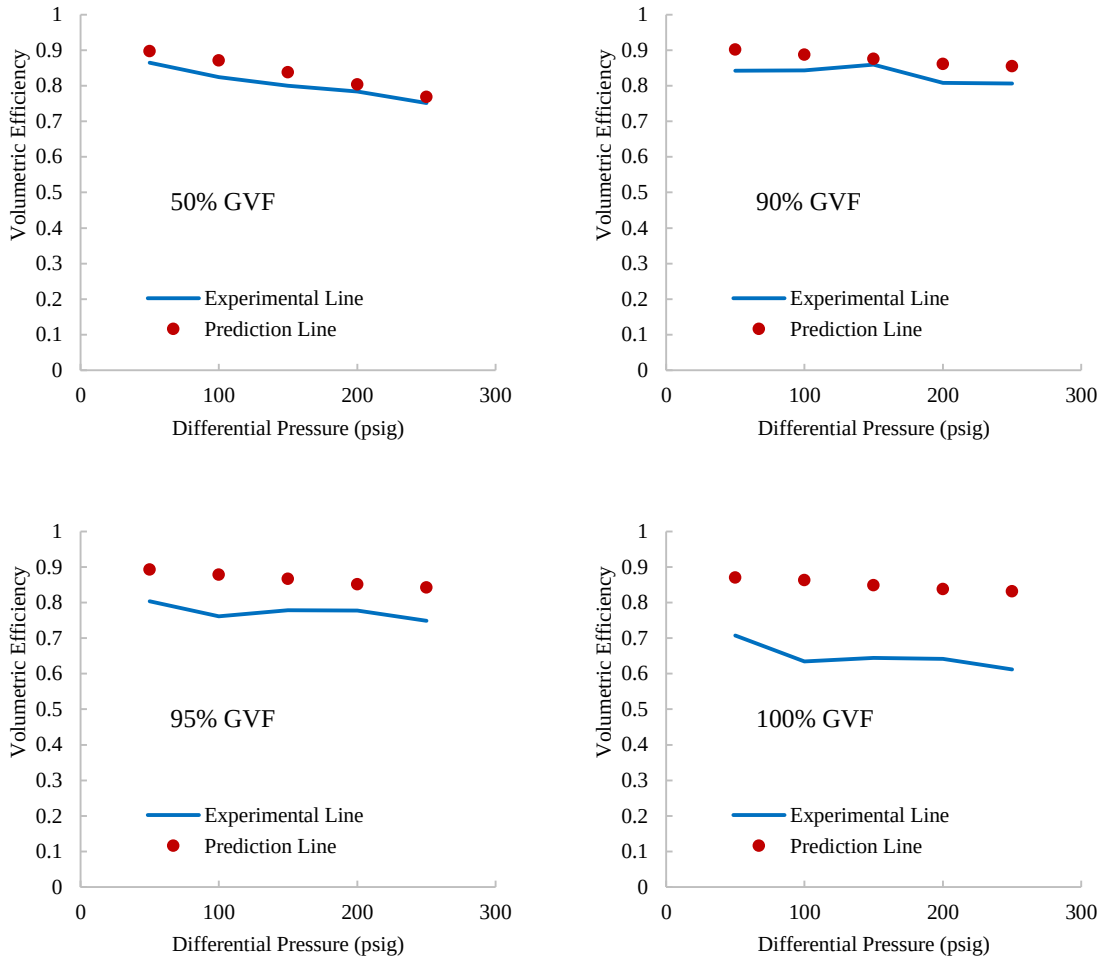

Figure 7.9 Comparison of prediction and experimental results of Leistritz pump

7.5 Volumetric Efficiency Prediction of Flowserve Pump

The Flowserve Pump was tested with oil and air. However, the experimental data of the Flowserve pump is incomplete. The pump inlet pressure and testing temperature are unavailable. The property of the working fluid is also unknown. In the simulation, the inlet pressure is assumed to be 100 psig and the inlet temperature is assumed to be 80 °F. Figure 7.6 shows the comparison between the prediction and experimental data. The

prediction shows the same trend with the experimental data. However, the test data shows that the volumetric efficiency decreases rapidly when the differential pressure is larger than 2000 psig. Since the relation of oil viscosity with temperature is not available, the viscosity is set to be constant in the program. With the increase of differential pressure, the viscosity will decrease due to increased temperature in the pump. The decreased viscosity will reduce the friction resistance in the clearance, which will lead to the increase of leakage flow rate.

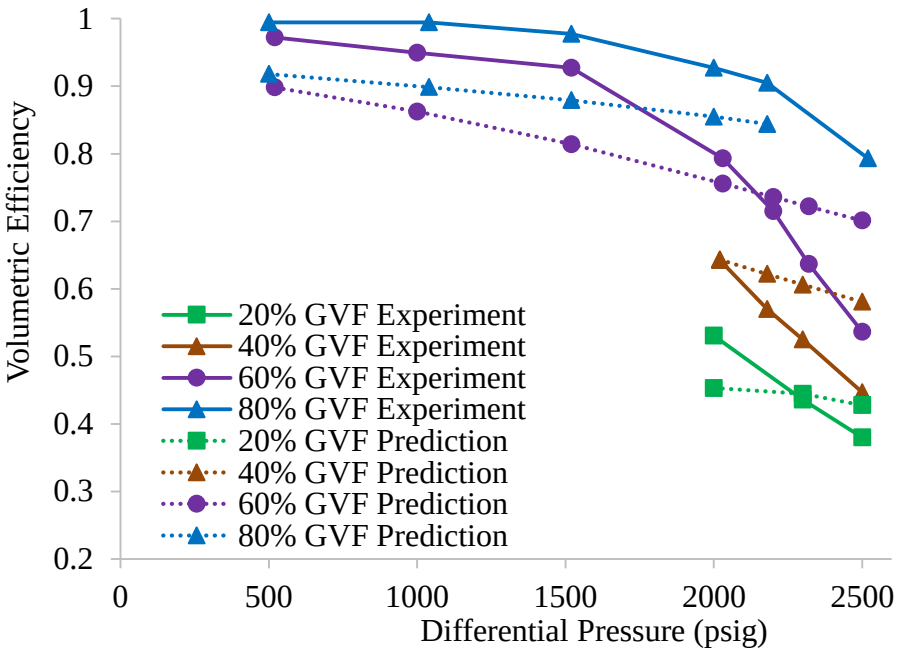

Figure 7.10 Comparison of prediction and experimental results of Flowserve pump

7.6 Mach Number Analysis

The leakage flow rate is deeply affected by GVF due to the characteristics of two phase flow. The sonic speed of two phase flow is much lower than that of pure gas or pure liquid, which has been presented in Figure 6.6. The leakage flow will be choked in the clearance once the velocity of the leakage flow becomes sonic speed. In this case, the velocity of leakage flow will not increase even with larger differential pressure between the two adjacent chambers. Besides, the leakage flow rate will not be affected by the downstream pressure. As a result, once the leakage flow is choked at one screw, the pressure in the downstream chambers could be much lower due to limited leakage flow rate.

Figure 7.4 and Figure 7.5 shows the Mach number at the exit of screws of the Leistritz pump. The choked condition is more likely to occur under high differential pressure and high GVF conditions. Typically, the choked condition is more likely to occur at the screw near the discharge side, where the pressure drops the most. However, the leakage flow is choked at the second screw at 250 psig differential pressure and 50% GVF as shown in Figure 7.12. This is because the GVF at the discharge is very low with a high differential pressure. Since the sonic speed of two phase flow is much larger at low GVF, the last screw can't be choked in this case.

For the Colfax pump, choked condition only occur at low suction pressure and high differential pressure flow conditions. This is because the Colfax pump has more cavities on the screws. The differential pressure over one cavity is reduced. Hence, the

possibility of being choked in the Colfax pump is small. The sonic speed of two phase flow is largely influenced by local pressure. The sonic speed at low pressure is much less than that at high pressure. Thus, the choked condition is more likely to happen with the suction pressure of 15 psig.

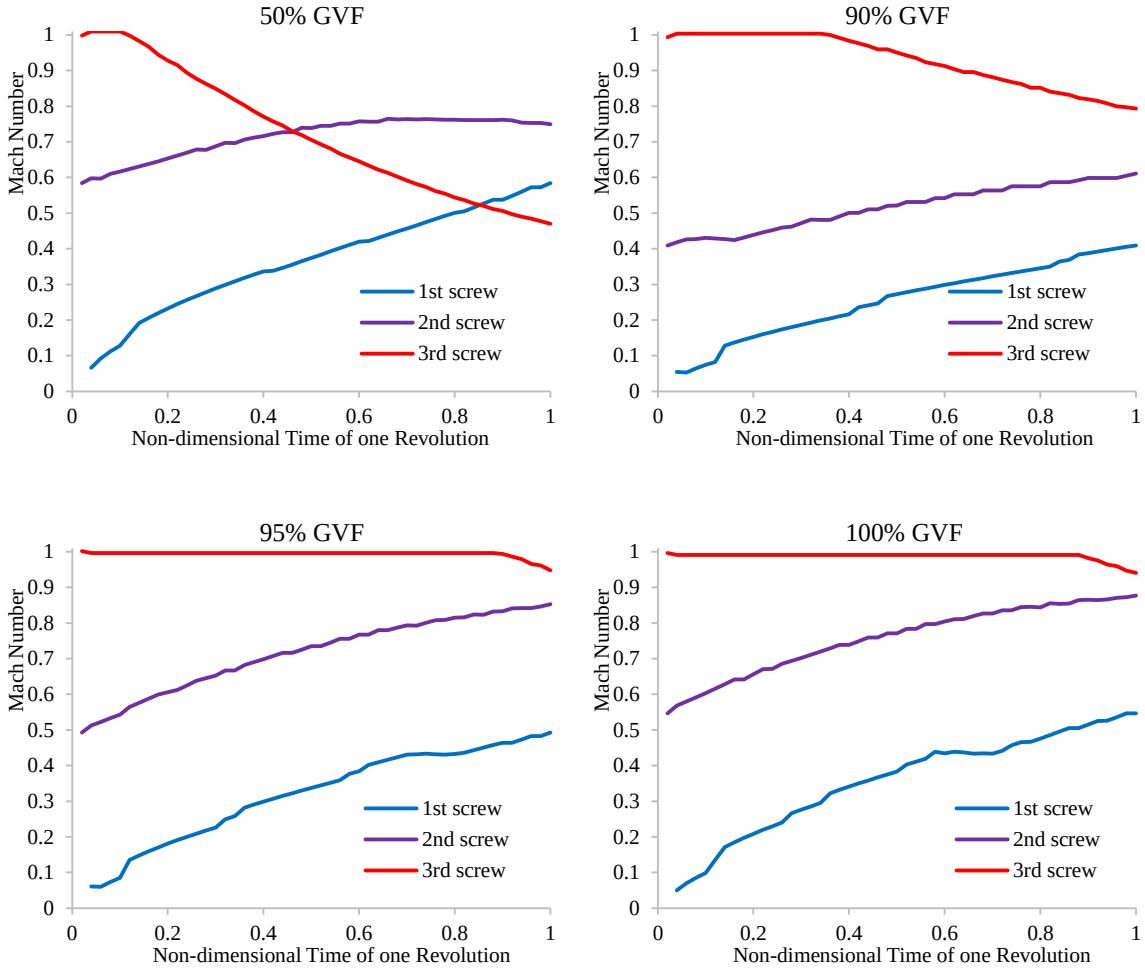

Figure 7.11 Mach number in the Leistritz pump with 100 psig differential pressure

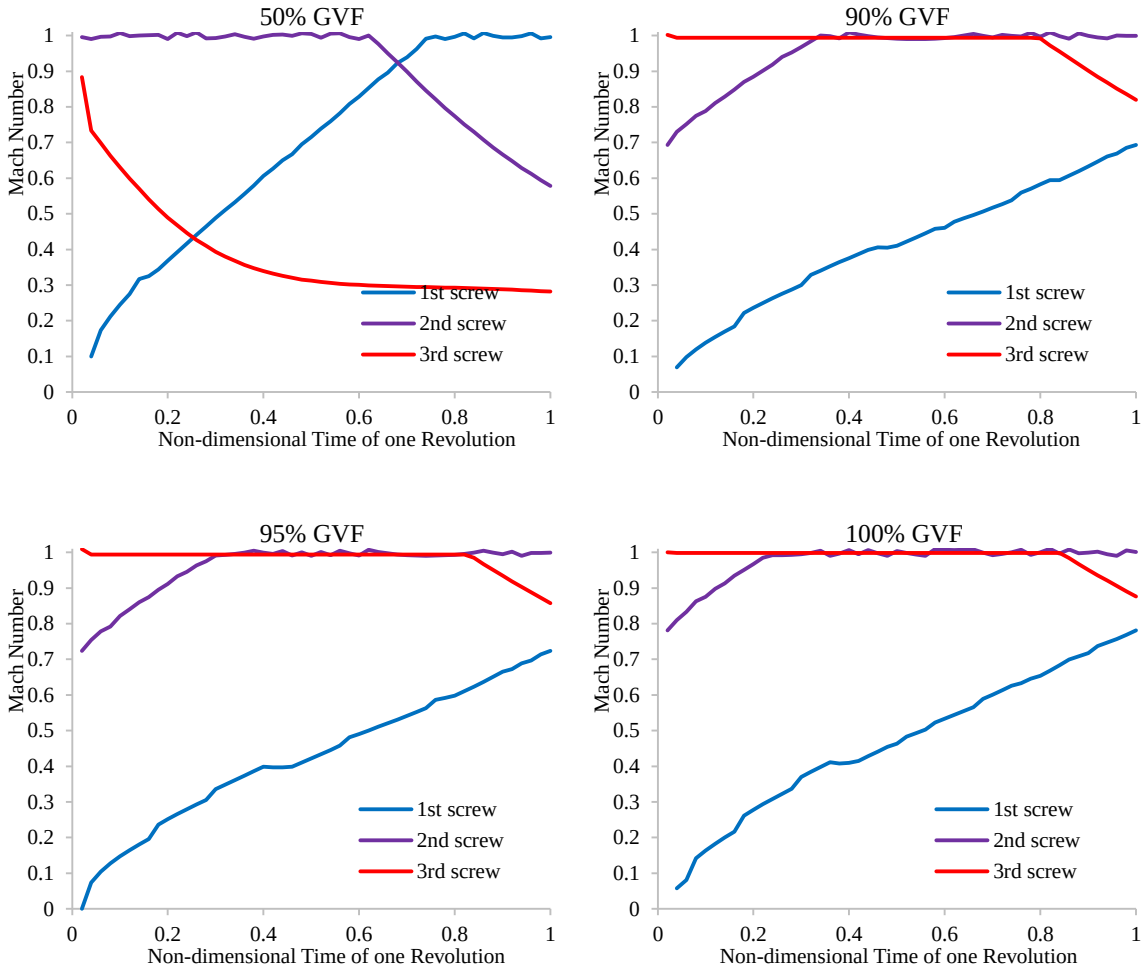

Figure 7.12 Mach number in the Leistritz pump with 250 psig differential pressure

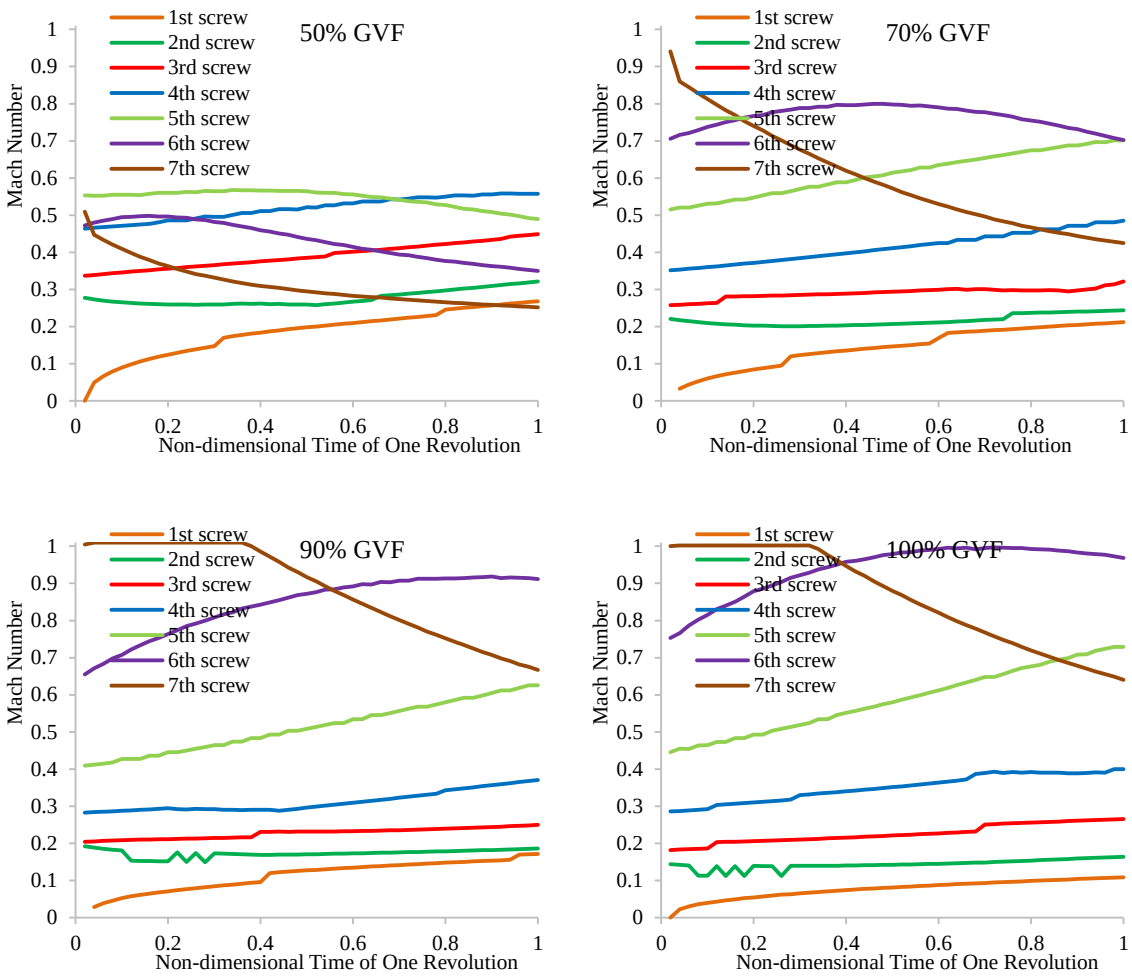

Figure 7.13 Mach number in the Colfax pump at 200 psig differential pressure, 15 psig suction pressure

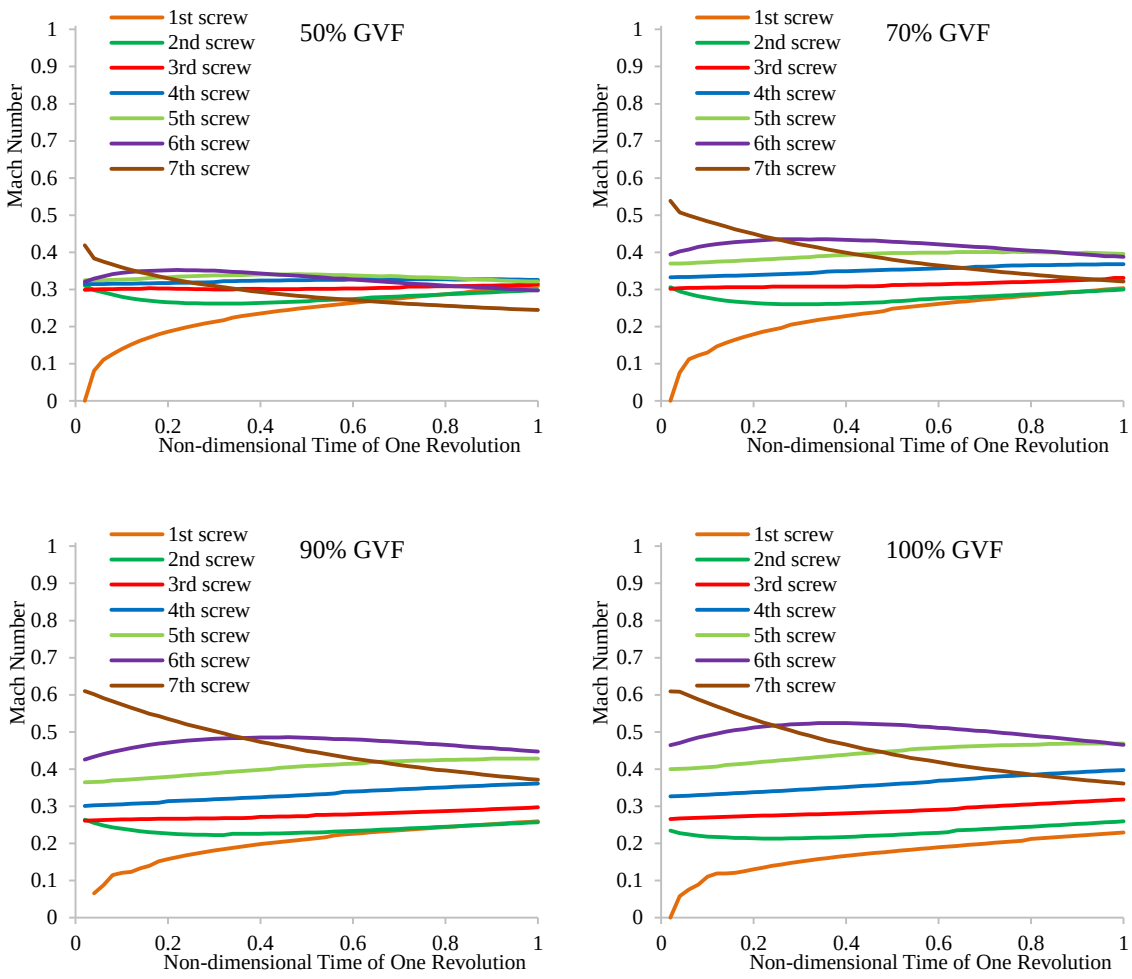

Figure 7.14 Mach number in the Colfax pump at 200 psig differential pressure, 100 psig suction pressure

7.7 Effect of Suction Pressure on Volumetric Efficiency

The suction pressure has an essential effect on the volumetric efficiency when twin screw pump operated with two phase flow. As shown in Figure 7.15, volumetric efficiency suffers significant decrease as suction pressure increases from 15 psig to 100 psig indicating less choked flow conditions.

Figure 7.16 shows the comparison of non-dimensional pressure distribution in the Colfax pump at 15 psig suction pressure and 100 psig suction pressure. It is found that the pressure distribution becomes more linear with increasing suction pressure. The pressure drop through the first screw is much larger with 100 psig suction pressure, which leads to the increased leakage flow rate over the first screw. Meanwhile, the pressure drop is more over the screws near the discharge side with 15 psig suction pressure. Because the leakage flow is more inclined to be choked near the discharge side with 15 psig suction pressure. As shown in Figure 7.13 and Figure 7.14, the choked condition occurs at the last screw with 90% GVF and 100% GVF with 15 psig suction pressure, while the Mach number of 100 psig suction pressure is much less.

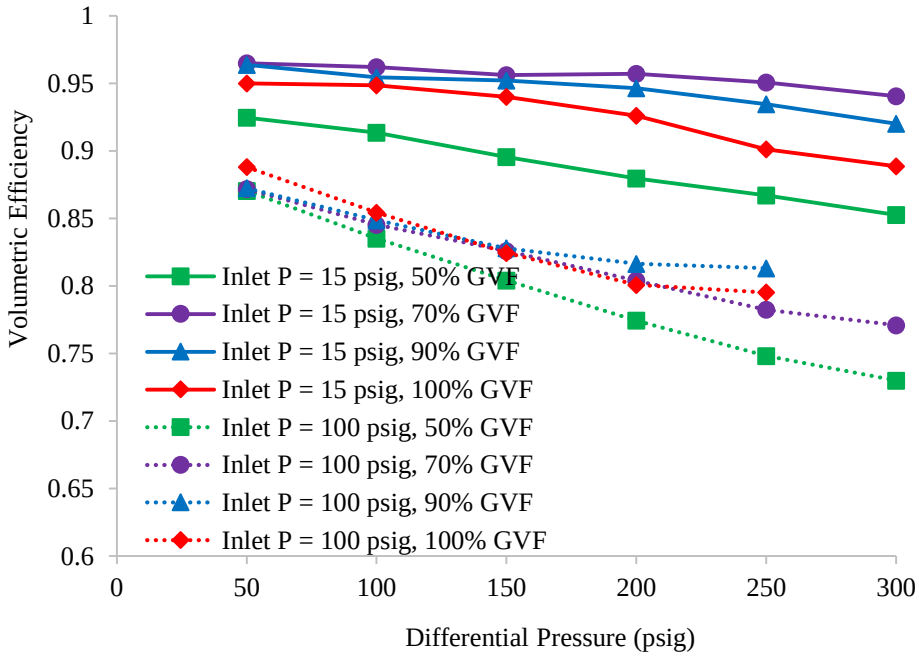

Figure 7.15 Comparison of volumetric efficiency for Colfax pump with different suction pressure (experimental data)

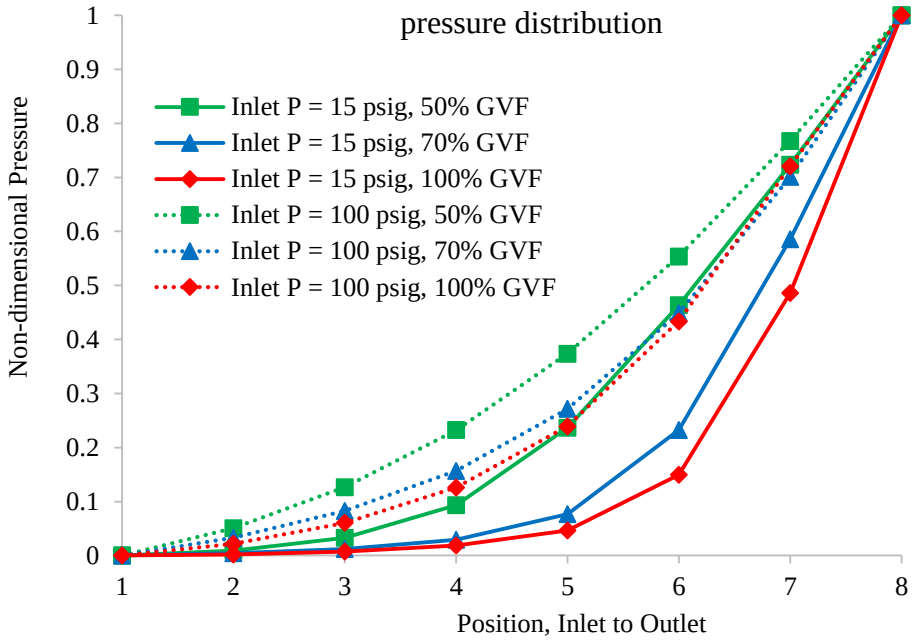

Figure 7.16 Comparison of pressure distribution for Colfax pump with different suction pressure

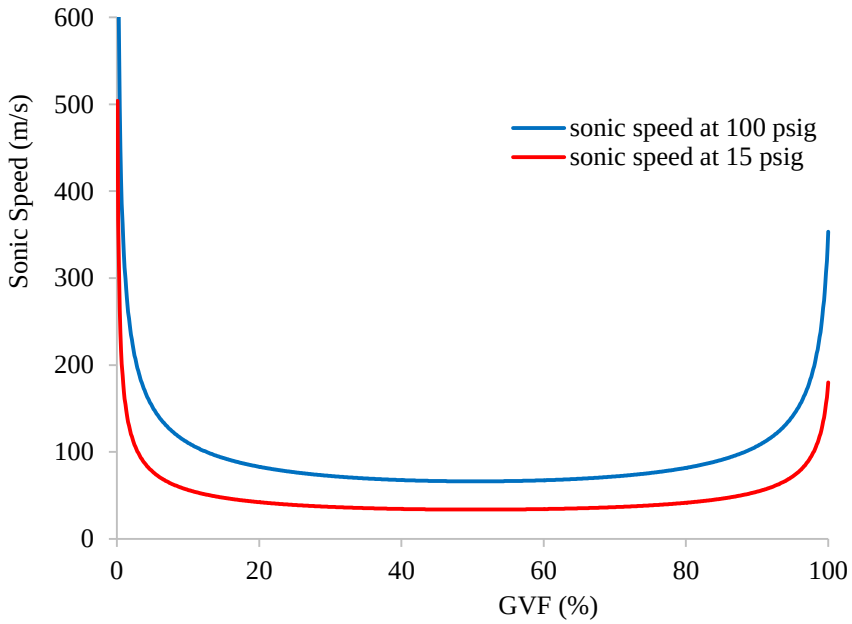

Figure 7.17 Comparison of water/air sonic speed at 100 psig and 15 psig

7.8 Effect of Water Cut on Pump Performance

Experimental test data shows that the volumetric efficiency of the oil and nitrogen test is lower than that of the water and air test for all testing conditions. As shown in Figure 7.18 and Figure 7.19, the prediction data also arrives at the same conclusion. Though the viscosity of oil is higher than the viscosity of water, the leakage flow rate of the oil test is larger than the leakage flow rate of water test. Previous experimental result also shows the same trend. Chan [6] found that efficiency doesn't increase with the increase of viscosity from 1 cp to 10 cP.

As show in Figure 7.20, the Mach number distribution of the oil test and the water test are almost the same. However, the sonic speed of oil and nitrogen mixture is larger than the sonic speed of water and air mixture. As result, the velocity of oil and nitrogen flow is larger than the velocity of water and air flow in the clearance, which leads to a larger leakage flow rate of oil test.

Hence, the friction loss in the clearance isn't the main factor to determine the leakage flow rate for the low viscosity flow. Instead, the pressure loss due to the expansion of two phase flow in the clearance has a larger effect on the leakage flow rate. Thus, though the viscosity of the oil is larger than the viscosity of water, the volumetric efficiency of oil/ nitrogen test is lower than the volumetric efficiency of water/ air test.

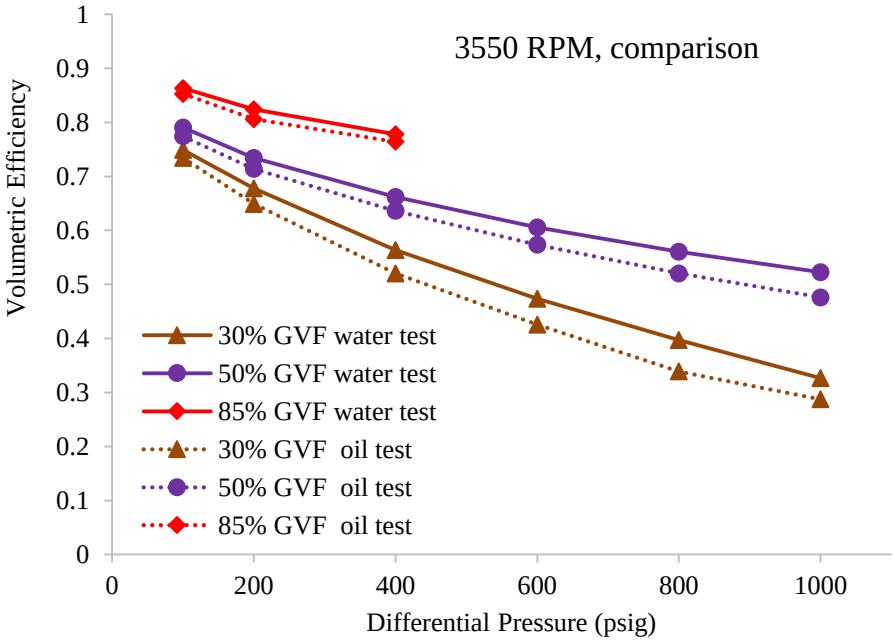

Figure 7.18 Prediction comparison of volumetric efficiency of water test and oil test at 3550 RPM

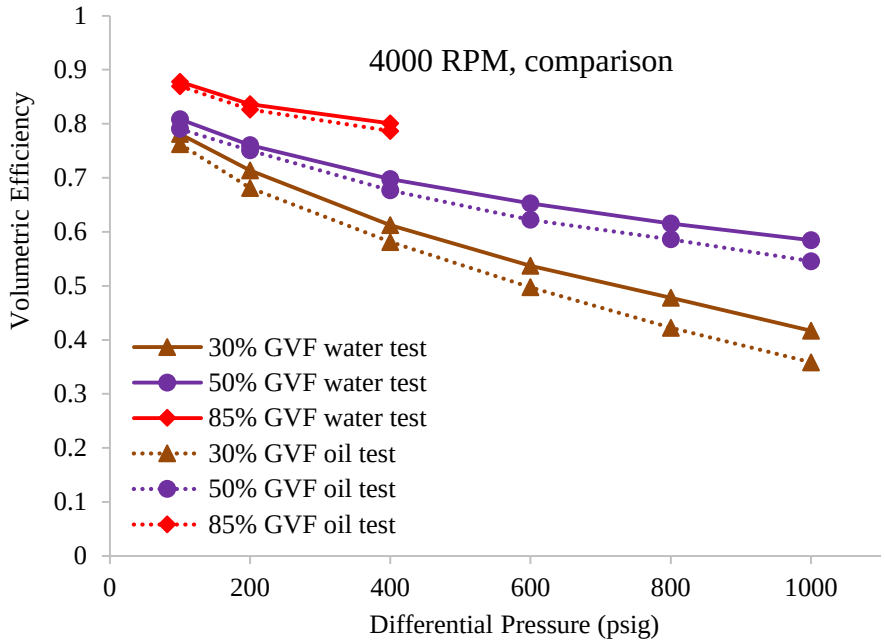

Figure 7.19 Prediction comparison of volumetric efficiency of water test and oil test at 4000 RPM

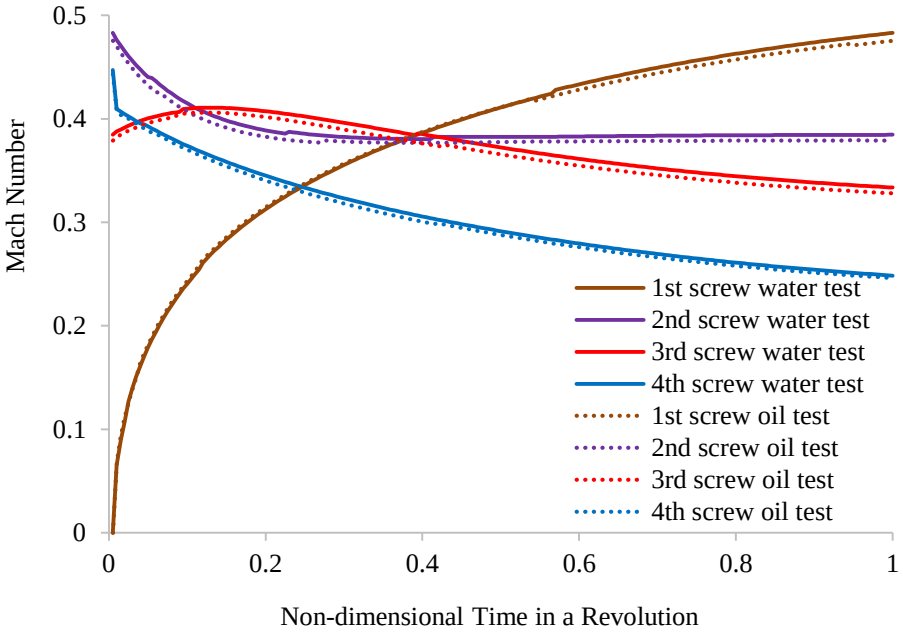

Figure 7.20 Comparison of Mach number for Can-K pump of water test and oil test at 4000 RPM, 1000 psig differential pressure, 50% GVF

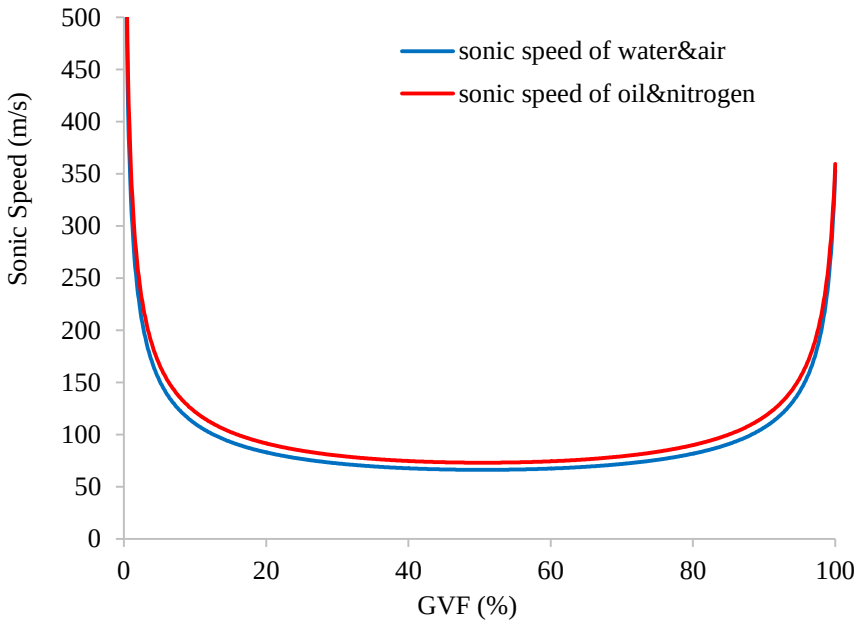

Figure 7.21 Comparison of sonic speed of water/ air and oil/ nitrogen at 100 psig

8 CONCLUSION

8.1 Experimental

In this research, the multiphase performance of a multistage twin screw pump has been investigated. Water-air mixture, oil-nitrogen mixture and oil-water-nitrogen mixture were selected as working fluids. The pump was tested with different differential pressures and different pump speeds. The GVF at the pump inlet varies from 0% to 85%. While water cut values of 0%, 50%, 80% and 100% were used.

Experimental results show that the curve of pressure distribution along the stages changes from concave-down to concave-up with the increase of GVF from 10% to 85% at the same differential pressure.

The volumetric efficiency increases as the GVF increases. The volumetric efficiency decreases with the increase of differential pressure. The volumetric efficiency of the oil test is lower than water test.

It is found the mechanical efficiency increases with the increase of differential pressure when the differential pressure is small. The mechanical efficiency decreases with the increase of differential pressure when the differential pressure is large. The mechanical efficiency becomes the maximum at about 600 psig differential pressure.

Compared with the single stage twin screw pump, the mechanical efficiency of Can-K pump is much lower. This is because the multistage pump has to overcome larger friction losses.

8.2 Analytical Model

An analytical model has been developed using MATLAB to predict the multiphase performance of twin screw pumps. A two phase Fanno flow model is used to model the leakage flow in the clearance. The compressibility of the leakage flow has been investigated.

The analytical model has been employed to predict the multiphase performance of various twin screw pumps. It has been demonstrated that the predictions match the experimental data well with the GVF ranging from 20% to 100% for the single stage pumps. A new method has been proposed to predict the multiphase performance of multistage twin screw pump. And it has been used to predict the performance of the Can-K pump with the GVF ranging from 10% to 85%.

The prediction shows that the GVF has a significant effect on the pressure distribution along the screws. With an increase of the GVF, the shape of the pressure distribution becomes steeper at the discharge side.

The possibility of choked flow condition has been investigated in this research. It is found the leakage flow is more likely to be choked with high differential pressure flow conditions. Besides, the sonic speed of two phase flow increases with the increase of the

local pressure. As a result, the choked condition is more likely to occur with low suction pressure conditions.

The Can-K pump shows different performance with different water cut. The volumetric efficiency increases with increasing water cut. Since the viscosity of the oil is very close to the viscosity of water. The viscosity isn't the dominant factor to determine the leakage flow rate. The sonic speed of the oil and nitrogen flow is higher than that of water and air flow. Thus the leakage flow of the oil and nitrogen has a higher velocity with the same Mach number, which leads to a lower volumetric efficiency.

8.3 Recommendations

In this research, the multiphase performance of a multistage twin screw pump has been investigated. However, the pump was tested with only one suction pressure. The effect of different suction pressure has not been investigated on the Can-K pump. Besides, a low viscosity oil was used as working fluid. The performance of the pump working with high viscosity oil hasn't been studied.

For the analytical model, the pressure distribution of the multistage pump is obtained by an empirical equation. New methods are still need to be developed to analyze the pressure distributions along the stages for the multistage pump.

REFERENCES

[1] Schlumberger. (2016, January 30). Integrated Lifting Solutions for Enhanced well Production. Retrieved from http://www.slb.com/services/production/artificial_lift.aspx

[2] Fleshman, R., and Lekic, H. "Artificial Lift for High-Volume Production." Oilfield Review, Spring 1999. 49-63.

[3] Zheng, D. Three Phase Erosion Testing and Vibration Analysis of an Electrical Submersible Pump. MSc Thesis, College Station: Texas A&M University, 2013.

[4] Dass, P. "Twin-Screw Pumps rival Traditional Artificial Lift Systems." E&P, 2009. 76-77.

[5] Karassik, I., Messina, J., Cooper, P., and Heald, C. Pump Handbook (3rd edition). McGRAW-HILL, New York, 2001. 3.99-3.122.

[6] Chan, E. Wet-gas compression in twin-screw multiphase pumps. MS Thesis, College Station: Texas A&M University, 2006.

[7] Vetter, G., and Wincek, M. "Performance Prediction of Twin-Screw pumps for Two-Phase Gas/Liquid Flow." Pumping Machinery, ASME, Fluid Engineering Conference (FED). Washington, D.C: ASME, 1993. 331-340.

[8] Egashira, K., Shoda, S., Tochikawa, T., and Furukawa, A. "Backflow in Twin-Screw-Type Multiphase Pump." SPEPF, 1998. 64-69.

[9] Feng, C., Yueyuan, P., Ziwen, X., and Pengcheng, S. "Thermodynamic performance simulation of a twin-screw multiphase pump." Journal of Process Mechanical Engineering , 2001. 157-162.

[10] Nakashima, C., Oliveira, S., and Caetano, E. "Thermodynamic Model of a Twin-Screw Multiphase Pump." Proceedings of ETCE, 2002. 877-885.

[11] Martin, A.M. Multiphase Twin Screw Pump Modeling for Oil and Gas Industry. PhD Thesis, College Station: Texas A&M University, 2003.

[12] Prang, A., and Cooper, P. "Enhanced Multiphase Flow Prediction in Twin-Screw Pumps." Proceedings of the 21th International Pump Users Symposium, 2004. 69-76.

[13] Rausch, T., Vauth, Th., Brandt, J-U., and Mewes, D. "A Model for the Delivering Characteristic of Multiphase pumps." 4th Conference on Multiphase Technology, Banff, Canada, 2004. 313-327.

[14] Vetter, G., Wirth, W., Korner, H., and Pregler. "Multiphase Pumping with Twin-Screw pumps - Understand and Model Hydrodynamics and Hydroabrasive Wear." 7th International Pump User Symposium, Turbomachinery Laboratory. Houston, Texas A&M University, 2000. 153-169.

[15] Nakashima, C., Oliveira, S., and Caetano, E. "Thermo-Hydraulic Model of a Twin-Screw Multiphase Pump." Proceedings of IMECE04, 2004. 251-260

[16] Xu, J. Modelling of Wet Gas Compression in Twin Screw Multiphase Pump. PhD Thesis, College Station: Texas A&M University, 2008.

[17] Rabiger, K., Maksoud, T., and Ward, J. "Thermo- and Fluid Dynamic Model of a Multiphase Screw Pump, Operating at Very High Gas Volume Fractions." Schriftenreihe der Georg-Simon-Ohm-Fachhochschule Nürnberg. Nr.35, November 2006.

[18] Rabiger, K., Maksoud, T., Ward, J., and Hausmann, G. "Investigation of the Fluid Dynamic and Thermodynamic Behaviour of Multiphase Screw Pumps Handling Liquid/gas Mixtures with Very High Gas Volume Fractions." BHR Group 2007 Multiphase Production Technology 13. 91-104.

[19] Rabiger, K., Maksoud, T., Ward, J., and Hausmann, G. "Theoretical and Experimental Analysis of a Multiphase Screw Pump, Handling Gas-Liquid Mixtures with Very High Gas Volume Fractions." Experimental Thermal and Fluid Science 32(2008). 1694-701.

[20] Rabiger, K. Fluid Dynamic and Thermodynamic Behaviour of Multiphase Screw Pumps Handling Gas-Liquid Mixtures with Very High Gas Volume Fractions. PhD Thesis, Nuremberg: University of Applied Sciences in Nuremberg, 2009.

[21] Kroupa, R. Investigation of a Multiphase Twin-screw Pump Operating at High Gas Volume Fractions. MSc Thesis, College Station: Texas A&M University, 2011.

[22] Morrison, G., Kroupa, R., Patil, A., Xu, J., Scott, S., and Olson, S. "Experimental Investigation of Wellhead Twin-Screw Pump for Gas-Well Deliquefication." Oil and Gas Facilities Journal, SPE, April 2014. 73-80.

[23] Patil, A. R. Performance Evaluation and CFD Simulation of Multiphase Twin-Screw Pumps. Ph.D. Dissertation, College Station: Texas A&M University, 2013.

[24] Morrison, G., Patil, A., and Cihak, D. "Evaluation of a Twin Screw Pump for Use in High Gas Volume Fraction Flows." ASME Fluids Engineering Summer Meeting, Puerto Rico, 2012. 1-9

[25] Turhan, Y. Efficiency and Leakage Analysis of a Twin-Screw Multiphase Pump. MSc Thesis, College Station: Texas A&M University, 2014.

[26] Brennen, C. E. Fundamentals of Multiphase Flow. Cambridge University Press, Pasadena, 2005. 220-246.

[27] Morrison, G., Patil, A., and Cihak, D. "Efficiency limit for multiphase pumps." 8th North American Conference on Multiphase Technology (BHR Group), Banff, Canada, 20-22 June, 2012. 17-29.

APPENDIX A

UNCERTAINTY ANALYSIS

A.1 Water Cut

The water cut is calculated based on the mixture density which is measured by the Coriolis flow meter,

$$\eta_w = \frac{\rho_m - \rho_o}{\rho_w - \rho_o} \tag{A.1}$$

Thus the uncertainty of the water cut is calculated with the following equation,

$$u_{\eta_w} = \left[\left(\frac{\partial \eta_w}{\partial \rho_m} u_{\rho_m} \right)^2 \right]^{0.5} \tag{A.2}$$

Which simplifies to,

$$\mu_{\eta_w} = \frac{1}{\rho_w - \rho_o} \mu_{\rho_m} \tag{A.3}$$

The measurement uncertainty of density is shown in Table 4.4. The uncertainty of 50% water cut and 80% water cut is given in Table A.1.

Table A.1 Uncertainty of Water Cut

Water Cut (%)	u_{η_w} (%)	u_{η_w}/η_w (%)
50	0.28	0.56
80	0.28	0.35

A.2 Liquid Flow Rate

For the water/oil test, it is found that the separator can't separate the gas and liquid thoroughly. There is some gas mixed in the liquid line, which leads to the measurement

error of the liquid flow rate. The liquid flow rate is calibrated with the following equation,

$$Q_l = Q_{l'} \frac{\rho_m - \rho_g}{\rho_l - \rho_g} \tag{A.4}$$

ρ_m is the density measured by the liquid flow meter. Thus,

$$\mu_{Q_l} = \left[\left(\frac{\partial Q_l}{\partial Q_{l'}} \mu_{Q_{l'}} \right)^2 + \left(\frac{\partial Q_l}{\partial \rho_m} \mu_{\rho_m} \right)^2 + \left(\frac{\partial Q_l}{\partial \rho_g} \mu_{\rho_g} \right)^2 \right]^{0.5} \tag{A.5}$$

The density of the gas is given by the following equation,

$$\rho_g = \frac{p}{Rp} \tag{A.6}$$

Thus the uncertainty of the gas density is,

$$\mu_{\rho_g} = \left[\left(\frac{\partial \rho_g}{\partial p} \mu_p \right)^2 + \left(\frac{\partial \rho_g}{\partial T} \mu_T \right)^2 \right]^{0.5} \tag{A.7}$$

The uncertainties of the liquid flow rate are presented in Table A.2.

Table A.2 Uncertainty of Liquid Flow Rate for 100% water cut test at 4000 RPM

GVF (%)	dP (psi)	Q_l (gpm)	μ_{Q_l} (gpm)	μ_{Q_l}/Q_l (%)
50	200	42.184	0.047	0.11
50	1000	28.187	0.032	0.11

A.3 Gas Flow Rate at the Pump Inlet

The gas flow rate at the pump inlet is calculated with the air flow rate at the flow meters with the following equation,

$$Q_g = Q_{g'} \frac{p_0 T_i}{p_i T_0} + Q_{l'} \frac{\rho_l - \rho_m}{\rho_l - \rho_g} \tag{A.8}$$

Thus, the uncertainly of the air flow rate at the pump inlet can be given as the following equation,

$$u_{Q_g} = \left[\left(\frac{\partial Q_g}{\partial T_0}u_{T_0}\right)^2 + \left(\frac{\partial Q_g}{\partial T_i}u_{T_i}\right)^2 + \left(\frac{\partial Q_g}{\partial p_0}u_{p_0}\right)^2 + \left(\frac{\partial Q_g}{\partial p_i}u_{p_i}\right)^2 + \left(\frac{\partial Q_g}{\partial Q_{g'}}u_{Q_{g'}}\right)^2 + \left(\frac{\partial Q_g}{\partial \rho_{\rho_m}}u_{\rho_m}\right)^2 + \left(\frac{\partial Q_g}{\partial \rho_g}u_{\rho_g}\right)^2 + \left(\frac{\partial Q_g}{\partial Q_{l'}}u_{Q_{l'}}\right)^2\right]^{0.5} \quad \text{A.9}$$

The uncertainties of the gas flow rate are presented in Table A.3.

Table A.3 Uncertainty of Gas Flow Rate for 100% water cut test at 4000 RPM

GVF (%)	dP (psi)	Q_g (gpm)	u_{Q_g} (gpm)	u_{Q_g}/Q_g (%)
50	200	42.170	0.460	1.09
50	1000	28.211	0.308	1.09

A.4 GVF

The uncertainty of the GVF at the pump inlet is given with the following equation,

$$\mu_{GVF} = \left[\left(\frac{\partial GVF}{\partial Q_l}\mu_{Q_l}\right)^2 + \left(\frac{\partial GVF}{\partial Q_g}\mu_{Q_g}\right)^2\right]^{0.5} \quad \text{A.10}$$

Which simplifies to,

$$\mu_{GVF} = \left[\left(\frac{Q_g}{(Q_g+Q_l)^2}\mu_{Q_l}\right)^2 + \left(\frac{Q_l}{(Q_g+Q_l)^2}\mu_{Q_g}\right)^2\right]^{0.5} \quad \text{A.11}$$

The uncertainties of the GVF are presented in Table A.4.

Table A.4 Uncertainty of GVF for 100% water cut test at 4000 RPM

GVF (%)	dP (psi)	GVF (%)	μ_{GVF} (%)	μ_{GVF}/GVF (%)
50	200	49.99	0.27	0.55
50	1000	50.02	0.27	0.55

A.5 Volumetric Efficiency

The volumetric efficiency is given by,

$$\eta_v = \frac{Q_g + Q_l}{Q_{th}} \tag{A.12}$$

Thus, the uncertainty of the volumetric efficiency is given with the following equation,

$$\mu_{\eta_v} = \left[\left(\frac{\partial \eta_v}{\partial Q_g}\mu_{Q_g}\right)^2 + \left(\frac{\partial \eta_v}{\partial Q_l}\mu_{Q_l}\right)^2\right]^{0.5} \tag{A.13}$$

Which simplifies to,

$$\mu_{\eta_v} = \frac{1}{Q_{th}}\left[\left(\mu_{Q_g}\right)^2 + \left(\mu_{Q_l}\right)^2\right]^{0.5} \tag{A.14}$$

The uncertainties of the volumetric efficiency are presented in Table A.5.

Table A.5 Uncertainty of Volumetric Efficiency for 100% water cut test at 4000 RPM

GVF (%)	dP (psi)	η_v (%)	μ_{η_v} (%)	μ_{η_v}/η_v (%)
50	200	0.743	0.0041	0.55
50	1000	0.497	0.0027	0.55

A.6 Polytropic Coefficient

The polytropic coefficient is given by,

$$n = \frac{In\left(\frac{p_{in}}{p_{out}}\right)}{In\left(\frac{p_{in}}{p_{out}} \cdot \frac{T_{out}}{T_{in}}\right)} \tag{A.15}$$

The uncertainty of the polytropic coefficient is given with the following equation,

$$\mu_n = \left[\left(\frac{\partial n}{\partial p_{in}}\mu_{p_{in}}\right)^2 + \left(\frac{\partial n}{\partial p_{out}}\mu_{p_{out}}\right)^2 + \left(\frac{\partial n}{\partial T_{in}}\mu_{T_{in}}\right)^2 + \left(\frac{\partial n}{\partial T_{out}}\mu_{T_{out}}\right)^2\right]^{0.5} \tag{A.16}$$

The uncertainties of the polytropic coefficient are presented in Table A.6.

Table A.6 Uncertainty of polytropic coefficient for 100% water cut test at 4000 RPM

GVF (%)	dP (psi)	n	μ_n	μ_n/n (%)
50	200	1.001	0.0106	1.06
50	1000	1.007	0.0047	0.47

A.7 Mechanical Efficiency (Isothermal)

The Mechanical efficiency (Isothermal) is given by,

$$\eta_{mech} = \frac{Q_l(p_{out} - p_{in}) + Q_g p_{in} \ln\left(\frac{p_{out}}{p_{in}}\right)}{P_{drive}} \quad \text{A.17}$$

The uncertainty of the Mechanical efficiency (Isothermal) is given with the following equation,

$$u_{\eta_{mech}} = \left[\left(\frac{\partial \eta_{mech}}{\partial Q_l} u_{Q_l}\right)^2 + \left(\frac{\partial \eta_{mech}}{\partial Q_g} u_{Q_g}\right)^2 + \left(\frac{\partial \eta_{mech}}{\partial p_{out}} u_{p_{out}}\right)^2 + \left(\frac{\partial \eta_{mech}}{\partial p_{in}} u_{p_{in}}\right)^2\right]^{0.5} \quad \text{A.18}$$

The uncertainties of the mechanical efficiency are presented in Table A.7.

Table A.7 Uncertainty of mechanical efficiency (isothermal) for 100% water cut test at 4000 RPM

GVF (%)	dP (psi)	η_{mech} (%)	$u_{\eta_{mech}}$ (%)	$u_{\eta_{mech}}/\eta_{mech}$ (%)
50	200	0.202	0.00085	0.42
50	1000	0.241	0.00061	0.25

A.8 Pump Effectiveness

The pump effectiveness is given by,

$$\eta_{eff} = \frac{Q_l(p_{out} - p_{in}) + Q_g p_{in} \ln\left(\frac{p_{out}}{p_{in}}\right)}{(Q_g + Q_l)(p_{out} - p_{in})} \quad \text{A.19}$$

The uncertainty of the pump effectiveness is given with the following equation,

$$\mu_{\eta_{eff}} = \left[\left(\frac{\partial \eta_{eff}}{\partial p_{in}}\mu_{p_{in}}\right)^2 + \left(\frac{\partial \eta_{eff}}{\partial p_{out}}\mu_{p_{out}}\right)^2 + \left(\frac{\partial \eta_{eff}}{\partial Q_l}\mu_{Q_l}\right)^2 + \left(\frac{\partial \eta_{eff}}{\partial Q_g}\mu_{Q_g}\right)^2\right]^{0.5} \quad \text{A.20}$$

The uncertainties of the pump effectiveness are presented in Table A.8.

Table A.8 Uncertainty of Liquid Flow Rate for 100% water cut test at 4000 RPM

GVF (%)	dP (psi)	η_{eff}(%)	$\mu_{\eta_{eff}}$ (%)	$\mu_{\eta_{eff}}/\eta_{eff}$ (%)
50	200	0.791	0.0012	0.15
50	1000	0.631	0.002	0.32